A Thesis for the Degree of Ph.D. in Engineering

Design and Fabrication of a Tooth-Inspired Tactile Sensor for the Detection of Multidirectional Force

February 2019

Graduate School of Science and Technology
Keio University

Nurul Adni Binti Ahmad Ridzuan

ABSTRACT

Demands on tactile sensors have been increasing rapidly. When they are thin and flexible, they can be attached to arbitrary surfaces and contribute to enhance precision in monitoring and handling objects. A capacitive-type tactile sensor with liquid dielectric is proposed to achieve both high accuracy and flexibility. There also are demands for tactile sensors that can detect multidirectional load in a narrow space. For such applications, the tactile sensors cannot have shapes of a sheet or a pad as reported in many of the previous work. Thus, in this thesis, a tactile sensor that has a three-dimensional format and can detect multi-directional force is designed and demonstrated, which is inspired by the anatomy of a tooth.

Chapter 1 summarizes background of the research. Tactile sensors are thoroughly surveyed, among which the highly accurate and flexible tactile sensor is detailed. The objective of this work is explicitly described.

Chapter 2 illustrates the design strategy of the sensor device. The inspiration of the design of the sensor, which is a tooth, is discussed.

Chapter 3 explains the design of the sensor device. The sensor consisted of a center pole that acts like a tooth, which can sense the direction of light touch or pressure applied on its enamel. The bottom of the center pole is equipped with four strain gauges, whose resistances change according to the movement of the center pole.

Chapter 4 illustrates the fabrication and assembly processes of the sensor device. The center pole is made of stainless-steel and is plugged into an acrylic base, just like a tooth that is plugged in the alveolar bone. The assembly process allows the sensor to have the strain gauges in a three-dimensional manner, which support the pole and detect the shear force applied to the pole.

Chapter 5 describes the experimental results. The sensitivity of the sensor device per unit 1 mm displacement is deduced to be -0.016 mm^{-1}, while sensitivity per unit 1 N load is -0.313 N^{-1}. The sensor is verified to be capable of detecting the magnitude and direction of the multidirectional load.

Chapter 6 summarizes the result of this study.

ACKNOWLEDGEMENT

First, I must give my high, respectful gratitude to my supervisor, Prof. Dr. Norihisa Miki for his guidance, supervision and help throughout this project. I have learned a lot throughout my seven years in Miki Laboratory, with many challenging yet valuable experiences in order to complete this task.

I would like to thank the members of Miki Laboratory from 2011 to 2017, for their guidance and support in fabricating the device for this project, in writing thesis and journals, in assisting me in my studies and improving my Japanese language skills, as well as in conducting my daily life in Japan. I also should like to express my gratitude to Ms. Iza Husna for her help and guidance in designing the measurement systems for my project. My deepest appreciation also goes to Assoc. Prof. Dr. Kenjiro Takemura, Assoc. Prof. Dr. Hiroaki Onoe, and Assist. Prof. Dr. Takeo Kato for their guidance in writing this dissertation. I am indebted to Mr. Akira Kikuzumi for his advice and support during the toughest time in my life. It has been great to know all of them during my time in Keio University.

I would like to express my eternal appreciation towards my parents, Mr. Ahmad Ridzuan and Mrs. Rusidah, and all my family members who have always been there for me no matter where I am and what condition I am in, for all their prayers, unconditional love, supports and patience. I am also indebted to my dear husband, Mr. Muhammad Hisyam for his beautiful heart and kind words, and for always being by my side lending ears and shoulders. I wish to thank all of them for being ever so understanding, tolerant and supportive.

Not to forget, I should like to acknowledge my very real debt to my sponsor, MARA Education Foundation (Yayasan Pelajaran MARA, YPM) of Malaysia for choosing me to receive the scholarship for Malaysia Japan Higher Education Program (MJHEP) for three years of my PhD studies. I would also like to thank Keio Leading-Edge Laboratory (KLL) of Science and Technology for providing three years of research grants, and Keio University for Research Encouragement Scholarship (研究のすゝめ奨学金) that I received during my third year of PhD studies. Finally, thanks to those involved in this project directly or indirectly. May their lives be showered with a lot of blessings.

Nurul Adni Binti Ahmad Ridzuan
Feb. 2019, Kusatsu, Shiga, JAPAN

For my parents,

Mr. Ahmad Ridzuan Mohd Noor

&

Mrs. Rusidah Mat Ibrahim

TABLE OF CONTENTS

LIST OF TABLES

CHAPTER 1

CHAPTER 5

CHAPTER 6

APPENDIX

LIST OF FIGURES

CHAPTER 1

CHAPTER 2

CHAPTER 3

CHAPTER 4

CHAPTER 5

APPENDIX

1

INTRODUCTION

1.1 Tactile Sensors

The widespread usage of smartphones introduces tactile sensor to the public, initially to the professionals who used them as personal digital assistant (PDA) in 1990s [1], and finally now to even infants for their interactive learning and digital playgrounds. It is not something strange if we own at least a thing that is equipped with tactile sensor nowadays. Besides for touch screens and panels, tactile sensors were also used in other industries, such as robotics, automobiles, and medical industries.

This dissertation reports about design and fabrication process of a tactile sensor for multidirectional force detection. The tactile sensor ability to distinguish the direction of force is crucially needed especially in medical industries, where medical imaging modality is recently exploited widely. Usage of tactile sensor is important especially in surgery. Nowadays, minimally invasive surgery (MIS) procedure is more preferred compared to the conventional open surgery due to the simple procedure and less recovery time. Tactile sensor for multidirectional force detection can be installed in endoscope or catheter for more accurate operation process during MIS. Other than medical industries, this kind of tactile sensor is also demanded in robotics industries. Flat, flexible tactile sensor might be needed to be applied as

robot skin, but the joints and legs of small robots need small, non-flat tactile sensor to guide its movement. Inspired by the sensitivity of a tooth which can sense direction of load applied to it precisely, a tactile sensor was developed using strain gauges.

1.1.1 Functions of Tactile Sensors

Research about tactile sensors had been done from decades ago [2]–[6]. Tactile sensors are installed to a lot of equipment and appliances, e.g. in machines factories, in medical appliances, artificial skin, touch panels for entertainment, etc. Each application requires its own special needs, for example, touch panels require tactile sensor for a light touch, but for an elevator door to operate its safe operation to not sandwich people between the automatic door, the sensor must need something different from what has been installed in a touch panel. Below are several types of tactile sensor that had been developed [7]. A tactile sensor that had been developed might has only one function, but there are also sensors that were designed to measure more than one variables [8].

1) Pressure sensor

Pressure sensor was firstly recognized as touch sensor, where the sensor only detects whether the 'touch' exists or not, but later researchers started to develop sensors that can distinguish the 'amount of touch' – or we call it load or pressure in the measurable way – that was received by the transducers [7]. That is why tactile sensor is commonly referring to pressure sensor. Pressure tactile sensor are generally built to detect pressure from vertical normal direction, but recently research on 3-axis pressure detection are actively done [9]–[12]. There are several ways that can be used in detecting the amount of pressure such as electrical way and optical way. This topic will be discussed in the section 1.1.2.

2) Slip sensor

Slip sensor is the sensor that detects relative slip displacement and speed between objects and the sensor itself. Some sensors that were developed also detect the very first few μm of slip just before the slip itself even happen. Slip perception is inevitable especially in developing robot's hand [13], [14]. For example, in holding fragile objects such as eggshells and glass, pressure from hand has to be as small as possible to avoid cracking. But, the lack of

pressure in holding objects will make the objects slip from the grip. Installing slip sensor in robot's hand will be one of the solutions for this problem.

3) Hardness perception sensor

Recently, research on hardness perception sensor has caught a lot of attention because of its demands to be applied in medical field [15]–[18]. Hardness perception sensor is a sensor that distinguish objects' hardness and softness. In medical field, hardness discrimination is inevitable especially in distinguishing tissues' properties. Researchers are developing sensors to measure hardness in several ways. For example, some sensors measure hardness and softness of an object by indentation, while some sensors are using vibrations to measure the change of frequency when the sensor is touched by the objects.

4) Texture perception sensor

Surface texture includes roughness and smoothness of an object. Texture perception sensors are usually developed to distinguish these characteristics of objects' surface. Surface texture perception sensor are widely used in designing robot finger and artificial skin. Texture perception usually measured statically, i.e. by indentation, or dynamically, where tactile perception sensor is slid along the surface of an object, and the frequency difference are measured and analyzed to distinguish the roughness or softness of the object's surface[19]–[21].

5) Thermal sensor

Thermal perception is one of the most important characteristics to measure in having safe interaction between human and environment. One example of thermal sensor that had been developed is by combining heat generating layer to the temperature sensor, and the thermal conductivity was measured during contact [22]. Another example is by measuring heat transfer speed using heat flux sensor [23].

1.1.2 Detection Mechanisms

In the previous section, the types of tactile sensor according to their functions are listed and discussed. One of the most developed type is the pressure tactile sensor. Pressure sensor could be defined as the transducer that measure the pressure or load distributions that act between an object and the contact surface. Pressure will cause deformations and distortions of the object and the contact surface, so basically a pressure tactile sensor detects the deformations and defines it in a measurable way. There are several ways of transduction principles and mechanisms that can be applied to pressure sensors. Listed below are some mechanisms that had been used to build pressure tactile sensors.

1) Piezoresistive pressure sensing

Piezoresistivity could be defined as the change of electrical resistivity of a resistor due to the application of mechanical strain. Piezoresistive tactile sensor was among the ones that frequently developed because of its simple structure and mechanism. There are two types of piezoresistive pressure sensing mechanisms, i.e. strain gauge mechanism and nanocomposite mechanism.

Strain gauge sensors are usually in the form of cantilever with a metal zig-zag shaped strain gauge fixed at the anchored side of the cantilever (Figure 1.1 (a)). Sometimes, the cantilever itself acted as the strain gauge (Figure 1.1(b)). The principle of piezoresistive effect was exploited to detect the pressure applied on the device. Piezoresistive effect usually occurs in conductors, such as metals, and semiconductors, like silicon (Si). Normally, the electrical resistance of a material is related to the length, L and cross-sectional area, A of the material. The relationship is shown in equation 1.1, where R is the resistance of the material, ρ is the resistivity, L is the length and A is the cross-sectional area.

$$R = \rho \frac{L}{A} \qquad \text{Eq. 1.1}$$

When load is applied on a material, the dimension of material will change, as depicted in Figure 1.2, and the ratio of the change to the initial dimension is called strain. The relation between stress (σ) and strain (ε) is shown in Hooke's Law, as in equation 1.2.

$$\sigma = \frac{\Delta L}{L} E = \varepsilon E \qquad \text{Eq. 1.2}$$

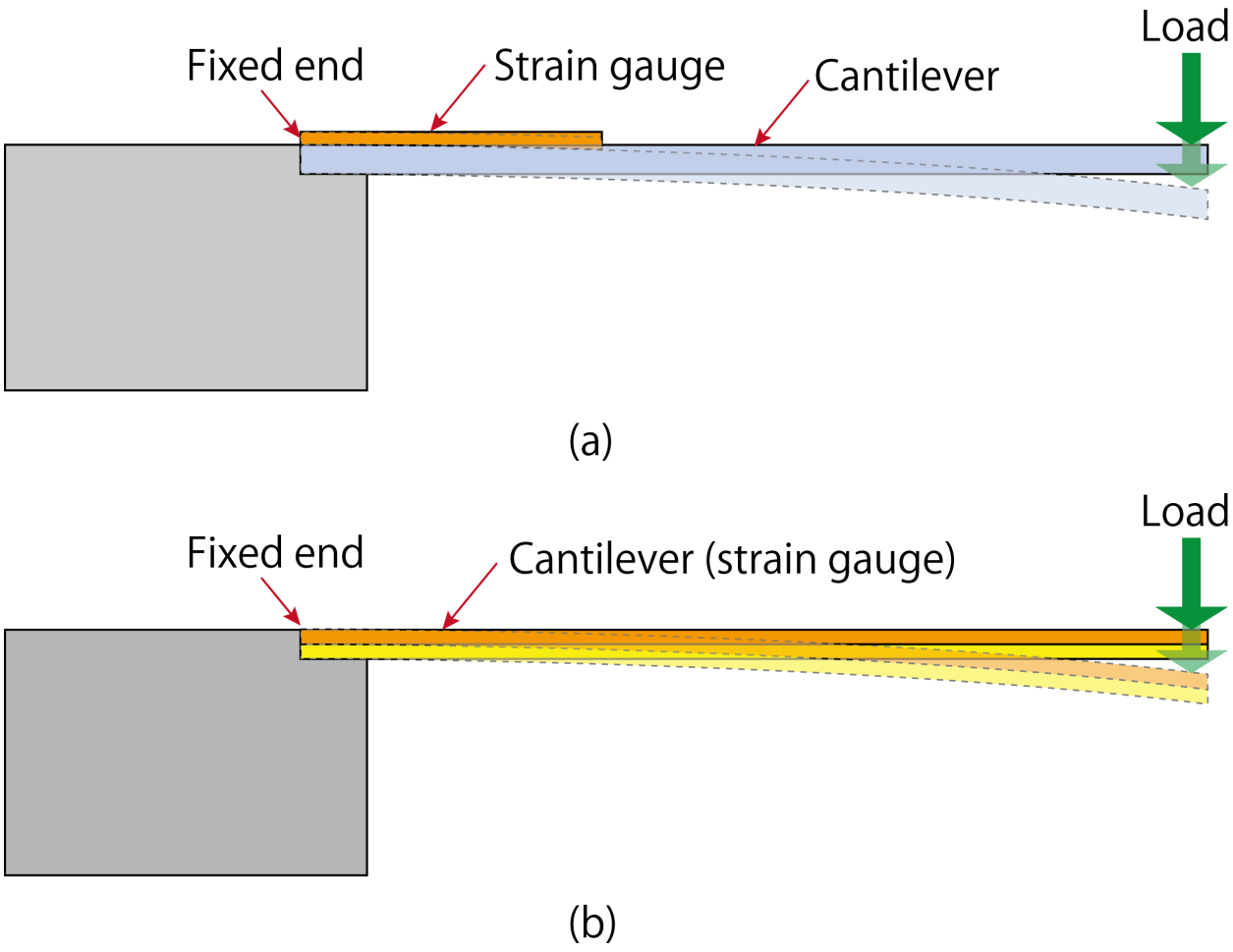

Figure 1.1 Cantilever type pressure sensor (a) with strain gauge attached at the top, and (b) the cantilever itself as strain gauge

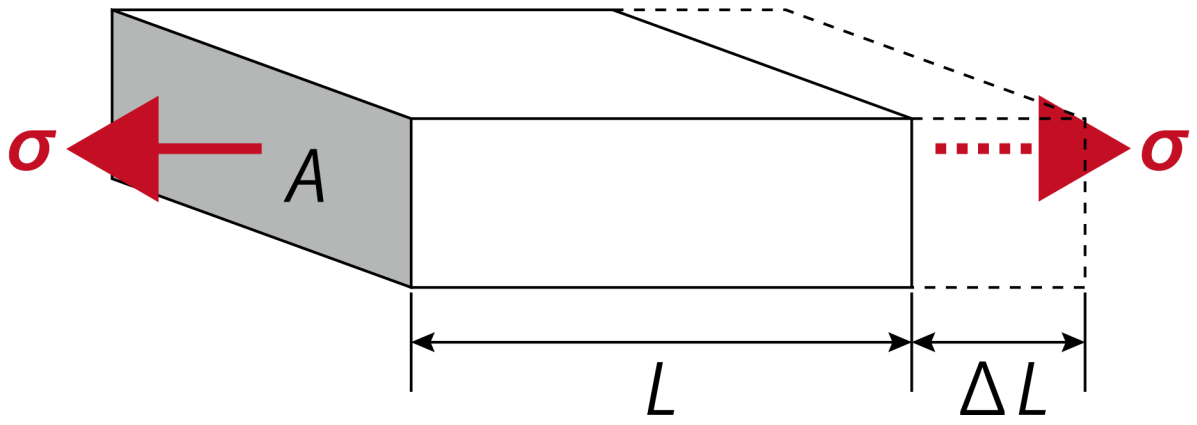

Figure 1.2 Change of length of a material with applied stress

Here, ΔL is the change in length and E is the modulus of elasticity, or also known as the Young's modulus of the material. In a piezoresistive material, as mentioned before, the change in the dimension of the material will cause the resistance to change. The relation of these variables is presented in equation 1.3.

$$\frac{\Delta R}{R} = G\frac{\Delta L}{L} = G\varepsilon \qquad \text{Eq. 1.3}$$

Here, ΔR is the change in resistance, and G is gauge factor of the material [24]. Substituting equation 1.2 into equation 1.3, the relation between the change of resistance ΔR and stress σ can be written as follows.

$$\Delta R = GR\frac{\sigma}{E} \qquad \text{Eq. 1.4}$$

In the field of microelectromechanical systems (MEMS), improvement of the accuracy of the piezoresistive strain gauge sensor usually focus on the material [25]–[28] and the design of the force conducting media [9].

Nanocomposite piezoresistive sensors were made of nanoscale conductive fillers that are embed in soft polymer matrices. When pressure is applied to the nanocomposite material, the soft, elastic polymer will be compressed, and the filler distributions become ununiformed and dense. This makes the electrical resistance decrease. On the other hand, when pressure value is decreased, the filler distributions will be sparser, and the electrical resistance will

increase. The structure of the nanocomposite sensor type is shown in Figure 1.3. While polydimethyl siloxane (PDMS) is the most used soft polymer matrix to make the composite [29], research on the filler includes using metal-based particles such as silver (Ag) [30] and nickel (Ni) [31], and also carbon-based particles such as carbon black [32], graphene [33], and carbon nanotubes (CNTs) [34], [35].

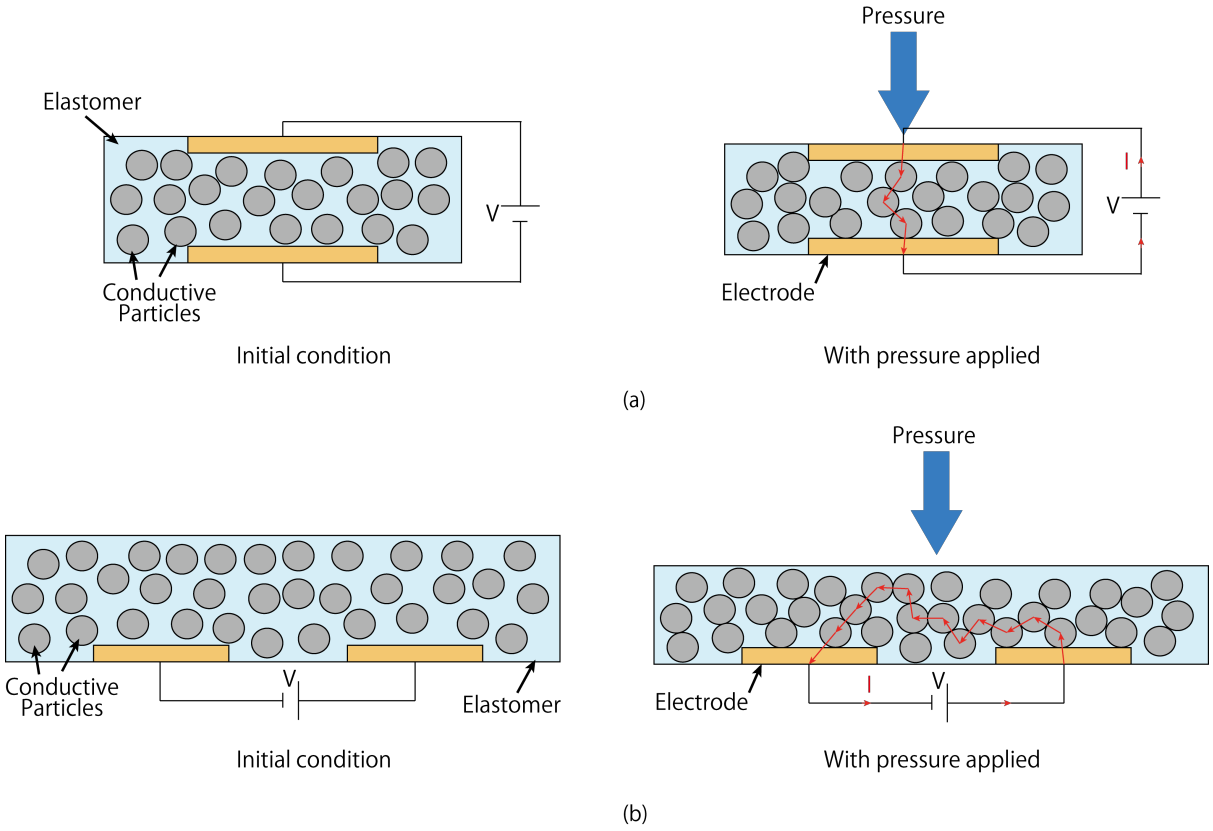

Figure 1.3 Principle of composite type sensor, before and after pressure application. (a) shows composite with parallel electrodes, while (b) shows composite with one-sided electrodes

2) Capacitive sensing

Capacitive sensor uses the principle of a capacitance to operate. The capacitance of a capacitor, C could be defined in the equation below

$$C = \varepsilon_0 \, \varepsilon_r \, \frac{S}{d} \qquad \text{Eq. 1.5}$$

where ε_0 is vacuum permittivity with a constant value of 8.854×10^{-12} $C^2N^{-1}m^{-2}$, ε_r is the relative permittivity of dielectric, d is the distance between two electrodes, and S is the effective surface area. Capacitive pressure sensors are usually built by manipulating the distance between two electrodes, d (Figure 1.4) or the effective surface area S (Figure 1.5).

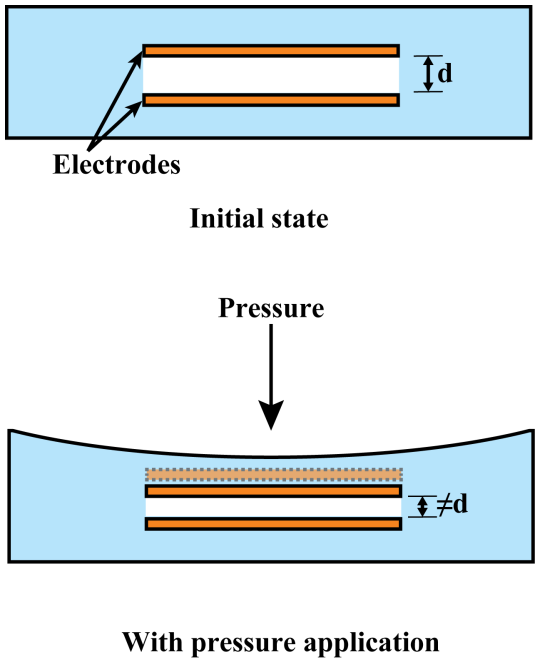

Figure 1.4 Principle of capacitive pressure sensor with change in the distance between two electrodes during pressure application

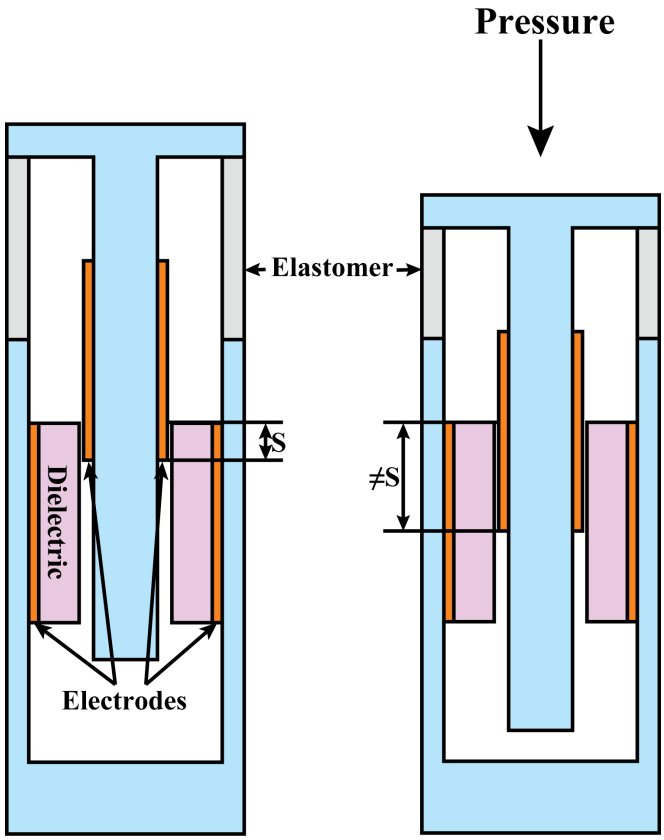

Figure 1.5 Principle of capacitive pressure sensor with change in the effective surface area during pressure application

Research on developing capacitive tactile sensor are now focusing on the dielectric materials [11], [36], [37] or the design of electrodes [11], [12] to increase the sensitivity of the sensor and for a better design in miniaturizing the sensor device. For the former type, flexible silicon elastomer namely PDMS is one of the most used materials to be the dielectric material of capacitive pressure sensor due to its obvious flexible properties [36], [38], besides the characteristic of human tissue friendly and biomedical compliance [39], [40]. Not only the material, there are also researches on the design and shape of the PDMS dielectric that were done to increase the sensitivity of the sensor. Among that were developed are V-shaped grooves and pyramids dielectrics [11], [41], [42]. Besides, there are also other material that the researchers are now eyeing to such as air [43], liquid [37], and nano needles [44]. Researches on the latter type of the sensor focus on the design of the electrodes [45] to increase the accuracy and sensitivity of the sensor, and also the material [12] to suit the needs of the sensor design.

3) Magnetic sensing

The working principle of magnetic tactile sensor is very much similar to the capacitive tactile sensor, except the measurable variable is obviously not the capacitance. There are several types of magnetic tactile sensor according to the measured variables. Among the most frequently developed are the one that measures magnetic flux or magnetic field intensity. These types of sensor utilize Hall effect [46] or giant magneto resistance (GMR) [47] to measure the aforementioned variables. The principle is as depicted in Figure 1.6. Force applied to the sensor will swift the position of the permanent magnet. Then, the change in the magnetic field vector will be measured by the Hall sensor.

There are also sensors that utilize the principle of Faraday's law of induction to measure the change in electromagnetic induction. Changes in magnetic flux will cause the change in induction voltage value [48]. One of the examples for this principle is shown in Figure 1.7. When load is applied on the sensor device, the distance between the detection coil and the excitation coil decreases, causing the change in voltage generated by the detection coil. The voltage change was related to magnetic field produced by the excitation coil that was located beneath the detection coil [49].

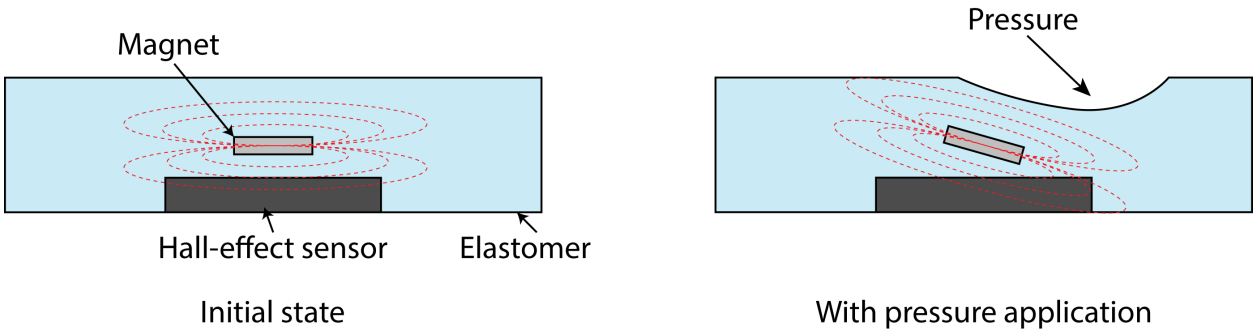

Figure 1.6 Principle of magnetic sensor with Hall-effect sensor. Figure shows the sensor in the initial state (left) and shift of magnetic field during pressure application (right).

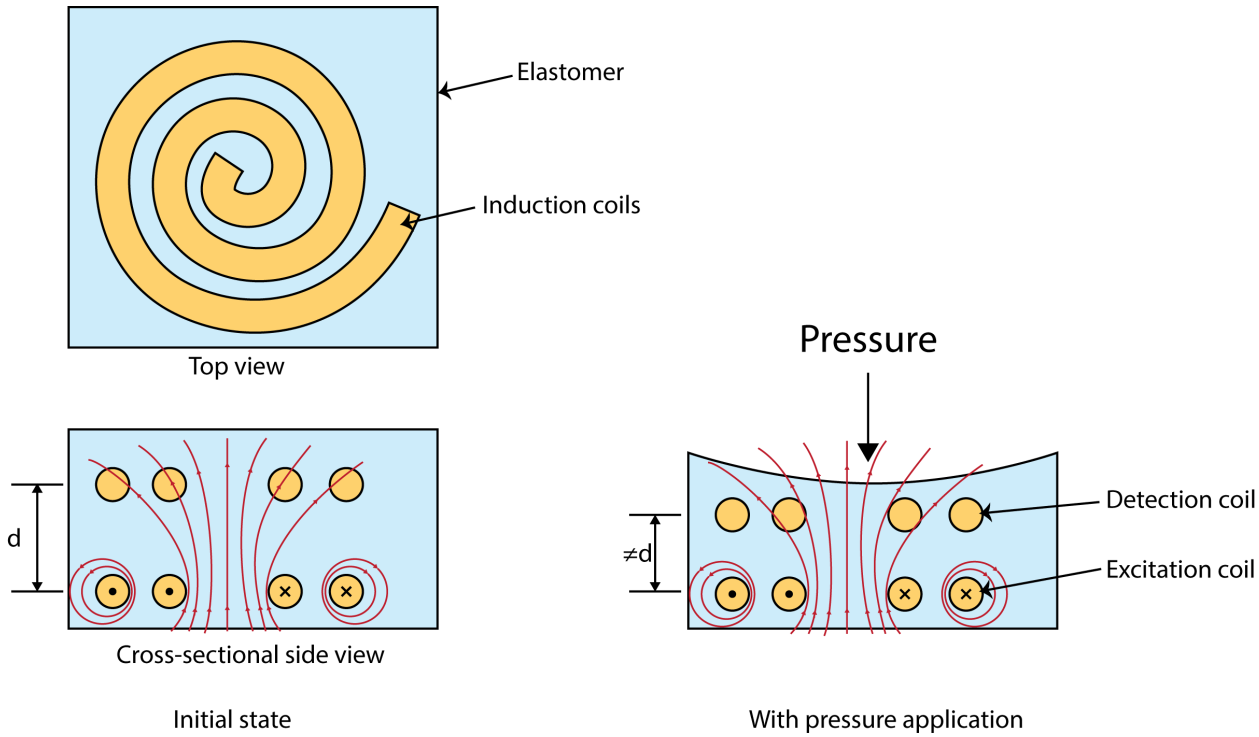

Figure 1.7 Principle of magnetic sensor with change in the distance between excitation coil and detection coil during pressure application. Change of distance between both coils will cause change in voltage generated by detection coil.

4) Piezoelectric sensing

Piezoelectricity is a property of a material to generate electricity in response to mechanical stress applied to it, as shown in Figure 1.8. The most common material that is used to develop piezoelectric tactile sensor is polyvinylidene fluoride (PVDF) [50]–[52] due to its flexible and lightweight properties. Piezoelectric tactile sensors are commonly applied to dynamic environments because the charges that are generated are usually dissipate very quickly. Besides its application in detecting dynamic pressure, piezoelectric tactile sensors are also suitable to be used in shape and texture discriminations [53].

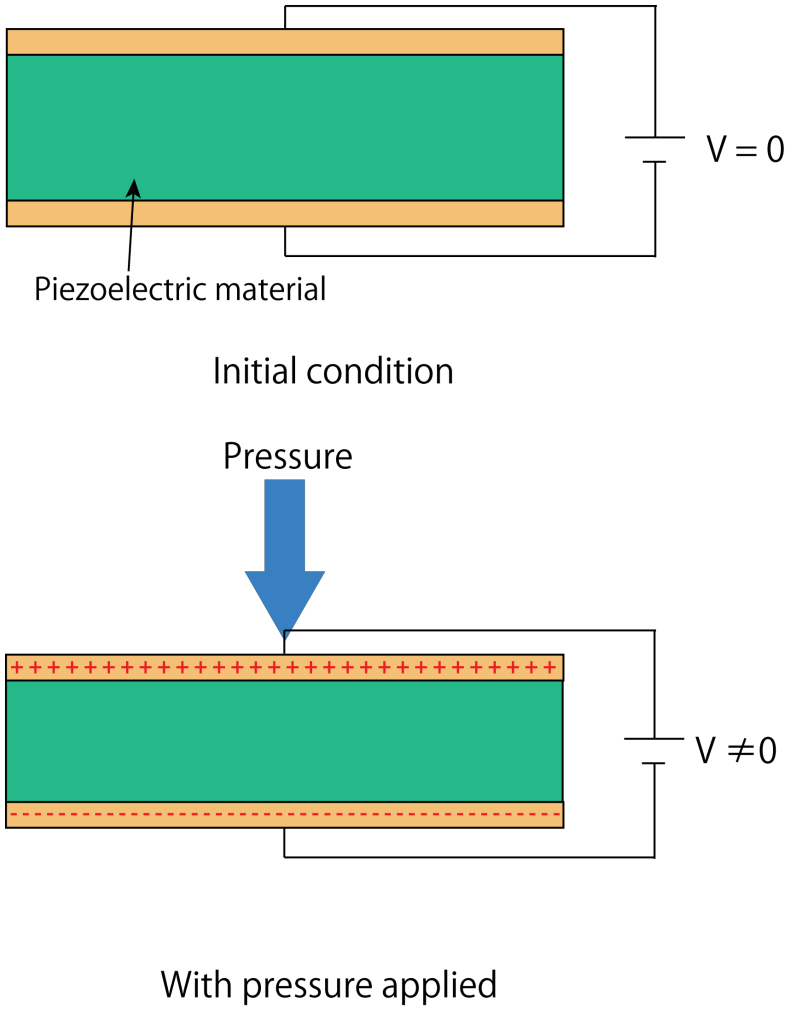

Figure 1.8 Principle of piezoelectric pressure sensing. Above is the piezoelectric material in initial condition, and below is the state during pressure application.

5) Optical sensing

In optical tactile sensor, optical fibers are typically utilized to transmit light, and then the changes in output light are then measured and analyzed to detect the tactile information. There are several principles that are used to tactile sensors. Among them, light intensity modulation and fiber Bragg grating (FBG) are the ones that are frequently used.

In the former principle, when pressure is applied to the sensor, the bending of the light fiber cause changes of the light intensity at the transmission side and output side of the fiber [54], [55]. Tactile information is then collected by evaluating the light intensity properties. The latter principle measures wavelength shifts that cause by external strain instead of light intensity [56]–[58]. The principles of optical sensing are shown in Figure 1.9 and Figure 1.10.

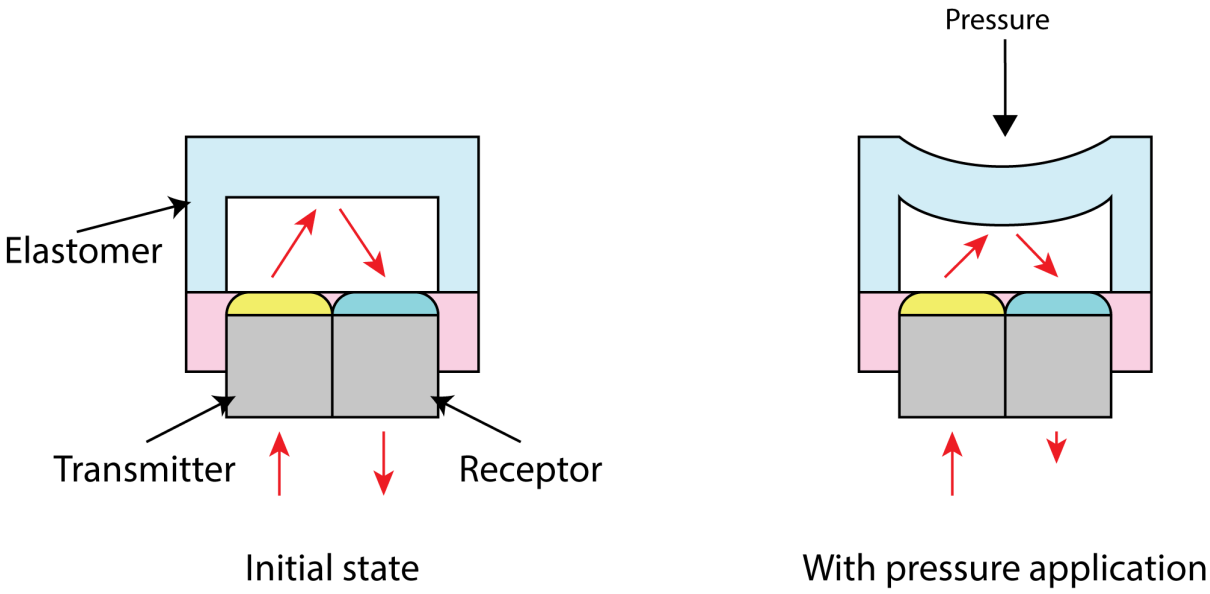

Figure 1.9 Principle of optical sensor with light intensity modulation. Figure on the left shows the sensor in initial state, while figure on the right shows the sensor during pressure application.

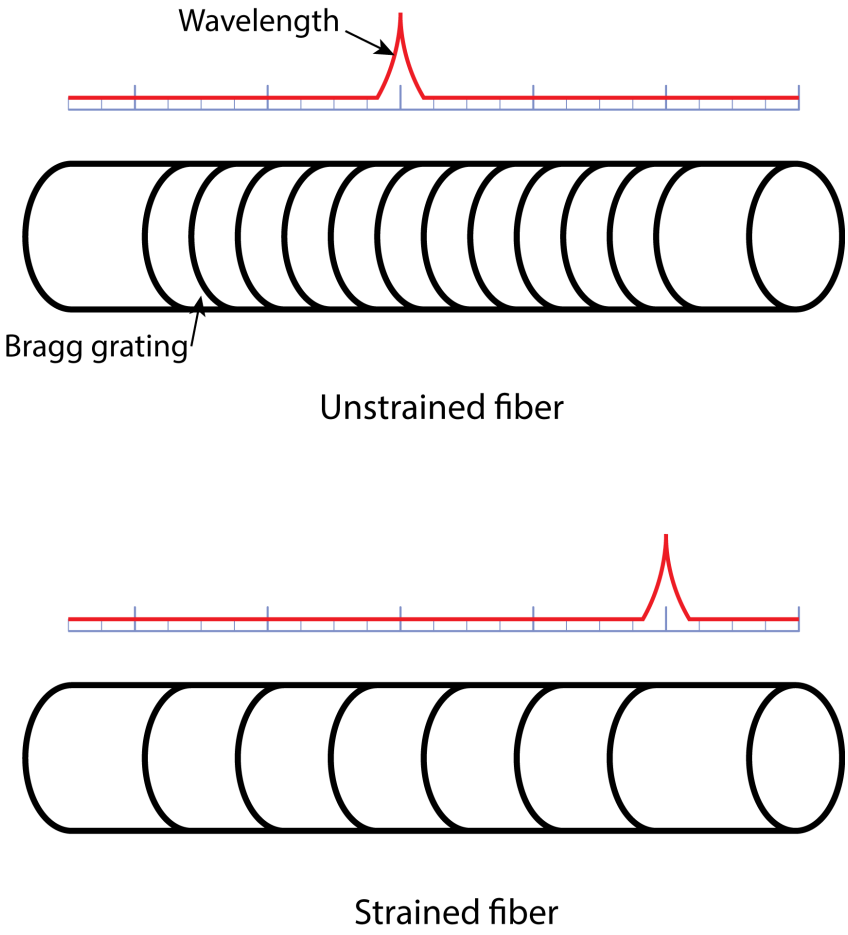

Figure 1.10 Mechanism of fiber Bragg grating, with the wavelength shift in strained fiber

Table 1.1 summarizes the pros and cons of each sensing mechanism [59].

Table 1.1 Pros and cons of detection mechanisms of pressure tactile sensor

Detection mechanism	Pros	Cons
Piezoresistive	• Simple fabrication process • High spatial resolution • Low cost	• High power consumption • Hysteresis
Capacitive	• Good sensitivity • High spatial resolution • Temperature independent	• High noise • Cross-talks • Complex measurement circuit • Hysteresis
Piezoelectric	• Good sensitivity • High dynamic range • High frequency response	• Dynamic sensing only • Charges leakage • Poor spatial resolution
Magnetic	• Good sensitivity • High dynamic range • High power output	• High power consumption • Low frequency response
Optical	• Wide sensing range • High spatial resolution • Good reliability	• Vulnerable to temperature change • Not flexible • Bulky in size

1.2 Bio-inspired Tactile Sensors

There is no bigger reason for researchers to design tactile sensor than to mimic the function of the skin. The function of the skin – here let's be specific to human's one – is not only limited to ensure our internal organs are safe and we don't look creepy with all the muscles, bones and arteries exposed, but also to provide one of the most important sense to guarantee better living: the sense of touch. The broad variety of 'sense of touch', i.e. differentiation of pressure, location and temperature was firstly recognized by a psychologist named Weber in 1846. His essay titled "Touch and Common Sensibility" attracted researchers to dig the information about this particular sense deeply and finally they added one more sense variation, namely pain [60].

1.2.1 Anatomy of the Skin

Human was said to have the sense of touch as early as six weeks old inside the mother's womb [61]. The formation of the skin includes three layers, specifically, from the outermost side, epidermis, dermis, and subcutaneous tissue. There are two types of the skin; i.e. the glabrous skin, or also known as hairless skin, which located at the lips, palm, and feet, and the hairy skin which covers the entire human body except the areas with the former skin type.

The skin can sense light touch, pressure, vibration, temperature and pain due to the existence of receptors. Touch receptors exist not only at the skin, but also in other organs such as tongue and the entire oral cavity [62], [63], surround the teeth [64], [65], and in internal organ such as pancreas [66], [67]. These receptors receive stimuli from the environment and translate them to informative nerve impulses. The impulses then are sent via the nerves to the central nervous system and finally to the brain to be recognized. The types of receptor that specifically senses temperature difference is called thermoreceptors, and the ones that senses pain is nociceptors. These types of receptors are in the form of free nerve endings. However, the main part of the discussion to be focused on here is the ones that can sense different type of touch; i.e. pressure, vibrations, soft touch, etc. they are called the mechanoreceptors. The types and locations of these receptors is illustrated in Figure 1.11.

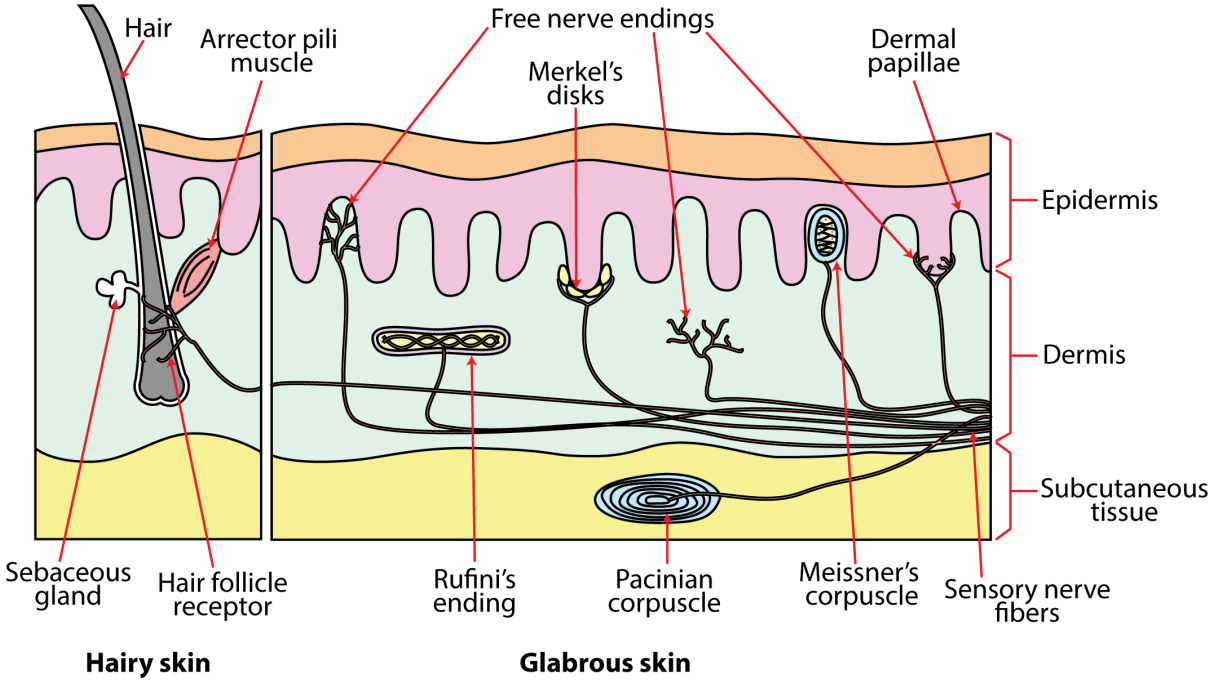

Figure 1.11 Location of tactile receptors beneath the surface of the skin

The function of the mechanoreceptors is to recognize shape, form, and spatial nature of an object. The glabrous skin has more sensitive mechanoreceptors than the ones in hairy skin, bur hairy skin has one more touch receptor that associate with the hair, i.e. hair follicle receptor. There are four major types of mechanoreceptors in the somatosensory system; i.e. Meissner's corpuscles, Pacinian corpuscles, Merkel's disks, and Ruffini's endings. These mechanoreceptors are responsible in receiving and recognizing tactile stimuli such as pressure, friction, roughness, softness, hardness, stickiness, etc. [68]–[76].

These four types of mechanoreceptors can be divided into two categories according to how they function in receiving stimuli from the environment: the rapidly-adapting (RA) receptors and the slowly-adapting (SA) receptors. The RA receptors, namely the Meissner's corpuscles and the Pacinian corpuscles, adapt quickly to the stimuli. It means that they respond at the beginning they sense the existence of the stimuli, and then rapidly remove the action potential generated by the stimuli. This function is important in adapting continuous stimuli, such as the ones that our shirts give to our skin. Pacinian corpuscles are sensitive to skin deformation caused by vibration, while Meissner's corpuscles are very sensitive to light touch. RA receptors concentrate especially at the sensitive areas of our body such as fingertips and lips [77]–[79].

On the other hand, SA receptors, i.e. the Markel's disks and the Ruffini endings, are the ones that keep responding until the stimuli are removed. The function of these type of receptors are to differentiate light pressure and discriminate static touch especially in determining shape, edges, and rough texture [80]. The presence of SA receptors makes us aware of stimuli that we have to respond to, for example in gripping objects so that they do not slip, and for the blinds to read Braille.

Besides the categories that differentiate how the receptors respond to stimuli, there is one more category to define the mechanoreceptors; i.e. the location beneath the skin. The placement of these receptors determines the receptive field of the receptors, where deeper receptors will have larger receptive fields, and vice versa [81]. In this category, the first one is the Type I receptors that are located near the surface of the skin, at the dermal papillae ridges. Two kinds of mechanoreceptors that can be categorized as Type I receptors are Meissner's corpuscles and Merkel's disks. Other than the two is Type II receptors that located deeper at the dermis layer and subcutaneous tissue of the skin. Because of the large receptive fields that Pacinian corpuscles and Ruffini's endings have, it is observed that their concentrations beneath the skin are lower than those in the Type I category [82]. The details of the characteristics of each mechanoreceptor are summarized in Figure 1.12 [7], [83].

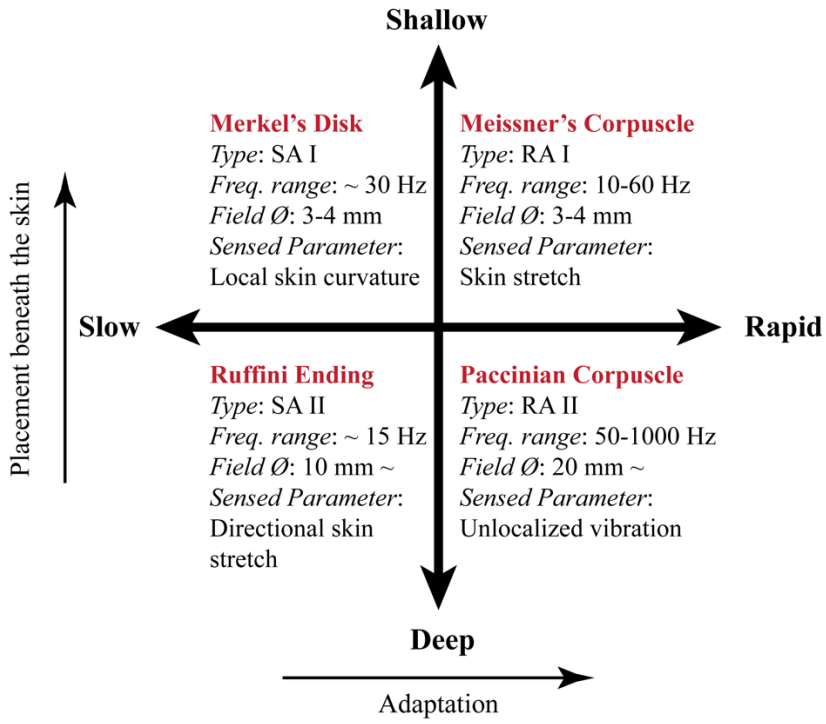

Figure 1.12 Characteristics of mechanoreceptors

1.2.2 Skin-inspired Tactile Sensors

Researchers all over the world are now taking the skin as an inspiration to design not only tactile sensor, but also other inventions [8], [84] for some features of the skin are proved to have significant effects on the skin's sensitivity to various kinds of tactile stimuli. Going through from the surface of the skin, to deep inside where the naked eyes could not see, there are special characteristics of the skin that support us to recognize light touch, pressure, vibration, slip, etc.

The surface of the palms and feet are different from other parts of our body because the existence of ridges. It is known that the pattern of the ridges is unique for each individual so that they are useful in one self's identification everywhere in the world, but actually their existence serves more than that. Research on mimicking the ridges to develop tactile sensor had been done several times to increase the sensitivity of tactile sensors in detecting shear force [85], discriminating curvatures of objects [86], and detecting objects' hardness and surface roughness [87].

The role of the hair to tactile sensing of the skin was not overlooked at as there are also sensors that were designed with almost the same features as the hair. Inspired by both hair and skin, there are tactile sensor that were built to sense wide range of tactile pressure, just like the hair which can detect small pressure and heavier forces would be sensed by the skin [88]. Not only human hair, vibrissae of mice and felines were also mimicked to some designs of tactile sensor as these whisker-like sensors are reported to be able to detect gas flow [89] and discriminate surface textures [90]–[92].

Right beneath the surface of the skin there lies the ridged dermal papillae, which seems like the sockets for epidermis-dermis connection. But for tactile sensor researchers, this 'socket' shape was an inspiration as tactile sensors were developed imitating the shape of dermal papillae to detect changes on object's shape surfaces [93], [94]. Going a slight deeper from the dermal papillae, there are distributions of tactile mechanoreceptors and free nerve endings, where tactile stimulations are detected and recognized, as explained in the previous section. Researchers are spurred by these various functions of mechanoreceptors, so they designed tactile sensor to detect various tactile stimuli, just like what the mechanoreceptors can do, such as pressure and temperature [95], and also sliding together with vibration [96]. Not stopping to only the mechanoreceptors, there are also effort to build the signal processing system of a tactile

sensor imitating the nerves that connects the mechanoreceptors to the central nervous system [97].

Besides the elements exists from the surface to deep below the dermis layer of the skin, the characteristics of the skin had inspired researchers to develop tactile sensor. One example is a flexible capacitive sensor developed with liquid as dielectric [37]. The main material of the sensor is a flexible silicon called polydimethyl siloxane (PDMS) that are elastic, just like the skin.

In this research, variation of the dielectric in between two conductive electrodes of a capacitor were studied to find the effect on the sensitivity of the pressure sensor. Contrary to the conventional capacitive sensor that used air [43] and solid materials [38]–[40] as the dielectric, in this research, two types of liquid have been used to fill the gap between two electrodes: i.e. deionized (DI) water and glycerin. Using these liquids as dielectric is expected to increase the sensitivity of the sensor device because the high permittivity values compared to air, which is 80 and 47 for DI water and glycerin, respectively, would increase the capacitance value of the sensing elements. Of course, there are solid materials that have higher permittivity values to be used, but the flexibility of the sensor device would be negatively affected if solid material is used as the dielectric.

The design of the sensor is illustrated in Figure 1.13. The pressure sensing concept is shown in Figure 1.14. The sensor was designed in 3×3 array of capacitive sensor elements. The sensor consisted of eight layers: bumps, top layer, top electrodes layer, top isolation layer, spacer layer, largely deformable PDMS layer, bottom electrodes layer, and bottom layer with escape reservoir. Most of the layers were made using the flexible and elastic PDMS membrane, except the electrodes and the largely deformable PDMS layer. The electrodes were made of copper on polyimide film, and the largely deformable PDMS was made using silicon based adhesive paste (Dow Corning® 3145 RTV MIL-A-46146 adhesive/sealant, Dow Corning Corp.). The function of each layer is summarized in Table 1.2.

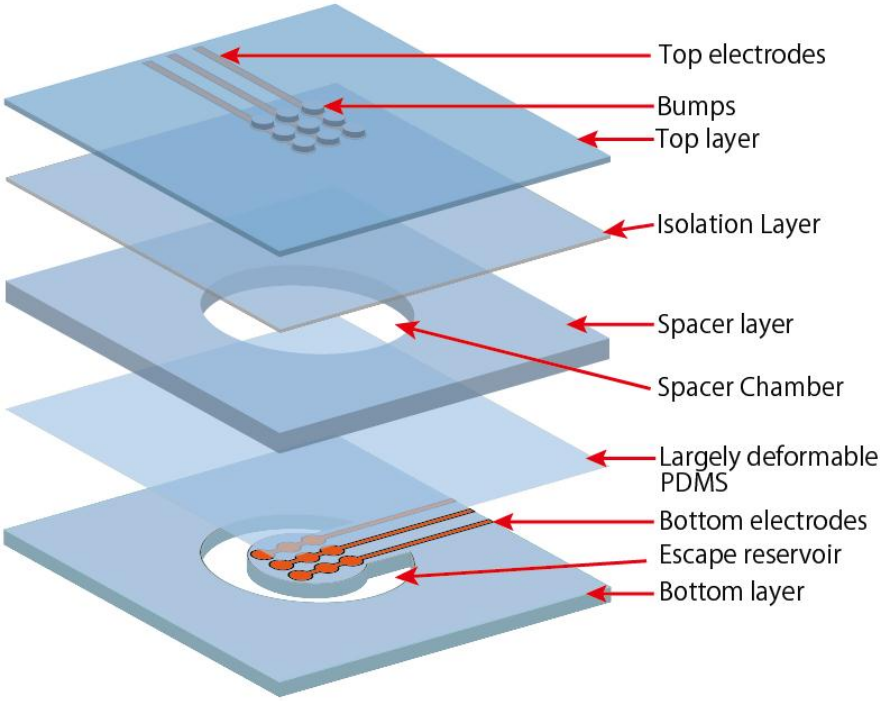

Figure 1.13 Design of capacitive sensor device in exploded view showing each layer

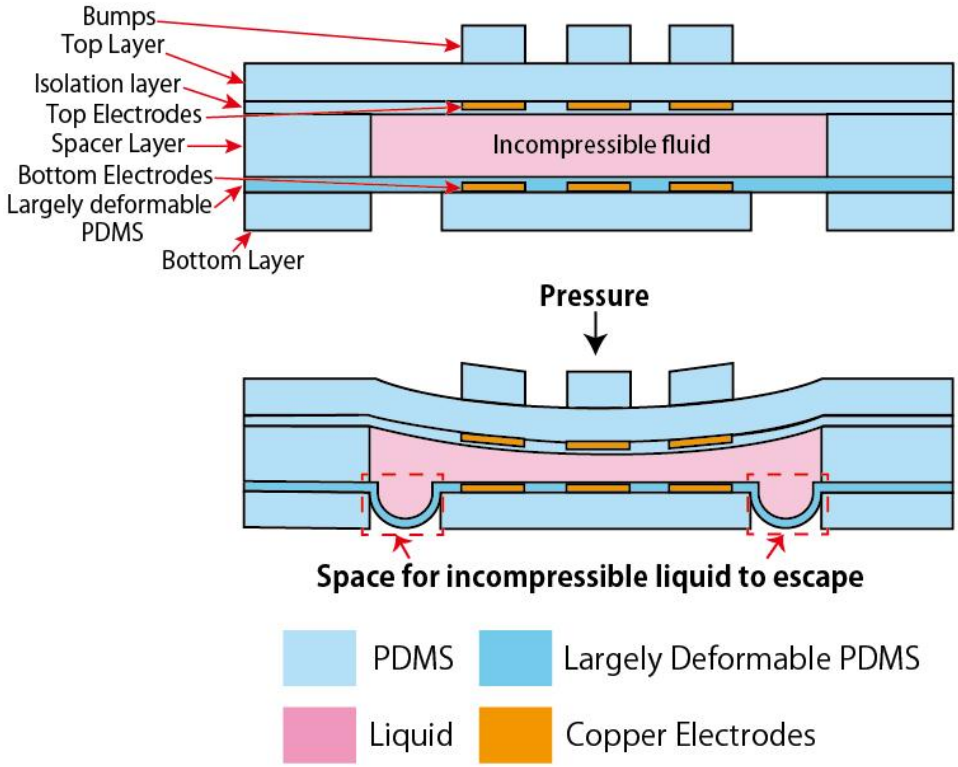

Figure 1.14 The cross-sectional view of the capacitive sensor device (top) and flowing-out of liquid from spacer layer during pressure application on the device (bottom)

Table 1.2 Layers of the capacitive sensor device with their respective functions

Layer	Function
Bumps	Enhancing the spatial resolution of the sensing element. Because the sensing elements were positioned in the inner surface of the device, the existence of bumps on the top of the device would be the indicator of the position of the electrodes in the device.
Top layer	Securing the top electrodes, while acting as the lid to cover the inner side of the sensor device
Top electrodes	As one of the electrodes for the capacitive sensing element
Isolation layer	As the cover for top electrodes, so that the top electrodes did not contact the liquid in the spacer layer directly. This is to prevent the oxidation of both liquids and electrodes.
Spacer layer	Chambering the liquids between two electrodes
Largely deformable PDMS layer	To allow the flow of the incompressible liquid in spacer layer to the escape reservoir without leakage outside the sensor device
Bottom electrodes	As one of the electrodes for the capacitive sensing element, the pair of the top electrodes.
Bottom layer	Supporting the bottom electrodes and the whole device. The escape reservoir for the liquids was also placed in this layer.

Prior work from the team in the same laboratory had designed the sensor with escape reservoir at the side of the sensing element array, as shown in Figure 1.15 [98]. This increased the size of the sensor device. Therefore, the idea of shifting the escape reservoir to the bottom layer of the sensor device has decrease the footprint of the device to 75%.

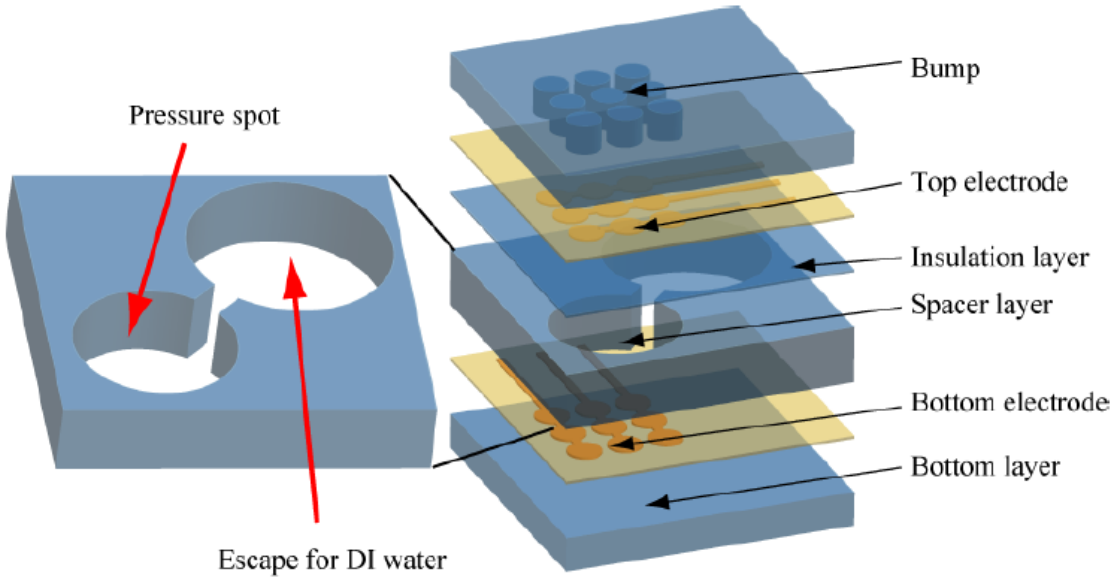

Figure 1.15 The design of the prior work of the capacitive sensor device with escape reservoir of the encapsulated liquid at the side of the liquid chamber

The device was fabricated mainly using photolithography process. The layers were made one by one, and then assembled to form top part and bottom part of the device. The parts were then bonded in the chosen liquid to encapsulate the liquid in the spacer chamber. The bonding process was called Bonding-in-Liquid Technique (BiLT) [99]. Details about the fabrication process are as follows:

1) Fabrication of layers made of PDMS

The layers that were made of PDMS were fabricated using soft-lithography technique. In this process, mold that represent the negative of the layer was made by patterning SU-8 2075 (Nippon Kayaku Co., Ltd.) with the thickness of 300 μm, on a glass substrate. The mold for the spacer layer, which was 500 μm in thickness, could not be patterned using the same material as the consistency of the SU-8 2075 liquid could not achieve that thickness when cured. Therefore, acrylic mold was made by machining process. PDMS (Silpot 184, Dow Corning Toray Co., Ltd.) was mixed well with the curing agent with the ratio of 10:1 in a plastic cup and placed in the vacuum desiccator for one hour or until all the air bubbles were dismissed. About 3 mL of the PDMS was then poured on the mold and spin-coated to get the desired thickness. After that, it was baked on a 100°C hotplate until hardened. After the PDMS membrane was cooled down to room temperature, the PDMS layers were released from the molds and the unnecessary parts were cut using a knife cutter. The process was illustrated in Figure 1.16.

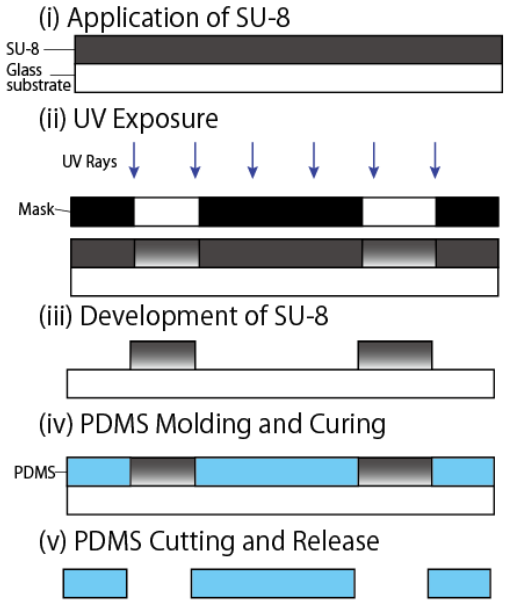

Figure 1.16 Fabrication process of PDMS layers using soft-lithography process

2) Fabrication of the largely deformable PDMS layer

As mentioned above, this layer was made using silicon based adhesive paste (Dow Corning® 3145 RTV MIL-A-46146 adhesive/sealant, Dow Corning Corp.). The paste was mixed with thinner (RTV Thinner, Dow Corning Toray Co., Ltd) in a plastic cup. The ratio of the mixture is 2 mL of thinner with every 1 g of the silicon elastomer paste. The mixture is then put in vacuum desiccator for about 30 minutes, or until all the air bubbles were dismissed. If the mixture of largely deformable PDMS was directly spin-coated on the glass substrate, the largely deformable PDMS layer would get adhered to the glass substrate too strongly. To resolve this problem, layers of amorphous fluoropolymer CYTOP were spin-coated on the glass substrate beforehand, so that the adhesion would be attenuated and the largely deformable PDMS layer would be easily released from the glass substrate. CYTOP type S (CTX-809SP2, Asahi Glass Co., Ltd.) was usually used as a release material, but as it has the non-adhesion characteristic, CYTOP type M (CTL-809M, Asahi Glass Co., Ltd.) that had been mixed with the solvent (CT-Solv. 180, Asahi Glass Co., Ltd.) with a ratio of 1:100 was firstly spin-coated on the glass substrate as the adhesion primer to enhance the adhesion between CYTOP type S and the glass substrate. The silicon elastomer paste was then spin-coated on the CYTOP layers. The film was left to harden at room temperature for 24 hours. The process was illustrated in Figure 1.17.

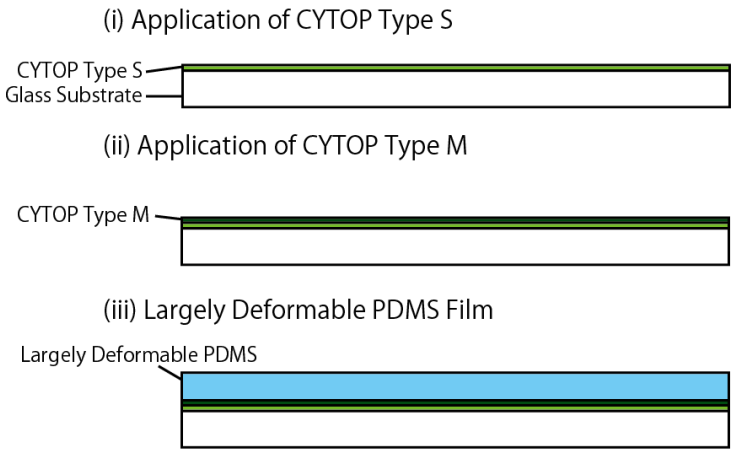

Figure 1.17 Fabrication process of the largely deformable PDMS layer

3) Fabrication of top and bottom electrodes

Adhesiveless polyimide copper clad laminate with 25 μm thick of polyimide film and 18 μm thick of copper layer (ESPANEX MC18-25-00FRFM, Nippon Steel Chemical Co., Ltd.) was used as the electrodes for this device. The details of electrodes patterning process are illustrated in Figure 1.18. AZ P4620 (AZ Electronic Materials K.K.), a positive type photoresist was used to pattern the copper electrodes using photolithography process.

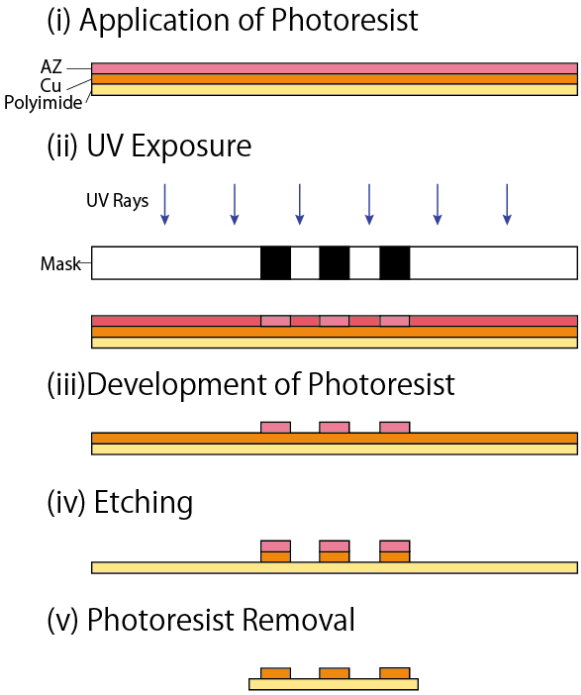

Figure 1.18 Fabrication process of the electrodes using photolithography and copper etching process

4) Bonding of the layers

Bump and top layer, copper electrodes films, spacer layer, largely deformable PDMS layer, and bottom layer had to be bonded together to complete the device fabrication process. The bonding processes consisted of two main steps; bonding using soft-etching technique to form top part and bottom part of the device, and BiLT to bond both parts together while in the same time encapsulating the liquid in the space chamber.

To bond bumps and top layer with copper electrodes film, and bottom layer with copper electrodes film, each layer was placed in the soft-etching chamber (SEDE-P, Meiwafosis Co., Ltd.) and was etched for 35 seconds. After the etching process was completed, the copper films were brought into contact with PDMS layers and cured on the 100°C hotplate for 3 minutes. The layers were then cooled-down to room temperature. For the spacer layer and largely deformable PDMS layer bonding, the process was just the same as mentioned above, but after the layers were cooled down to room temperature, the largely deformable PDMS layer was cut according to the spacer layer size and released from the glass substrate slowly. The bonded spacer layer-largely deformable PDMS layer and bottom layer-copper electrodes film were finally bonded together using the same process. The processes were illustrated in Figure 1.19.

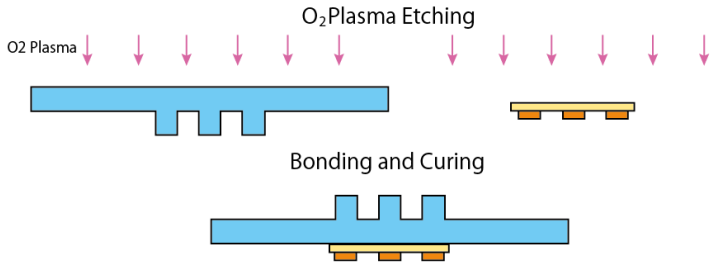

(a)

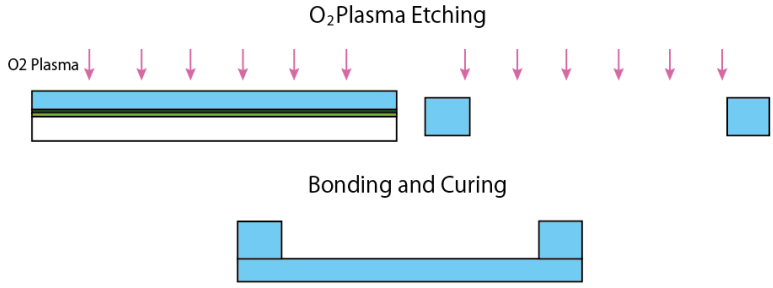

(b)

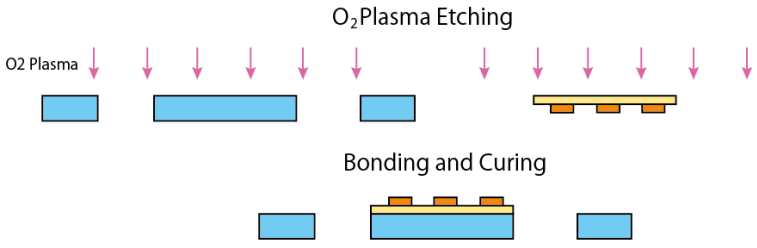

(c)

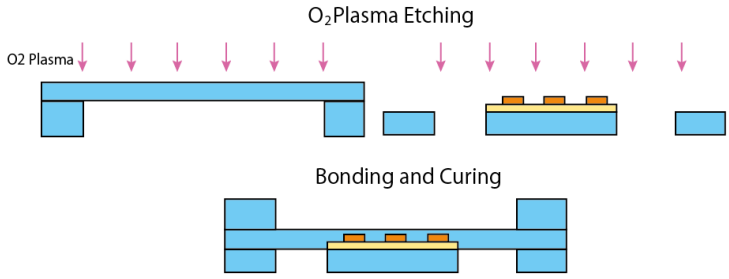

(d)

Figure 1.19 The bonding process of (a) the bumps and top electrodes, (b) The largely deformable PDMS layer and the spacer layer, (c) the bottom layer and bottom electrodes, and (d) the layers in (b) and (c)

To perform the BiLT, firstly, UV curing silicon resin (ThreeBond 3164, ThreeBond Co., Ltd) was spin-coated on a glass substrate. The silicon resin was then transferred to the spacer layer. The layers were then overlapped in the liquid and put on the mask aligner where UV rays were exposed. The details were illustrated in Figure 1.20.

The fabricated device was shown in Figure 1.21. The device was flexible and deformable as the material used exhibits those characteristics. Experiments were done to test the performance of the sensor device in the terms of sensitivity enhancement. For comparison purpose, a sensor device with the same design was made without liquid encapsulated in the spacer chamber as the control condition for the experiment. The space was left with air in between the two electrode layers for this control sample.

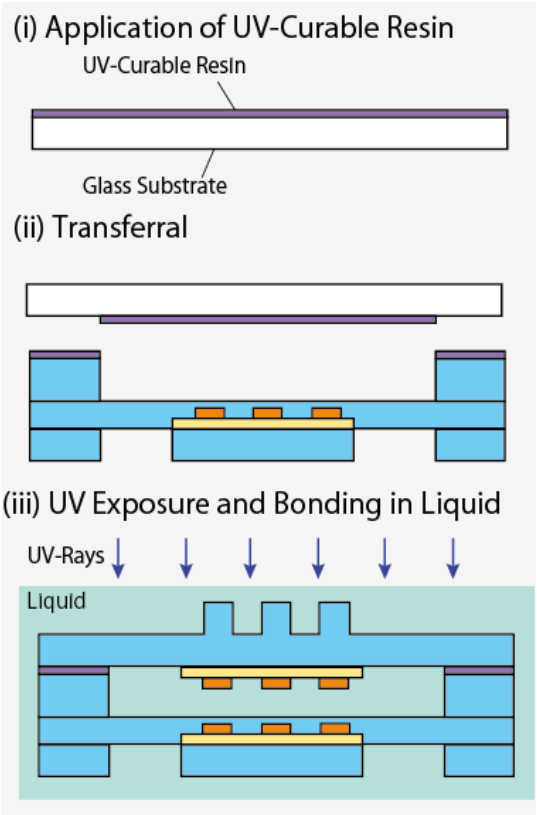

Figure 1.20 BiLT process

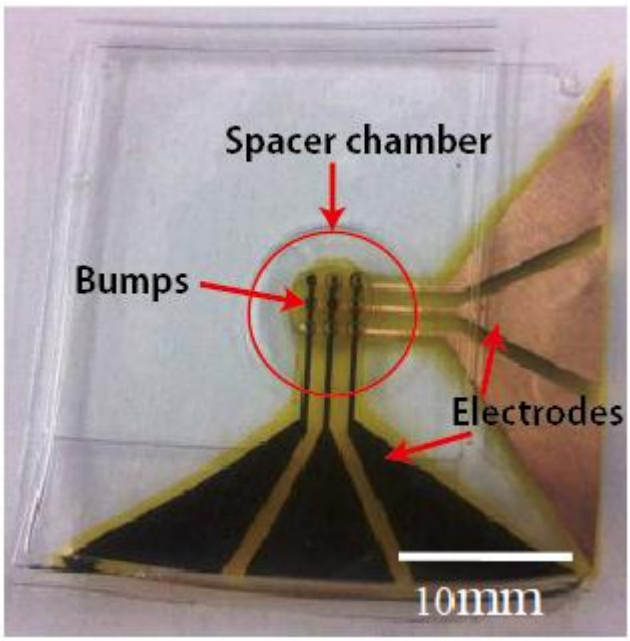

(a)

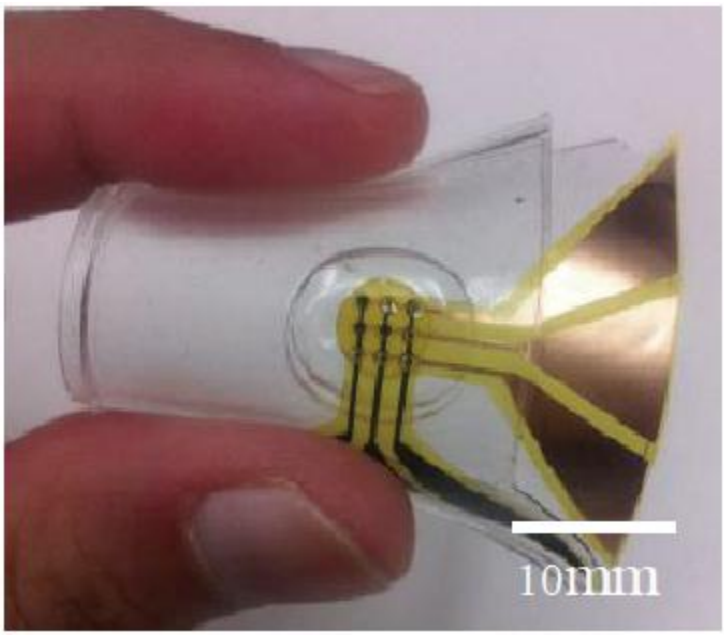

(b)

Figure 1.21 (a) The fabricated capacitive sensor device with liquid as dielectric, and (b) flexibility of the device

The experiment was done by applying normal force gradually to the bump of the middle sensing element of the device. The amount of force was controlled by the microstrength evaluation testing machine (Micro Autograph MST-I, Shimadzu Corporation), while at the same time, the capacitance values of the device were measured using a capacitance-to-digital converter (AD7746, Analogue Devices Ltd).

The result of the experiment is shown in Figure 1.22. There was no leakage of the liquid observed during the procedures of experiment. From the deformation test result shown in Figure 1.22 (a), deformations of the devices with liquid as dielectric were smaller than the one without liquid by 20%. The reason behind this phenomenon is the repulsion forces from liquids are larger than that from air. However, given the high dielectric performance of the encapsulated liquids, we consider that the proposed escape reservoir functioned sufficiently. The trend of the result in the graph of deformation vs applied pressure was observed to be similar, where a steep and linear initial rise up until the pressure of 100 kPa and gradual increase in the deformation over 100 kPa. The sensitivity of the sensor device can be observed as the gradient of capacitance difference vs applied pressure graph in Figure 1.22 (b). The change in the capacitance difference ($C-C_0$) of the devices with liquid encapsulated were constantly increased and almost proportional to the pressure applied. On the contrary, the change in $C-C_0$ of the device without any liquid encapsulated was found to be increasing at first, but did not show a significant change after 100 kPa pressure applied. From this result, we could conclude that the devices with liquids encapsulated as dielectric were more sensitive as compared to that without liquid as dielectric; especially for detecting large pressure, i.e. from about 100 kPa to about 800 kPa.

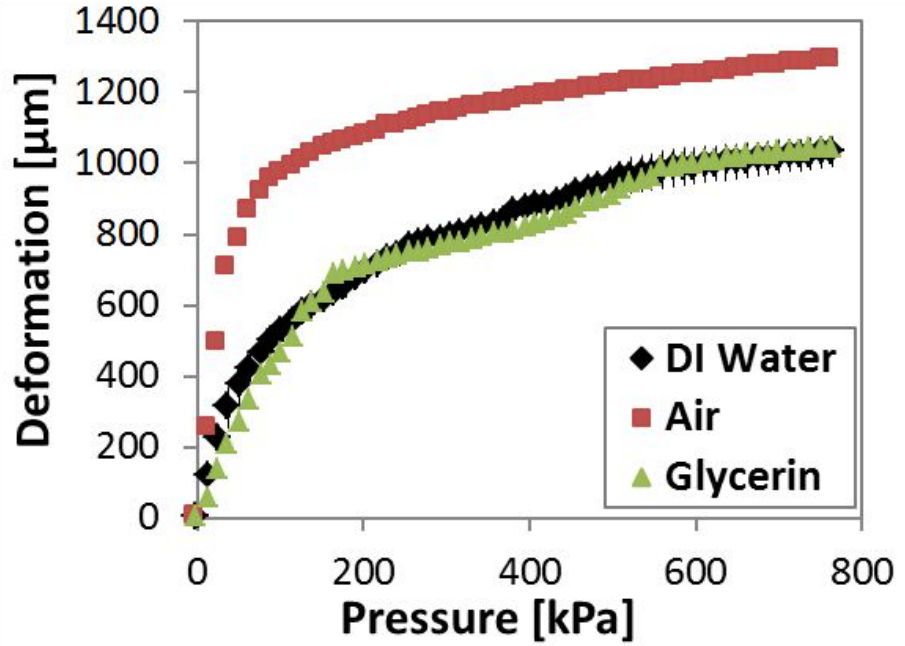

(a)

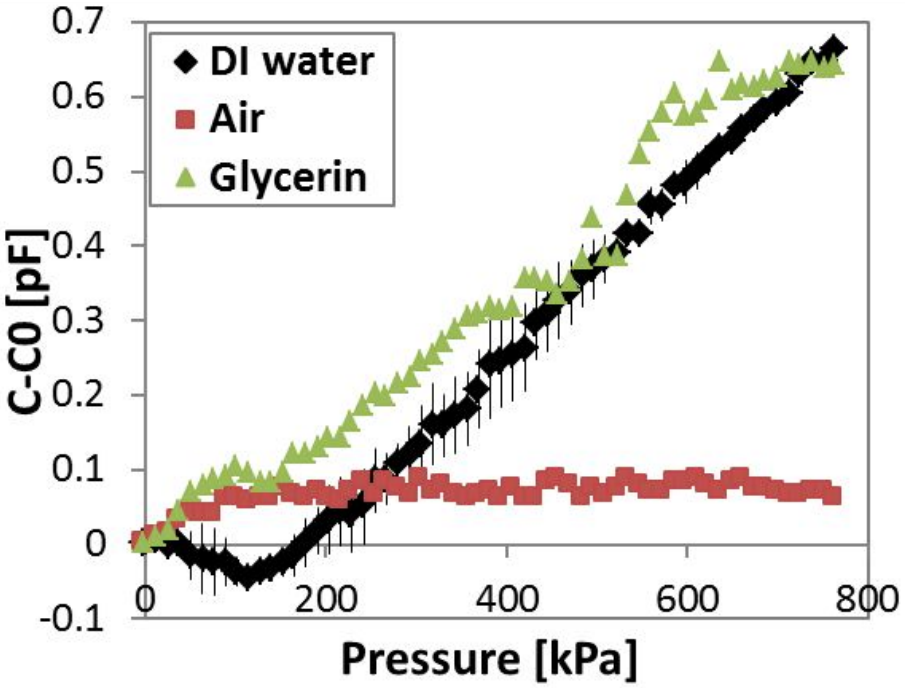

(b)

Figure 1.22 Result of the experiment on capacitive sensor device comparing the devices with DI water, glycerin, and air as the control sample. (a) Relationship between the deformation of top electrode and pressure applied to the device, and (b) relationship between capacitance difference and pressure applied to the device.

1.3 Objective of Study

Most of the tactile sensors that had been developed inspired by the skin were flat and flexible, just like the skin. The sensors are usually to be mounted to robots as the skin, so it is true that there is more demand for flat and flexible tactile sensor. However, to be used in small and narrow channel, e.g. inside the body during MIS procedures and in pipeline during pipeline inspection, etc., the tactile sensor has to be non-flat, small, and can be fitted to the tip of the devices or robots, just like how cameras did in this time being.

Taking MIS procedure as an example, besides adequate dimension of size, a sensor device for MIS need to be able to detect forces from different directions and distinguish hardness and softness of human organ's tissues. Focus on the research of non-flat tactile sensors were also done by some researchers, e.g. the tactile sensor that were developed inspired by fore finger [100], roughness discrimination artificial fingertip sensor [101], and also skin inspired tactile sensor for surface texture perception [102]. Focusing on the ability for a sensor to detect multidirectional load, there are some researchers who decide to take the road not taken by others, by not mimicking the skin. For example, a three-dimensional load sensing tactile sensor was built in donut shape [103], and a capacitive tactile sensor with liquid metal electrodes was developed inspired by a ball-point to detect the location of hard bump in soft tissue [12]. Other than that, a load direction recognizable tactile sensor was also designed in micropillar arrays [104]. Function-wise, these tactile sensor looks promising, but the complicated wiring systems and large sensing elements makes them difficult to miniaturize. From the view of safety and better quality of life, for example, in applying this sensor for MIS, the need for high indentation in localizing subcutaneous blood vessels may be the drawback for this sensor which can actually be made low-costly and specifically for MIS [105] as high pressure may cause tissue injuries.

Robots for pipeline inspection are another example of the application of non-flat tactile sensor. Several types of robots had been developed to inspect thousands of kilometers of various diameters of pipelines [106]–[108]. These robots have to move inside the pipelines, travelling a few kilometers through T and U junctions to inspect the internal surface of the pipelines whether there are corrosions or cracks. Usually, a charge-coupled device (CCD)-based camera would be installed in front of the robots to do the recording, but for inspection, going through a recorded video of hundreds of kilometers of pipelines would be challenging and time consuming. Hence, some robots are now equipped with sensor modules like

ultrasound sensor, microwave sensor, laser sensor, and etc. to aid the inspection task [109]. Tactile sensor might not help in detecting cracks and corrosions inside a pipeline, but tactile sensor is needed in forward motion and steering mechanism for pipeline bends. Therefore, tactile sensor for multidirectional force detection is desirable to this application. To date, walking robot are helpful in inspecting small diameter pipelines, but the complexity of building tactile sensor for its legs had been a major limitation in developing this technology [109].

Therefore, in this dissertation, design and fabrication process of a bio-inspired tactile sensor for multidirectional load sensing will be discussed. This particular sensor cannot be made inspired by the skin for the shape cannot be flat and flexible to fit the expected application. Consequently, inspired by the structure of a tooth and how it can sense pressure, this sensor is designed and fabricated by using the principle of strain gauges. Besides its simple structure that can be further miniaturize, the developed tactile sensor is also costly economical, and has uncomplicated data analysis system.

1.4 Overview of Thesis

This thesis consists of six chapters. The first chapter is this chapter, explaining about the background and objective of the research.

Chapter two explains about the design strategy and how the design of the sensor can be realized inspired by the anatomy of a tooth.

The design of the proposed sensor device is explained in the third chapter. The chapter will begin with some discussions about mechanisms chosen for the proposed device, a couple of designs that were proposed before, followed by the details of the final design.

Chapter four discusses about the fabrication process of the proposed sensor device. The details of the fabrication process of each part of the device will be explained first in this chapter, and then the assembly process will be specified next.

The experiments that were done to prove the concept of the sensor device is listed in detail in chapter five. The experimental results and discussions will also be explained thoroughly in this chapter.

Chapter six summarizes all of the topic that has been discussed and presents some views about the future prospects of this particular research.

Enjoy reading!

2

DESIGN STRATEGY

2.1 Inspiration

As mentioned in the previous chapter, a lot of tactile sensor has been designed inspired by the skin, for the skin is the best organ that defines sense of touch. However, there are also other parts of our bodies that do the same function, with different approach. In this research, the design of the sensor device was inspired by a tooth to suit the function of the sensor device.

2.1.1 Anatomy of a Tooth

The teeth are bones that are not wrapped with muscles, fat, and skin, instead the surface is bare. So, the teeth are exposed to anything that are coming near it, including tactile stimuli. Of course, every one of us had experience how our teeth always did a good job in recognizing and discriminating tactile stimuli, whether in sensing light touch and hard pressure, or distinguishing the direction of touch and pressure. Unlike skin, a tooth is hard and not deformable, and it is proven that there are no tactile receptors under the surface of the enamel. Fortunately, there is a thin layer between the tooth and its socket where mechanoreceptors are distributed. This layer is called periodontal ligaments. The anatomy of a tooth is illustrated in Figure 2.1 [64], [65], [110].

With the width of only 0.15 mm to 0.4 mm, periodontal ligament, which located between the cementum of root on the tooth and the socket wall of alveolar bone, contains soft, fibrous, and flexible substance such as collagen, oxytalan fibers, and ground substances. Besides, it also contains nerves, blood vessels, lymph vessels, and of course, periodontal receptors including mechanoreceptors. The functions of periodontal ligaments are including:

1) Supporting the tooth, including maintaining it in the right position during eruption, excessive occlusal loading, and after extraction.

2) Protecting the tooth from excessive occlusal force by absorbing the load like a cushion.

3) Sensing light touch and pressure that occur on the surface during mastication. The existence of mechanoreceptors explained this phenomenon.

4) Helping in the forming, maintaining, and repairing of cementum and alveolar bone.

5) Providing nutrient supply required by the cells of the ligament through the blood vessels.

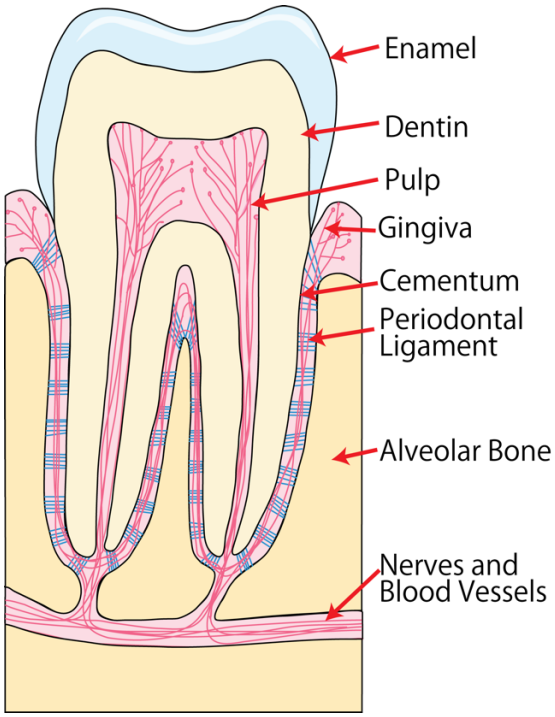

Figure 2.1 Anatomy of a tooth

2.1.2 Movement and Pressure Sensing

For the sensory function of periodontal ligaments, the periodontal receptors include nociceptors and mechanoreceptors. Nociceptors are responsible in detecting pain, while mechanoreceptors help in detecting physical deformation of the membrane and proprioception of the teeth during food munching process. Both RA and SA mechanoreceptors distributed in a high concentration in periodontal ligament, thus a very small force, e.g. that is caused by a thin metal foil that is placed in between two teeth, can readily be sensed by the teeth.

The mechanoreceptors in periodontal ligament fires when the deformations of the fibrous substance of the ligament are detected. The physical characteristics of periodontal ligament, especially with the presence of collagen and the ground substance, is like a viscoelastic material. So it responds to force in a non-linear, viscoelastic manner [111], [112]. During loading on the surface, the periodontal ligament on the pressure side of the tooth will be compressed, while the one at the tension side will be stretched. This compress and stretch movement will stimulate the mechanoreceptors and the sensing information will then be sent to the central nervous systems via the nerves. The deformation of periodontal ligament during these stimulations is depicted in Figure 2.2.

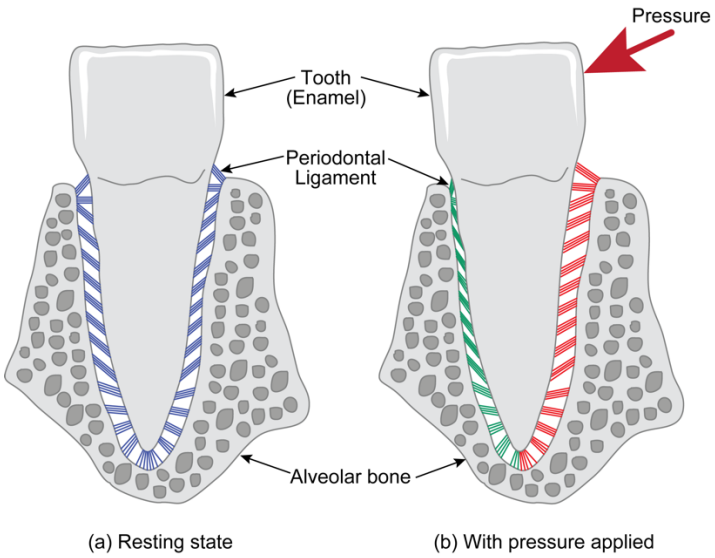

Figure 2.2 A tooth in (a) resting state and (b) during pressure application to its enamel. Periodontal ligaments in blue were in resting state, red in stretched state, and green in compression state.

2.2 Design Concept of the Sensor Device

The idea of the design was using the concept of a tooth, where a pole, which act like a tooth, was going to be placed around a material that could sense the movement of the pole when load is applied to it. The concept is illustrated in Figure 2.3.

The structure of a tooth seems common with tactile sensor designs, as a lot of force sensors had been designed with a pole, post, probe or mesa structure. The tooth-inspired tactile sensor device is quite similar to whisker type sensor device, in terms of the force would not be directly applied to the sensing elements, like the ones inspired by skin. In this type of sensor, force would be applied to the sensor part that is moveable, and the movement of the part would trigger the sensing elements, like strain gauges, that are attached to it. One of the examples is this whisker sensor for underwater induced vortex detection [113], which has quite a similar design with our proposed sensor. The sensor was built using three-dimension printing technology, making its size of 8 mm in diameter and 160 mm in length. For MIS application, small-scale sensor has been made inspired by hair-cell, with the diameter only 420 μm [114]. It has a detectable shear force range below 5 mN and post's maximum displacement of only 15 μm. Building a mesa structure [115] or a probe [116] on a flat sensor element was proven to increase the detectable shear force range.

All of these sensors have a similarity with the proposed sensor in this research, which has protruding structure such as pole, post, probe or mesa structure. However, unlike the usual whisker type sensors with flat sensing elements, the proposed sensor has three-dimensional sensing element structure, just like the periodontal ligaments of the teeth. Besides, unlike some whisker-like sensor which the protruded structure glued on the flat surface, this proposed sensor was inserted and glued inside a hole to set a limit in the displacement of the pole to avoid over-bend that can cause destructive effect on the durability of the sensor device itself.

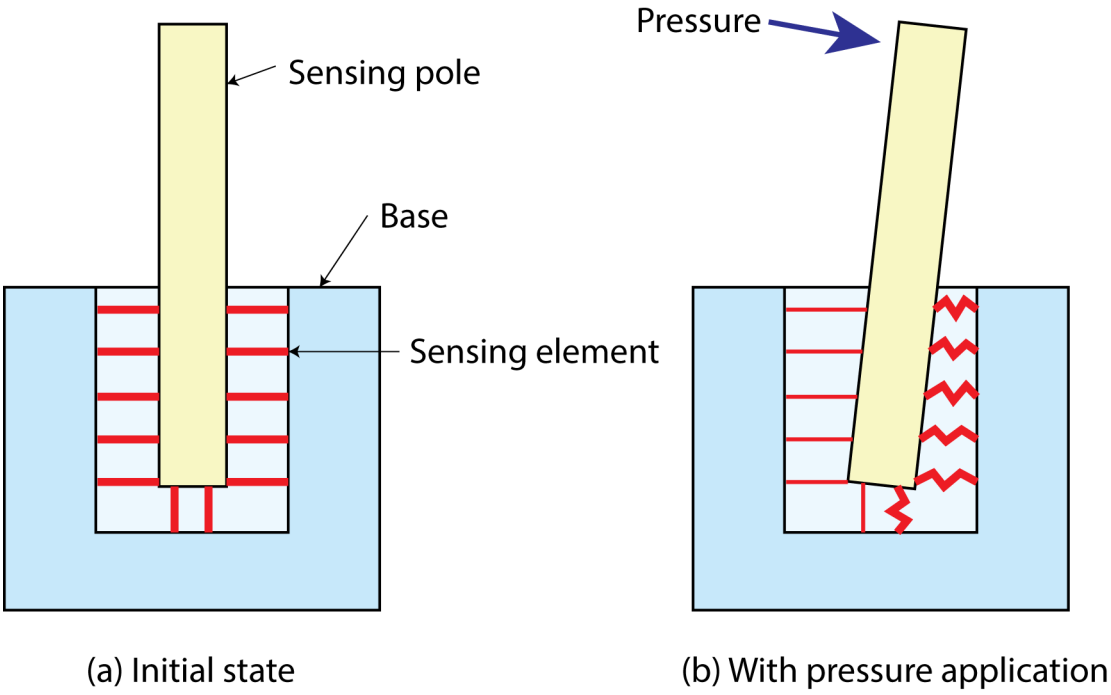

Figure 2.3 Principle of pressure tactile sensor inspired by the anatomy of a tooth, in (a) initial state, and (b) When pressure is applied to a side of the sensing pole, the sensing elements at the pressure side is compressed (jiggly red lines) and sensing element at the tension side is stressed (thin red line)

2.3 Size and Limitations

The sensor device is aimed to be applied to aid operations in narrow areas such as MIS procedures, pipeline inspection, etc., thus the size has to be small enough to fit the equipment used during the procedures.

For MIS procedures, the tip of the sensor device for MIS must be smaller than 10 mm in diameter [117], and the material of the sensor has to be lightweight [118].Other than that, the range of detectable force of the sensor for MIS should be up to 16 N, but most of the procedures in endoscopic surgery, e.g. tissue palpation, require a force sensor that can detect pressure lower than 1 N [119].

For pipeline inspections done by engineers, for example in oil and gas industries, the pipeline size are various; the small ones are only a few mm, and the big ones could reach a few thousands mm [120]. Researchers are developing robots with tactile sensors to aid the

movement of robots during pipeline inspections, together with cameras for better view on what is happening inside the unreachable areas [109]. The motion of pipeline robots are quite slow, about 50 mm/s for small robots [106]. Range of detectable force are not mentioned because it is subject to the weight and speed of the robot itself, but it is desirable for the wiring to be less complicated and lightweight, because inspection robot could not carry heavy load because of the limitation of power supply despite of long travelling distance [109].

Using these two examples of the application of non-flat tactile sensor, in this research, the sensor device would be designed to measure force less than 1 N, with size less than 10 mm in diameter. Besides, the material used had to be lightweight and biocompatible. Simple wiring and data processing are necessary, and the sensor should be able to detect force in motion, but low frequency motion would be sufficient. The gap between sensing pole and the base would set the limit of the displacement of the sensing pole. However, the displacement of the sensing pole itself could be higher, according to the length of the pole. As illustrated in Figure 2.4, taking the bottom of the pole as the fixed fulcrum for the pole, the displacement of the pole can be calculated as follows;

$$d_1 = \frac{l_1}{l_2} d_2 \qquad \text{Eq. 2.1}$$

Here, d_1 and l_1 is the displacement and length of the pole at any point above the sensing element that would be the possibility of the pressure point, and d_2 and l_2 is the displacement and length of the pole at the pole movement limitation point near the surface of the base, where the sensing element would be mostly affected by the movement of the sensing pole. The movement of the pole should be in a rotation, thus the displacement of the pole d_1 and d_2 should be in a curve line. However, assuming that the displacement is sufficiently small, d_1 and d_2 could be regarded as a straight line. Longer pole could compromise higher displacement. Nevertheless, because the sensor is aimed to be applied to narrow spaces, a few mm of pole displacement would be sufficient for the application. Therefore, this tooth-like design would be suitable for small-scale tactile sensor, provided that the sensing element can detect small displacement from applied force.

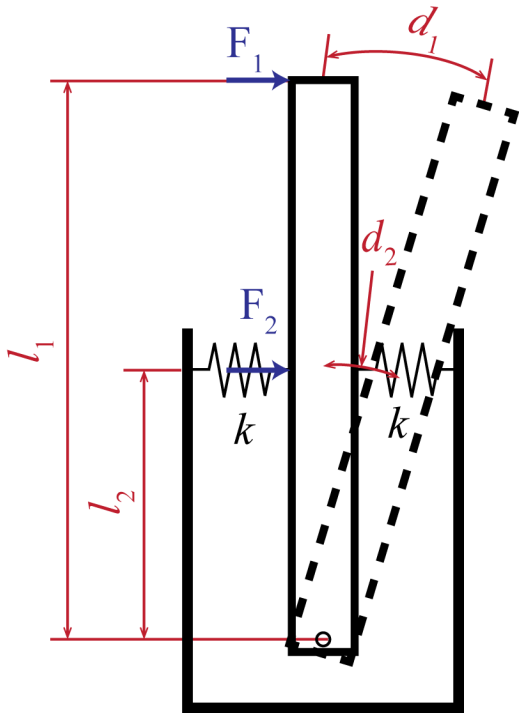

Figure 2.4 Limitation of displacement of sensing pole

Magnitude of force applied to the sensing element could also be calculated from the lever mechanism. If F_1 is the force applied to the side of the pole with distance from the bottom of the pole l_1, taking the bottom of the pole as the center of torque, force applied to the sensing element nearest to the surface of the base, F_2, would be

$$F_2 = \frac{l_1}{l_2} F_1 \qquad \text{Eq. 2.2}$$

The sensing element of this sensor should be elastic so that the pole could return to its initial position after force is unapplied to the side of it. Assuming the sensing element is purely elastic, F_2 could also be written as follows.

$$F_2 = 2kd_2 \qquad \text{Eq. 2.3}$$

k is the spring constant of the sensing element's material. Inserting equation 2.1 to equation 2.3,

$$F_2 = 2kd_1 \frac{l_2}{l_1} \quad \text{Eq. 2.4}$$

It is shown in equation 2.4 that besides the spring constant k of the sensing element, the displacement of the pole d_1 and the ratio of distance of sensing element to the distance of applied force from the bottom of the pole (l_2/l_1) would affect the force applied to the sensing element. Force applied to the side of the sensing pole F_1 can be calculated by substituting equation 2.2 to equation 2.4.

$$F_1 = 2kd_1 \left(\frac{l_2}{l_1}\right)^2 \quad \text{Eq. 2.5}$$

The length of the pole might be important in determining the amount of force that can be applied to the sensor device, as the working principle of this sensor device is similar to the lever mechanism. However, as described in equation 2.5, what is more important is the relative length of the position of sensing element and the position of the applied force. Therefore, having adequate length of protruding side of the sensing pole would give larger sensing range for the sensor device.

3

DESIGN

3.1 Choosing the Best Mechanism

3.1.1 Requirement for the Proposed Device

Force that has to be detected by the sensor device would not be applied directly to the sensing element. Force will be added to the side of the sensing pole, and the movement of the sensing pole would trigger the sensing elements at the bottom sides of the pole. Therefore, several requirements had to be fulfilled to realize this sensor device. The requirements are listed as follows:

1) Sensing element has to be flexible enough to deform according to the movement of the center pole

Because the sensing element would be attached to the center pole, the flexibility of the sensing element would be the main characteristic that has to be taken into account. As shown in equation 2.5, using material that has higher spring constant k would require higher force F_1 for the same displacement d_1 of the pole. Hard and rigid sensing element would set limit on the

movement of the center pole; therefore, flexible and soft sensing elements are desirable in this proposed sensor device.

2) The sensor can detect static and dynamic force

Force sensing in narrow spaces could be static or dynamic, depending on the objective of the sensing activity. For example in MIS procedure, static force sensing is used in tissue's grasping and hardness or softness sensing [121], while dynamic force sensing is used in cutting and suturing [122].

3) Sensing element has to fit the device

As discussed in section 2.3 Size and Limitation, the device would be developed in a small size, thus the sensing element has to be small enough to fit the bottom surrounding of the center pole.

4) Sensing element can be fabricated in three-dimensional structure

The sensor device would be developed inspired by the anatomy of the tooth. Unlike most of the whisker-like sensor which has two-dimensional flat sensing element, the sensor device inspired by tooth has three-dimensional sensing element surrounding the center pole.

The suitable mechanism for the proposed tactile sensor can be concluded from the discussion above, by eliminating the mechanisms that are unsuited the design of the sensor device. Optical sensors are usually bulky [55]; thus, it cannot fit the proposed size of the sensor. Magnetic sensor, especially the one with Hall effect sensor also has limitations in size [123]. Electromagnetic induction sensors might be fabricated in small scale, but they consume more power and has eddy current effect that can disturb the sensors' performance [59]. Piezoelectric sensors have the advantage in the term of size, but static force sensing using the said sensor type would be difficult because the charges induced in the piezoelectric material usually dissipate rapidly [124], causing insensitivity in static force sensing.

The ones that are left after the elimination process are capacitive sensing mechanism and piezoresistive sensing mechanism.

3.1.2 Capacitive Sensor Array with Liquid as Dielectric

The research of this sensor was discussed in section 1.2.2. In applying the concept and mechanism of the sensor device to the proposed tooth-like sensor device, the result from the research of the design and fabrication of capacitive sensor array with liquid as dielectric seems promising, especially the sensitivity enhancement of the sensor with liquid as dielectric. However, the sensing element of the sensor inspired by tooth need to be made in three-dimensional structure, as mentioned in section 3.1.1, therefore major revision on the design of the sensing element need to be considered if this sensor is to be applied to the tooth-like tactile sensor. Moreover, the capacitive sensor was very sensitive to electrostatic charges from the surroundings. A robust, inert packaging need to be design to the sensing element before applying it to sensor devices so that the signal from the sensor could be noise free and data processing could be done more smoothly. Additional packaging might increase the dimension of the sensing element, thus capacitive sensing element might not be the best candidate for the tooth-inspired tactile sensor.

As the capacitive type mechanism was eliminated from the candidature to be applied to the proposed tactile sensor, piezoresistive mechanism will be tested in cylindrical, tooth-like tactile sensor device.

3.1.3 Nanocomposite Piezoresistive Sensor

3.1.3.1 Design and Fabrication Process

The first attempt to develop cylindrical sensor was designing the sensor device using nanocomposite piezoresistive principle [34], [125]. The material of the nanocomposites was chosen from several types of elastomers: i.e. PDMS (Silpot 184, Dow Corning Toray Co., Ltd.) and elastic adhesive material (Dow Corning® 3145 RTV MIL-A-46146 adhesive/sealant, Dow Corning Corp.). The variant of the fillers were Ag powder and multiwalled carbon nanotubes (MWCNTs) powder [126]. Result of the experiment showed that the combination of MWCNTs and PDMS elastomer had a suitable mechanical and electrical properties to be applied to the sensor device. The poles were made from 30-mm- and 50-mm-long polyoxymethylene (POM). The diameter of sensing pole was 3 mm and 1 mm for the outer and inner diameter respectively, while for the bigger pole that would be the base of the device, the diameter was 6 mm and 4 mm respectively for outer and inner side. The concept of the sensor device is shown in Figure 3.1.

3.1.3.2 Fabrication Process

The composite was made first, and then the sensor components was assembled as illustrated in Figure 3.2. Multi-walled carbon nanotubes (MWCNTs) (20-50 nm, Wako Pure Chemical Industries, Ltd.) was used as the filler of the composite without further purification. The polymer matrix, PDMS prepolymer (Silpot 184, Dow Corning Toray Co., Ltd.) and MWCNTs were measured to be 1:0.15 by weight ratio. The MWCNTs and PDMS prepolymer were directly mixed for five minutes using a glass rod in a clean room ambience. After that, PDMS curing agent (Silpot 184 CAT, Dow Corning Toray Co., Ltd) was added to the mixture with PDMS prepolymer–curing agent ratio of 25:1, and the mixture was stirred for another five minutes. The mixture was then left in a desiccator for one hour until no more air bubbles were visible.

After that, the sensor device was fabricated through the following processes:

1) Four copper electrodes were adhered to the inner side of the outer rod, along the length of the rod. Then, it was adhered in upright position on a glass substrate. Adhesive tape was used to make sure the rod stays put.

2) About 10 μL of PDMS–MWCNTs composite that was prepared beforehand was injected into the outer rod using micro syringe to form the base of the composite. The device was then baked for one hour on a hotplate with temperature of 100°C so that the base hardened.

3) The device was removed from heat. Another 170 μL of PDMS – MWCNTs composite was injected into the outer rod.

4) The inner rod was inserted into the outer rod to be the center pole of the sensor device, and the position was adjusted to be in the middle of the outer rod. The device was baked for about 3 hours to harden the composite.

3.1.3.3 Evaluation and Discussion

The fabricated device is shown in Figure 3.3 (a). It was assumed that when pressure is added to one side of the device, the concentration per unit area of the piezoresistive nanocomposite will change, thus causing the change in resistance of the materials [127]. Trend of the resistance change would differ if the pressure was added to the side with electrodes or the side in between two electrodes. During pressure application, the resistance of the nanocomposite was read between the combination of two electrodes of the device, six pairs simultaneously using the circuit that was built consisted of semiconductor relays IC (AQW 614, Panasonic Corporation) and an open source electronics prototyping platform, Arduino UNO.

Result of the experiment when pressure was applied to the side of the center pole towards electrode C and between electrode C and D is shown in Figure 3.4 (a) and Figure 3.4 (b) respectively. The result for this design of sensor seemed promising, but as shown in Figure 3.4, the pressure added to the sensor device had to be more than 300 kPa for it to show difference for each pair of electrodes, and no data obtained when pressure was applied lower than 100 kPa. In this experiment, 100 kPa was equal to 0.1 N. This phenomenon occur because of the mixing ratio of conductive filler to the polymer matrix was not enough to have an effect by added pressure below 300 kPa. More condense composite might be needed for this device but adding more conductive filler would sacrifice the flexibility of the composite [126]. Also, there are a lot of things to be considered when using nanocomposite piezoresistive materials to develop a sensor, such as tunneling resistance inside the composite [128]–[130], contact resistance between the composite and metal electrodes[130]–[132], creep behavior [130], etc. All of these matters affected the resistance of the device and caused a lot of noises in the system. This made the data processing complicated.

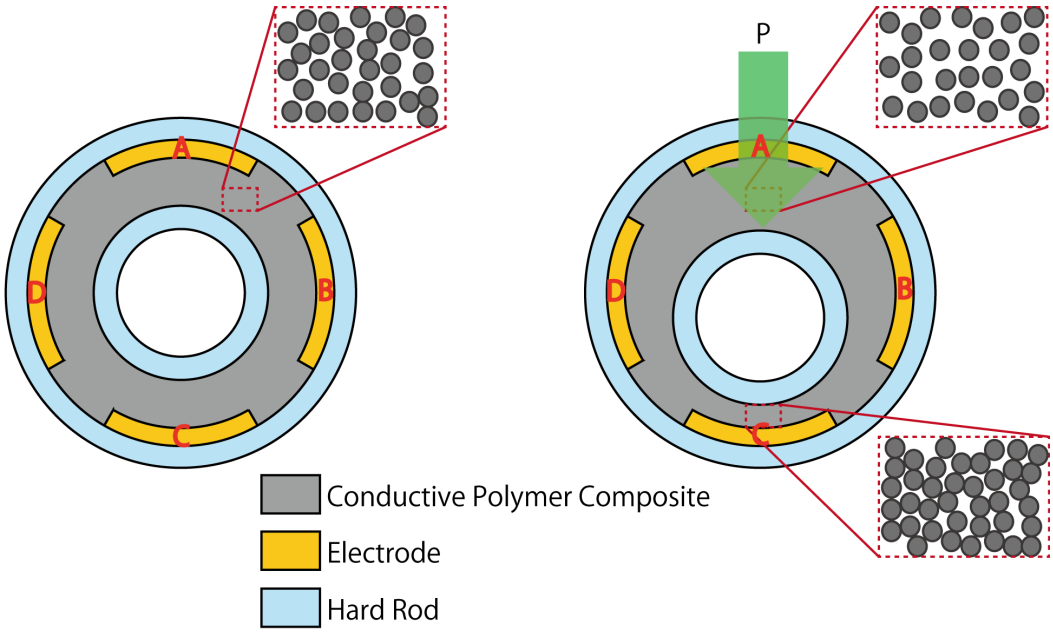

(a) Initial state and pressure added to the side with electrode C

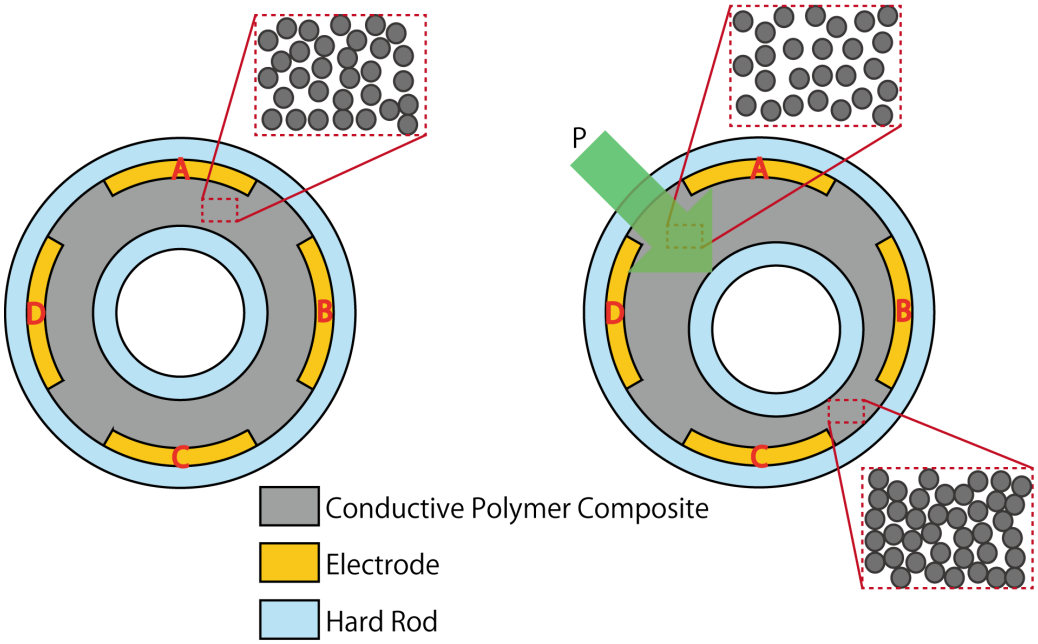

(b) Initial state and pressure added to the side between electrode B and C

Figure 3.1 Top view showing the concept of the nanocomposite device, with (a) the initial state and when pressure is added to the side with electrode C, and (b) the initial state and pressure added to the side between electrodes B and C

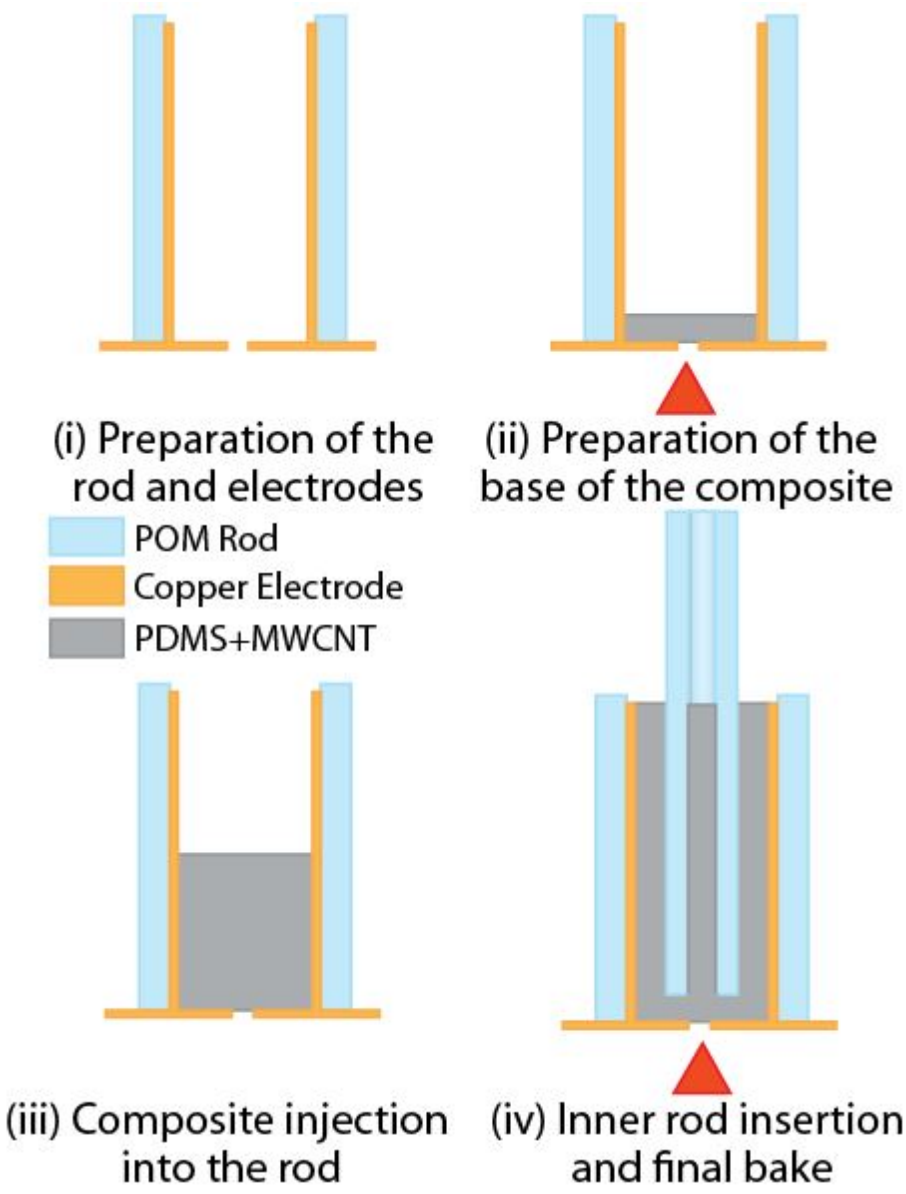

Figure 3.2 Fabrication process of the piezoresistive sensor device with polymer nanocomposite

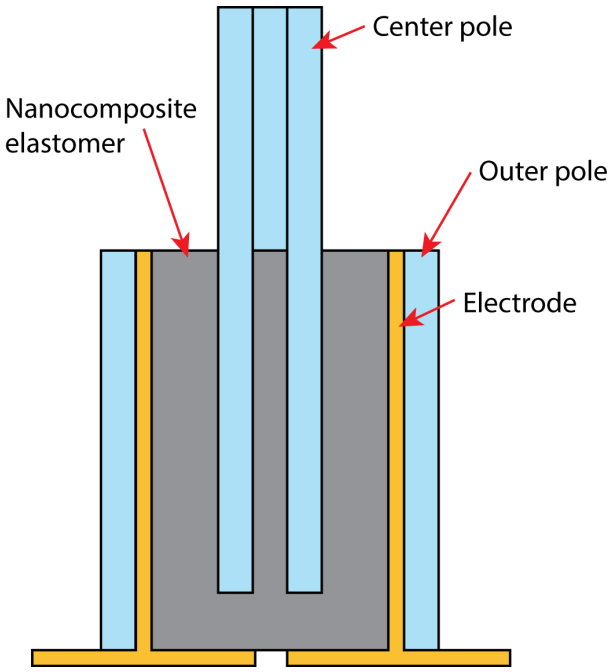

(a)

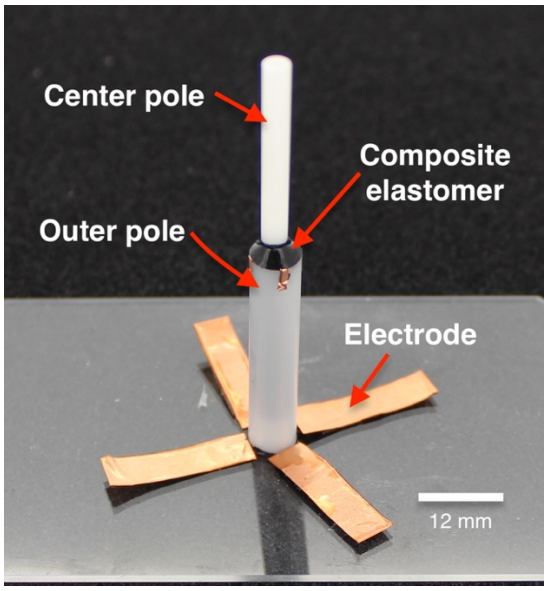

(b)

Figure 3.3 (a) Cross sectional illustration of the device and (b) the fabricated sensor device with nanocomposite elastomer

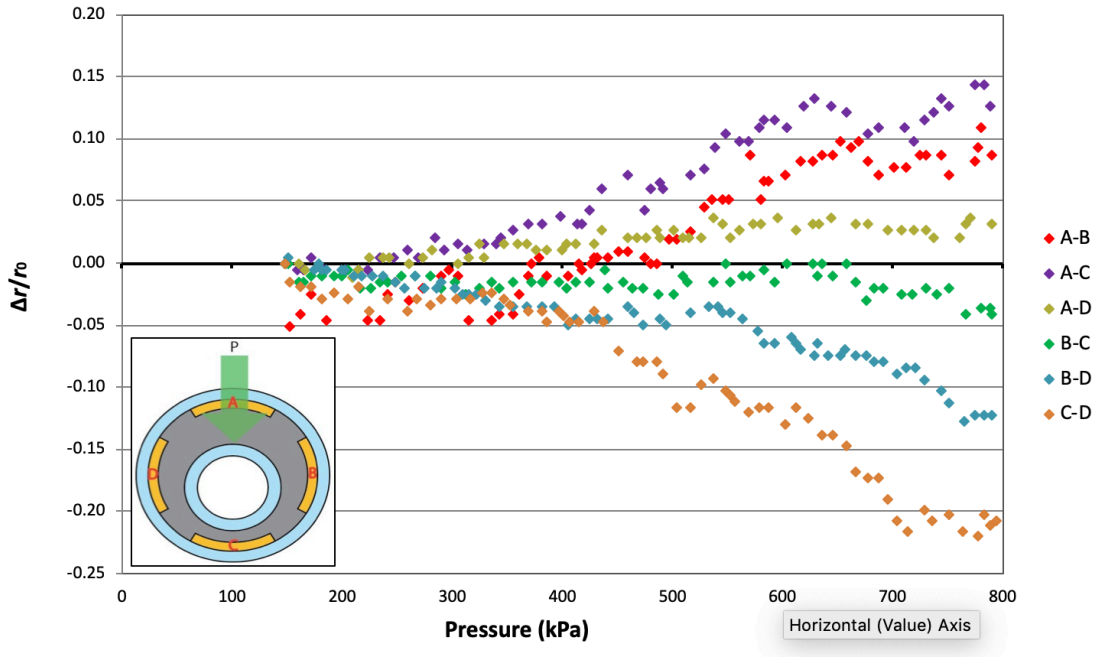

(a)

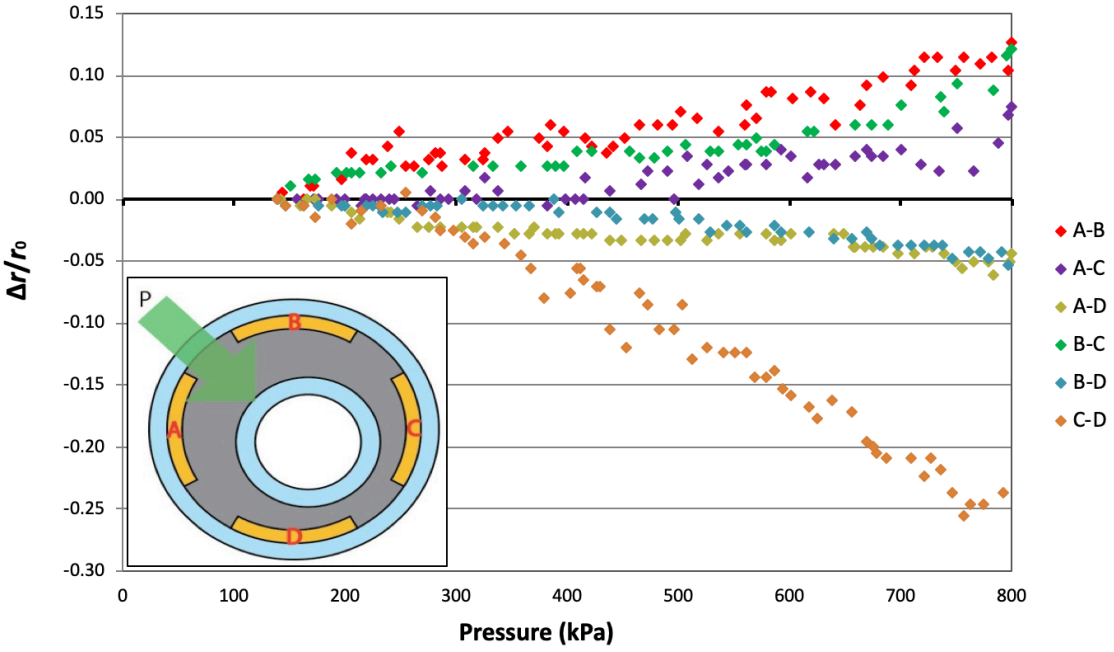

(b)

Figure 3.4 Result of the experiment shows the relationship between resistance change ratio $\Delta r/r_0$ of six pairs of electrodes and pressure added to the side of the device (a) to electrode C and (b) between electrodes C and D

3.1.4 Copper Strain Gauge Piezoresistive Sensor

3.1.4.1 Design

Second attempt was using copper strain gauges that were placed in between two poles. The poles used for this device was similar to the ones used for the nanocomposite device. The copper strain gauge was made by photolithography process, and it was padded with PDMS elastomer inside the pole. The padding was placed to make sure that the copper strain gauge would stay in its position, and the deformation of the copper could happen because of the elastic properties of the PDMS itself. The strain gauge was placed near the tip of the outer rod as the deformation at the particular position would be the highest according to equation 2.1. The concept of pressure sensing is shown in Figure 3.5. The sensing concept was much simpler than the previous design, where the load to the center pole made from hard polymer rod would cause deformation of the compressed strain gauge so the data processing is uncomplicated and direct.

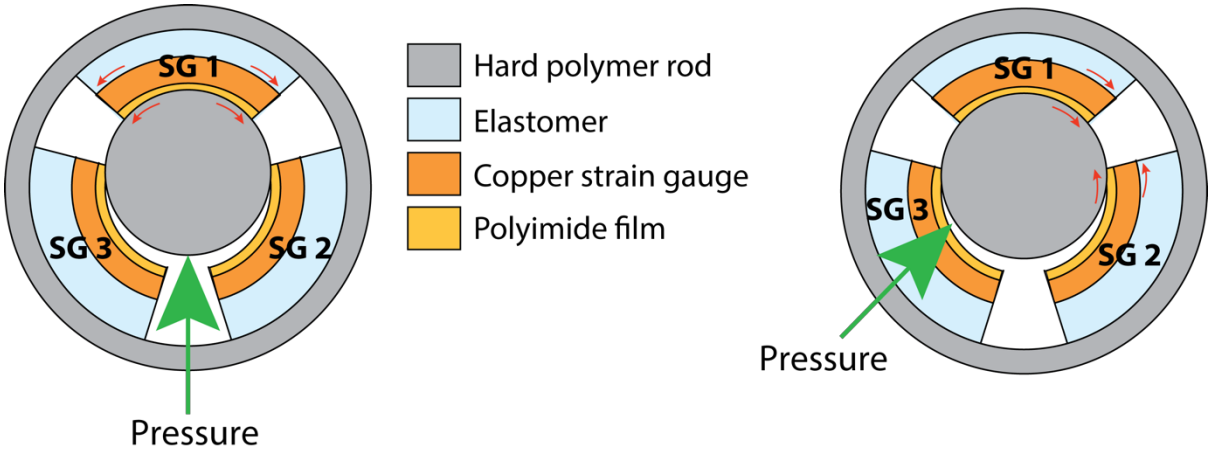

(a) (b)

Figure 3.5 Pressure sensing concept for device with copper strain gauge. Red arrows show the deformation of copper strain gauges when pressure is applied to (a) the side with a strain gauge, and (b) the side in between two strain gauges

3.1.4.2 Fabrication Process

The fabrication process of the strain gauges is shown in Figure 3.6. The strain gauges were made using photolithography process. Photoresist were spincoated on the adhesiveless polyimide copper clad laminate with 25 µm thick of polyimide film and 18 µm thick of copper layer (ESPANEX MC18-25-00FRFM, Nippon Steel Chemical Co., Ltd.) film. The film was then masked with a patterned photomasked and exposed to ultraviolet (UV) light. The exposed film was then immersed in the developer solution to remove the unwanted parts of the photoresist. After that, the developed copper film was etched and finally, the photoresist was removed from the film by immersing the film in acetone.

PDMS liquid that had been mixed with the curing agent was spincoated on a glass susbtrate. While the PDMS is still in liquid state, the fabricated strain gauge-polyimide film was placed on the surface of the PDMS liquid. The membrane was then baked to harden and removed from the glass substrate.

Wires were soldered to the strain gauges before the membrane was wrapped around the inner rod. Both the inner rod and the membrane with strain gauges were then inserted to the outer rod. The fabricated device is shown in Figure 3.7.

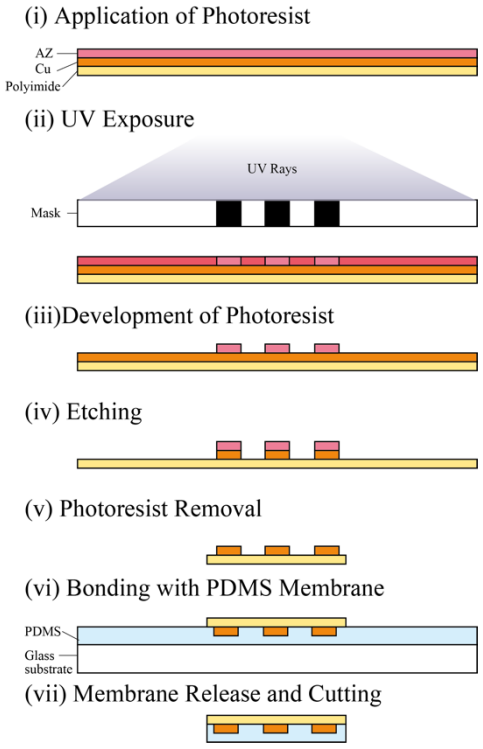

Figure 3.6 Photolithography process to fabricate the strain gauge for the sensor device

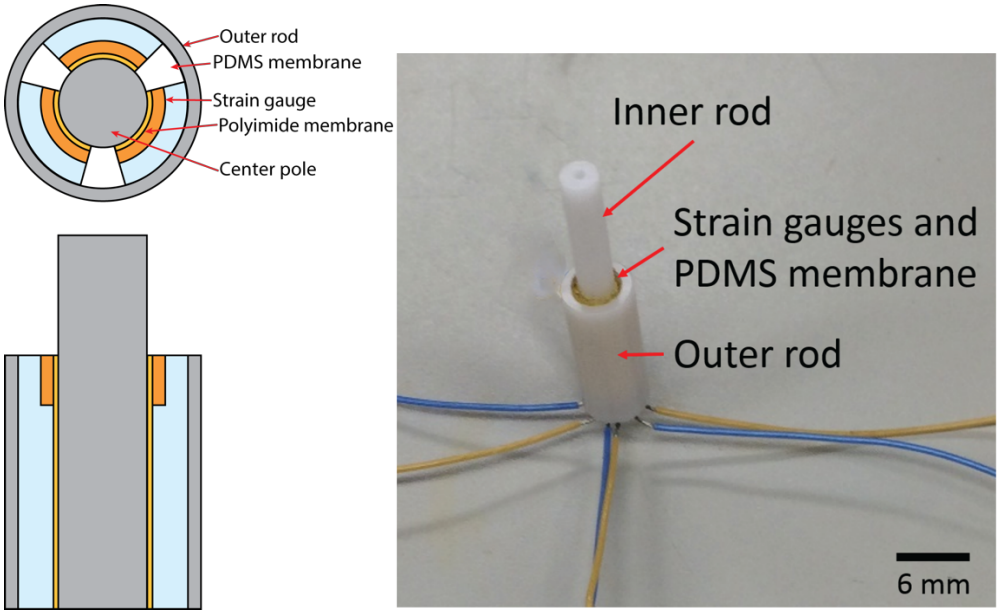

(a) (b)

Figure 3.7 (a) Top view and cross-sectional diagram of the device, and (b) the fabricated device with copper strain gauges

3.1.4.3 Evaluation and Discussion

The device was tested where load is applied to the sides of the pole with an electrode sequentially from SG 1, SG 2, and SG 3, as shown in Figure 3.5 (a), 100 s with 100 s intervals, while the strain gauges were connected to a Wheatstone bridge circuit to measure the resistance changes that were relative to the applied load. The resistance reading showed a small change only when quite a large pressure was applied by hand to the sensor device, but unfortunately, the change was not significant and there were no further change after the first change. The result of the experiment is shown in Figure 3.8. From the result, it is sure that the sensor could give a reading to multidirectional pressure, but still there are insignificant change for the third strain gauge. Also, from the graph, it is obvious that the signal to noise ratios (SNR) were quite small even with an RC filter, with 3, 4.5, and 0.5 for the first, second, and third strain gauges respectively. From the experiment, it was proved that the pressure needed for this experiment was only large pressures, not to the scale that can be measured by the experimental equipment that was used for pressure application, and also it could not detect different values of pressure. Moreover, the fabrication process of this device was intricate, especially in making sure whether the strain gauges were positioned in the right place or not, because the process of inserting the center pole can cause the strain gauge shifted from the place it should be at because

of the large friction between PDMS membrane and the inner surface of the outer rod. The unstable reading from SG 1 during pressure application towards SG 3 was believed to cause by the vague position of the strain gauges inside the device.

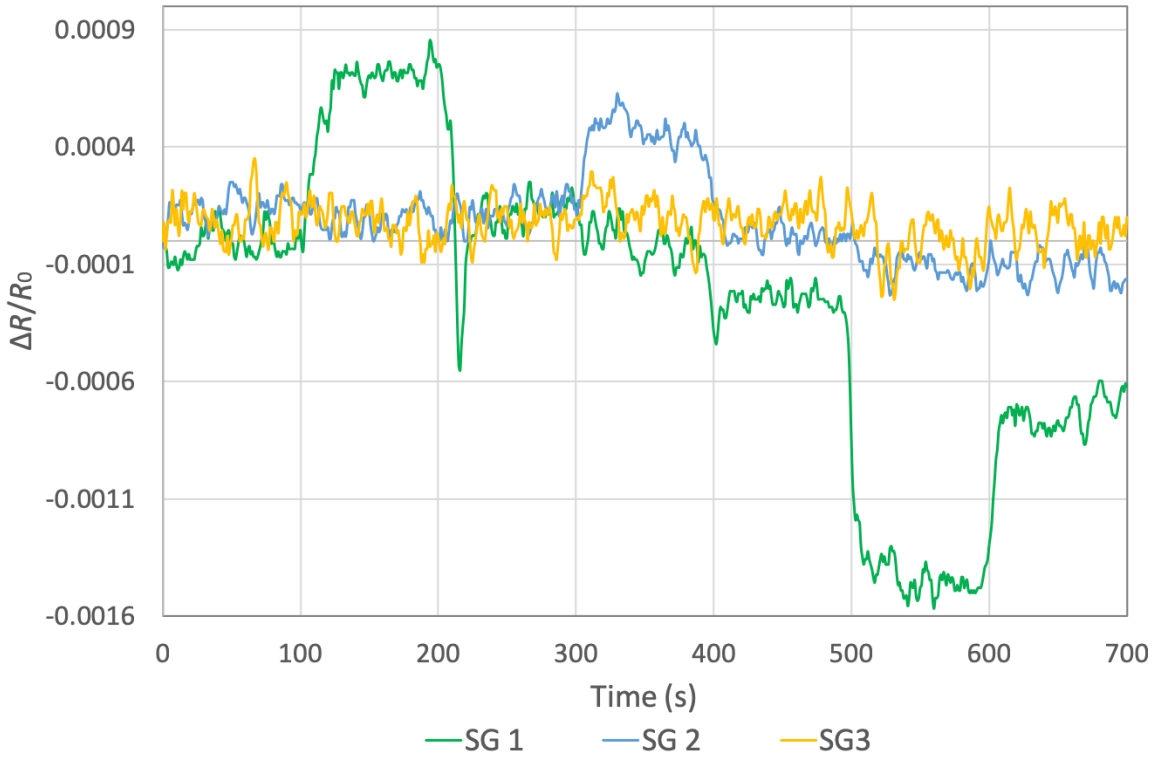

Figure 3.8 The result of the experiment to the sensor device with copper strain gauges, where pressure was added to the side of the device with strain gauges sequentially from SG 1, to SG 2, to SG 3, 100s each with 100s intervals

3.2 Design Improvement

3.2.1 Design

The first two designs of the cylindrical sensor had several characteristics that are unsuitable to be used in surgery equipment, as mentioned in the previous section. Therefore, improvement has been made in designing the device, while taking the disadvantages of the previous devices into account in deciding the new design of the device.

Principle of strain gauge was used where four strain gauges were placed surround a stainless-steel pole, with all the strain gauges were set to be leaned upward against the pole. The design is shown in Figure 3.9. The dimension of the device is illustrated in Figure 3.10.

In the previous devices, the space for the pole to move was too narrow, so the changes of the piezoresistive materials became too small to be detected. Also, the elastomer used was too hard to have effect from small pressure. Therefore, in this research, the piezoresistive material, or in this case, the strain gauges, were not sandwiched between two poles. Besides, softer elastomer was used to adhere the pole to the base of the device so that the pole can move more freely compared to poles in the previous devices.

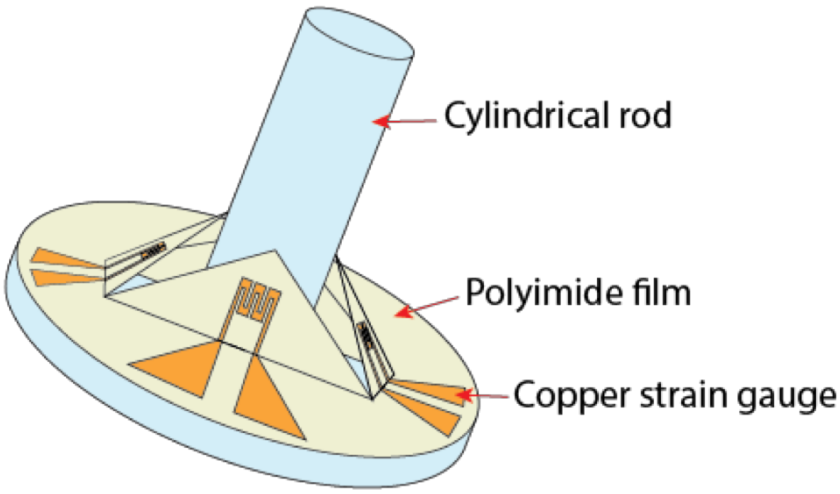

Figure 3.9 Design of the newly proposed device

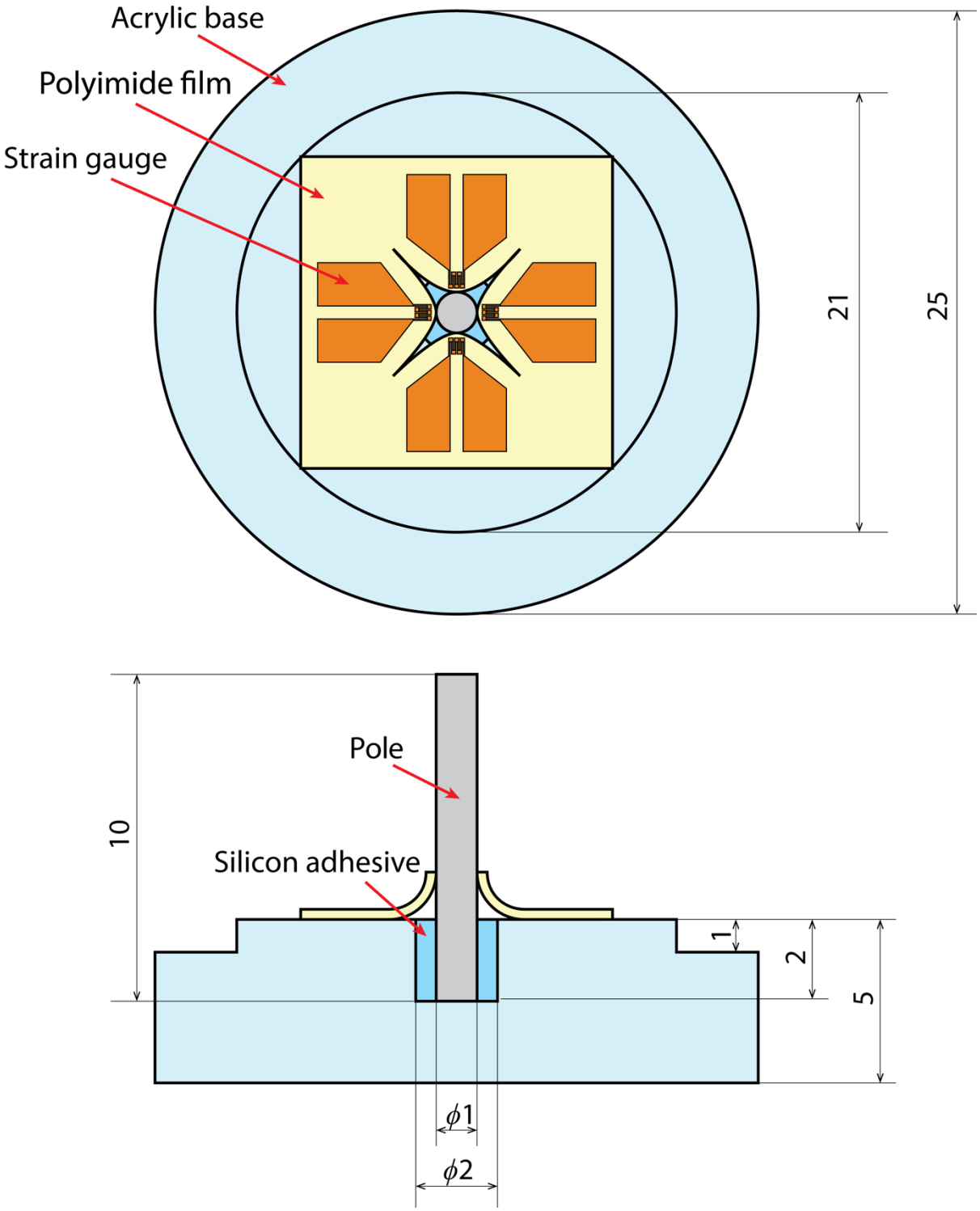

Figure 3.10 Dimension of the proposed device

3.2.2 Material

Details about materials used to make the device are as follows:

3.2.2.1 Base

The base of the device is made using 5mm thick acrylic plate. Comparing to the anatomy of a tooth, the base is the alveolar bone to the device, where it contained the socket to the tooth. Acrylic was chosen to be the material of the base because of its characteristics, as follows:

1) Costly inexpensive

2) Easy to cut and machine

3) Light weight

4) Non-toxic polymer

3.2.2.2 Pole

The center pole, which act as the 'tooth' for the device. Stainless steel is easy to shape, and it was easy to find stainless steel in a small diameter to be used to the device. Stainless steel has good characteristics that made it suitable to be used to the sensor device, such as:

1) Excellent corrosion resistance

2) Good strength

3) Ductile and easy to shape

4) Costly inexpensive

3.2.2.3 Strain Gauges

In this research, the strain gauges were made using copper. In electronic industries, copper is widely used in wiring because it is costly inexpensive compared to gold and silver. The properties of copper are:

1) Good electrical conductor

2) Good thermal conductor

3) Easy to shape

4) Unreactive to water

5) Resistant to corrosion

3.2.2.4 Elastomer

Polymer adhesive called 3145 RTV MIL-A-46146 adhesive/sealant (Dow Corning Corp.) was elected to be used as the elastomer to glue the pole to the base of the device. This polymer adhesive is softer and more elastic, with Young's Modulus of 1.1 MPa according to the insert, compared PDMS, which has Young's modulus of 2.66 MPa for 10:1 of base per curing agent ratio [133]. The characteristics of this polymer adhesive is as follows:

1) Can be cured in room temperature

2) High tensile strength and elongation

3) Excellent adhesive properties

3.2.3 Principle of the device

The position of the strain gauges that were curled up and leaned against the pole made them compressed, so the length of the gauges was decreased from the initial length. The strain gauge has the properties where the resistance increases when the length decreases, and vice versa, as mentioned in section 1.1.2 (1). Parallel to that principle, in this device, when load is applied to one side of the pole, the strain gauge at the opposite side will be further decreased, and the strain gauges that were on the same side of the applied load will be released from their initial compression, thus make them longer. This phenomenon will cause difference in the readings of each strain gauge once load is applied to the side of the device. The principle of the device is depicted in Figure 3.11.

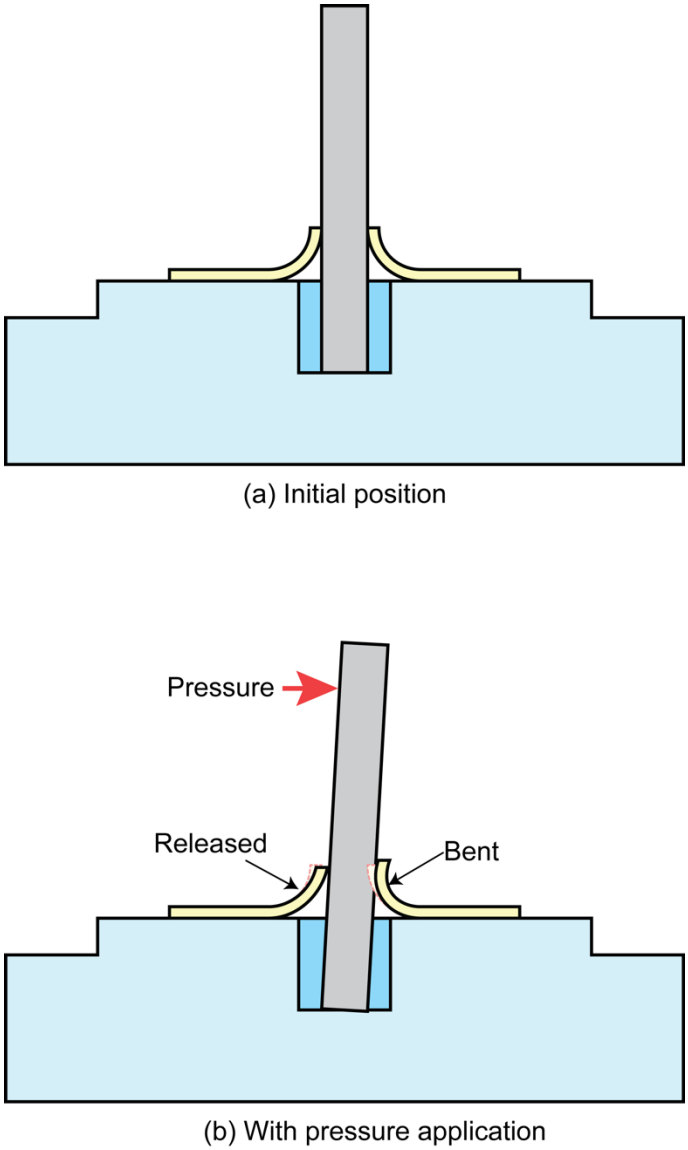

Figure 3.11 Pressure sensing concept of the device. (a) shows the device in initial state, while (b) shows the device during pressure application

Assuming the change of strain of the strain gauge $\Delta L/L$ is linearly proportional to the displacement of the sensing pole at the position of sensing element d_2,

$$\frac{\Delta L}{L} = X\, d_2 \qquad \text{Eq. 3.1}$$

where X is the linear coefficient of the relation. Inserting equation 3.1 to the equation 1.3, and referring to figure 2.4 for the relation of displacement of the sensing pole, resistance change ratio $\Delta R/R$ of the strain gauge would be

$$\frac{\Delta R}{R} = G\, X\, d_2 = G\, X d_1 \frac{l_2}{l_1} \qquad \text{Eq. 3.2}$$

The relation in equation 3.2 shows that the change of resistance of the strain gauge would be proportional to the relative length of the position of the sensing element and the position of force applied to the pole. Designing adequate length of the sensing pole would increase the sensing range of the sensor device.

4

FABRICATION PROCESS

4.1 Fabrication Process of Each Component of the Sensor Device

4.1.1 Base

The base of the device was made using acrylic plate. 5-mm-thick acrylic plate was machined to the dimension as shown in Figure 4.1 and the photograph is shown in Figure 4.2.

4.1.2 Pole

Stainless steel wire with a diameter ϕ 1 mm was cut to 10 mm in length. The edges of the wire were then polished using sand paper to smooth the sharp surfaces. Figure 4.3 and Figure 4.4 show the dimension and photograph of the stainless-steel pole, respectively.

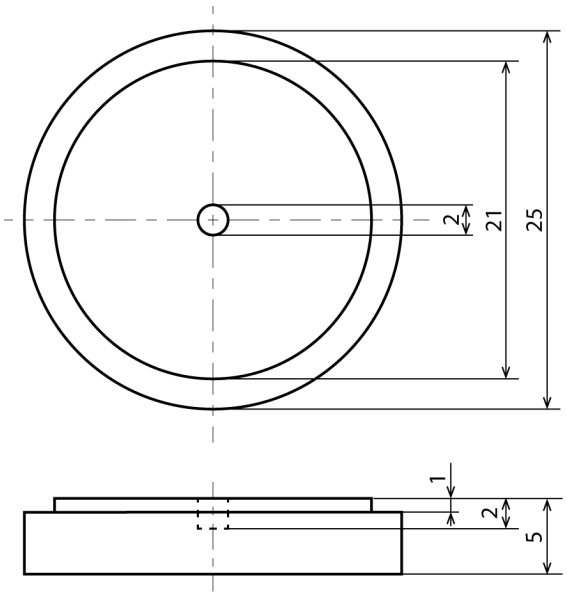

Figure 4.1 Dimension (in mm) of the base of the device, top view (above) and side view (below)

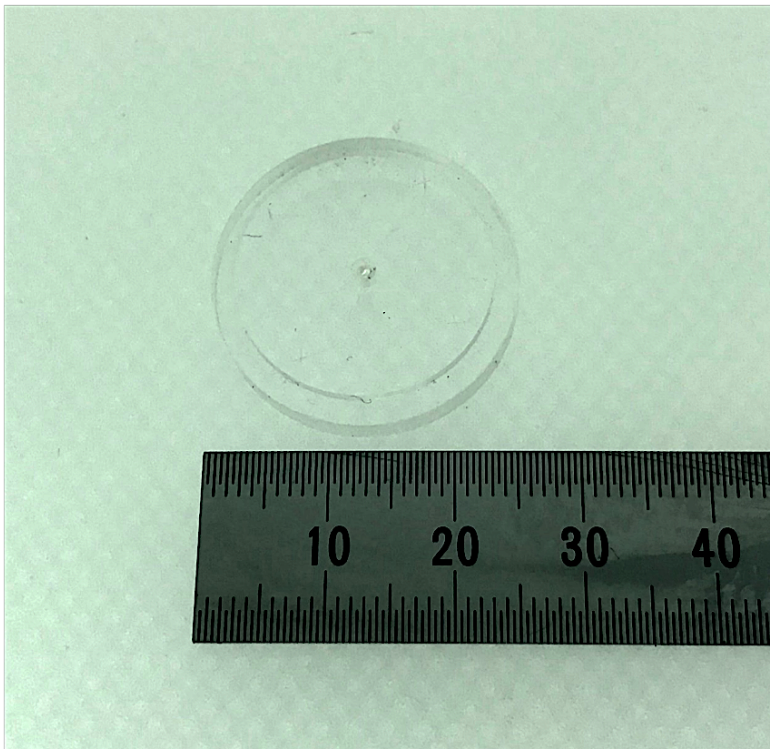

Figure 4.2 The acrylic base

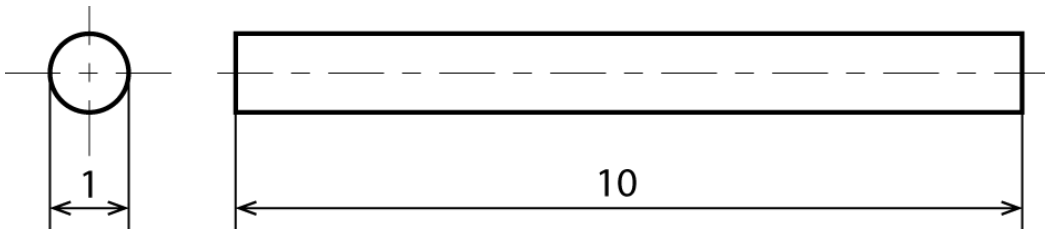

Figure 4.3 Dimension (in mm) of the center pole of the device, top view (above) and side view (below)

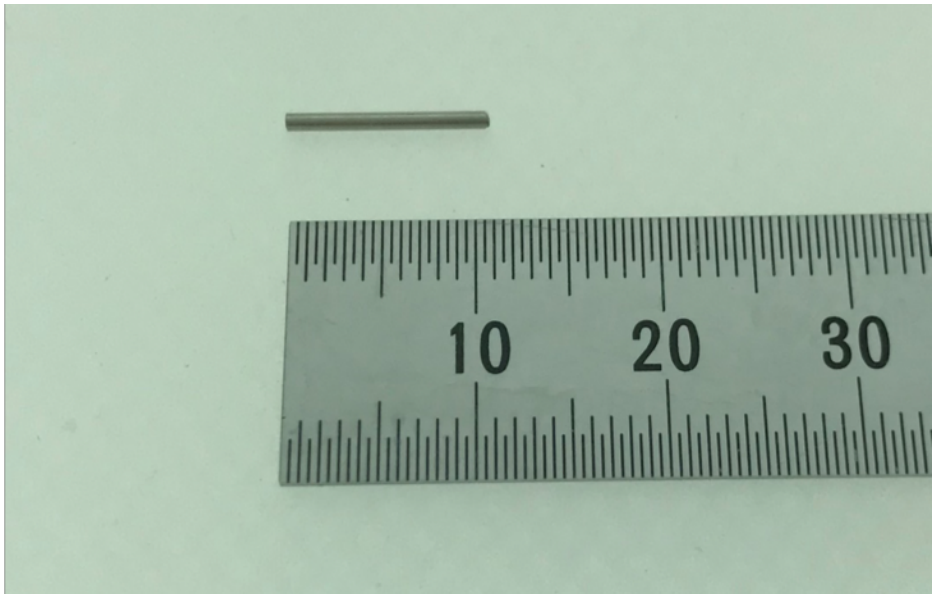

Figure 4.4 The center pole

4.1.3 Strain Gauge

A strain gauge is typically a zig-zag shape thin metal wire printed on a polymer film. The widely used polymer film as the base of a strain gauge is polyimide. Compared to other types of polymer films, polyimides have a better chemical, mechanical, and thermal properties. Polyimides also have high heat resistance level, excellent mechanical strength, and are good insulators. Metals could be easily deposited on the surfaces of polyimides, and the usage of contact metals helps in designing electronic wires on the polyimides' surfaces. In this research, copper strain gauges were patterned on a polyimide film because it would offer better fabrication process and a robust device.

To fabricate the strain gauges for the proposed device, there were several matters to be considered. The device has to be small enough and the strain gauge has to fit the small area, besides still being sensitive to a small movement. The area at the device to be fit with strain gauges is illustrated in Figure 4.5. From the figure, it was known that the area that might be bent and affected by the movement of the center pole is within the red dotted circle with the diameter of 2 mm. On the acrylic base, this area was the hole that was made to insert the pole. So, the strain gauge film in this area would not stick to the acrylic base and this will make the strain gauge film deflected upward to lean against the center pole. There were four strain gauges had to be fitted in the area. So, the limit of the dimension of the strain gauge is within the triangular green areas, as shown in Figure 4.5.

The proposed strain gauges' dimensions are shown in Figure 4.6. More details can be found in the Appendix section of this dissertation. The thinnest part of the strain gauge would be 50 μm in width. There are several ways to make strain gauges. In the MEMS field, photolithography process is one of the most well-known process to make thin films. In the previous research [37], [134], copper electrodes and copper strain gauges were made by etching copper films which initially covered the polyimide film. The film was an adhesiveless polyimide copper clad laminate with 25-μm-thick of polyimide film and 18-μm-thick of copper layer (MC18-25-00FRM, Nippon Steel Chemical Co., Ltd.). In this process, as shown in Figure 4.7, positive type photoresist was spin-coated on the copper layer and patterned to the desired shape using UV light and a photomask. The photoresist was then developed to expose the part of the copper film that had to be etched, and then etching process was done. After the cleaning and cutting process, the film was ready to be used. The example of the outcome is shown in Figure 4.8.

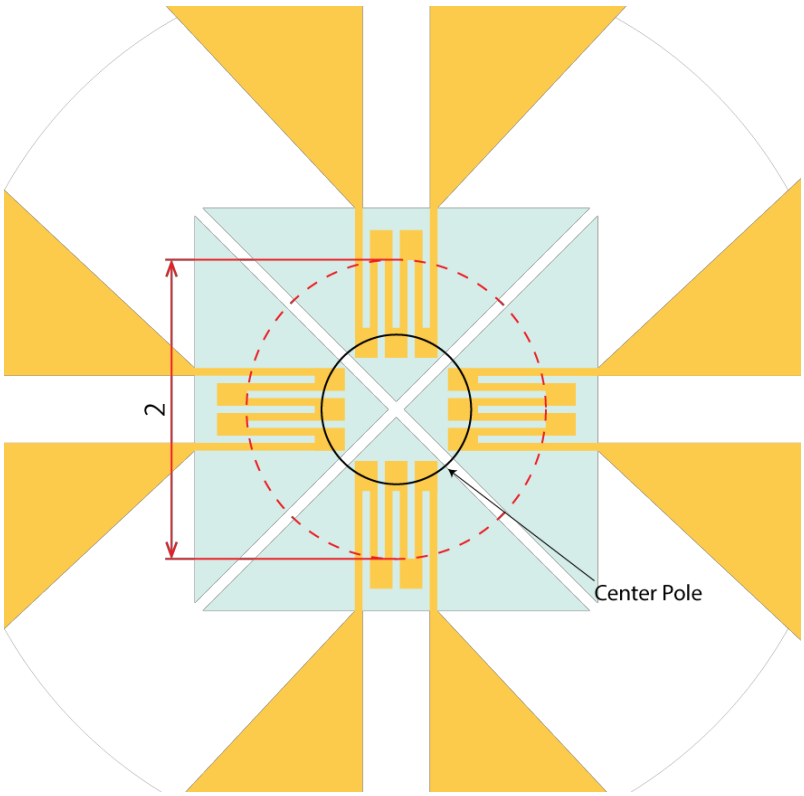

Figure 4.5 The strain gauge area around the center pole. Within the red dotted circle is the hole on the base of the device, and the green areas are the strain gauges areas.

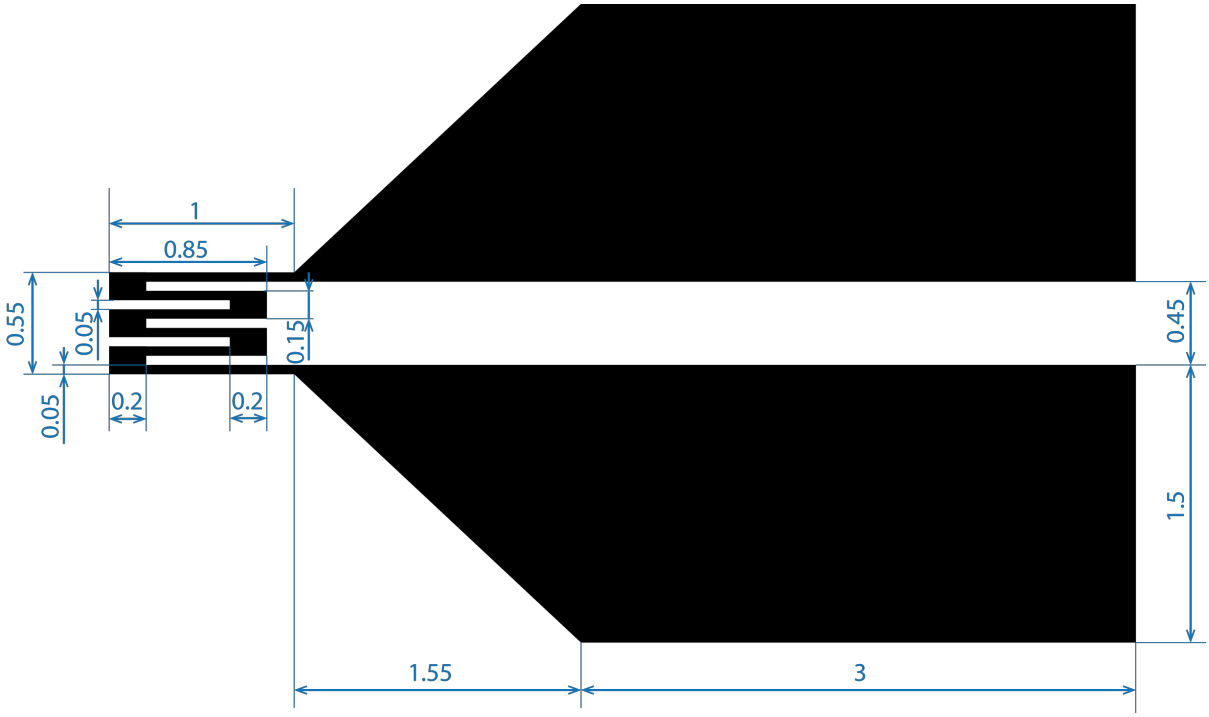

Figure 4.6 Dimension of the strain gauge in mm

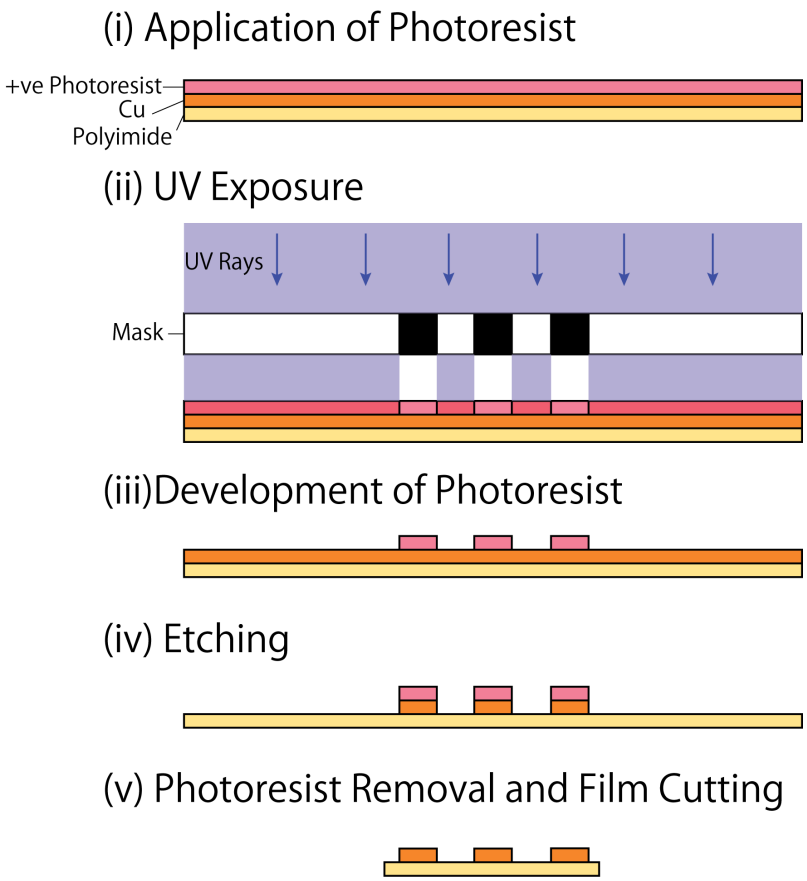

Figure 4.7 Electrode patterning process including etching process

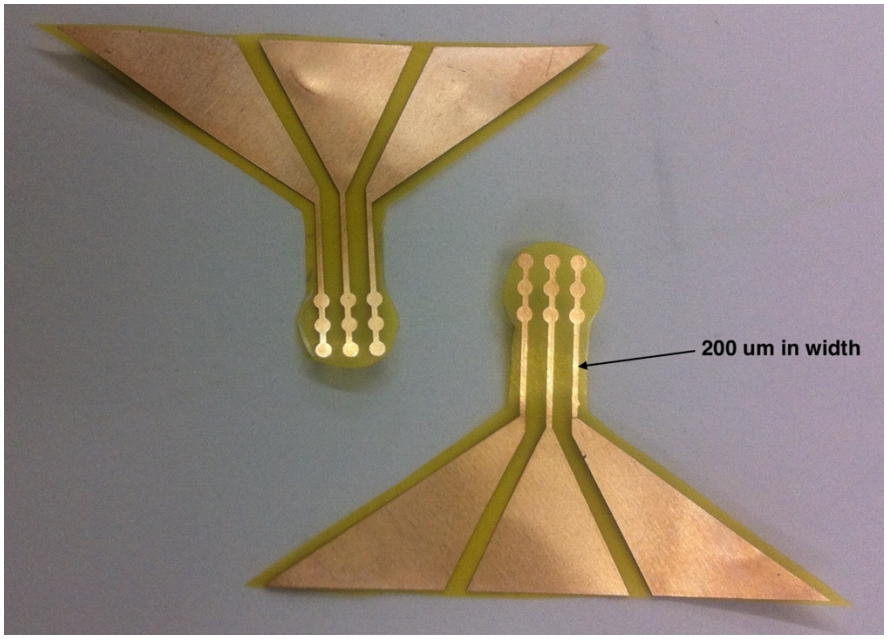

Figure 4.8 Electrodes that had been patterned with copper etching process

Wet etching process will usually cause undercut and etch bias, as shown in Figure 4.9, because of the different etch rates for lateral and vertical direction, or also known as anisotropic etching. So, the end product would normally have some difference in dimension from the mask in width. As reported in the previous device in [37], as shown in Figure 4.8, the thinnest part of the electrodes is designed to be 200 μm in width. This dimension is flexible, which means difference in the dimension of electrodes' wiring were tolerable and would not affect the sensing mechanism of the device. So, using this method to pattern the electrodes was completely acceptable.

However, in this research, the finest part of the strain gauge would be the most important part for the sensing mechanism of this sensor device. The width of the strain gauge will determine the resistance values. Therefore, using the etching method to fabricate the strain gauge would not be suitable in this case. Other method that can be used to pattern the strain gauge is metal vapor deposition, such as physical vapor deposition (PVD), chemical vapor deposition (CVD), and electrochemical deposition (ECD). In this research, PVD process, or more specifically resistive thermal evaporation technique is used to pattern the strain gauges.

Resistive thermal evaporation is a process that uses electrical energy to heat material to its evaporation point so that it can be deposited to form a thin film at the designated substrate. This process requires a very high vacuum environment, so that the vaporized material's molecules can travel as far as possible before it collides with gas molecules. Collisions with gas molecules would cause the vaporized molecules to change their directions, thus can affect the consistency of coverage on the substrate. Furthermore, some gas molecules can interact with the vaporized molecules, hence the purity of the film will be affected if there are gas molecules exist during the vaporization process [135].

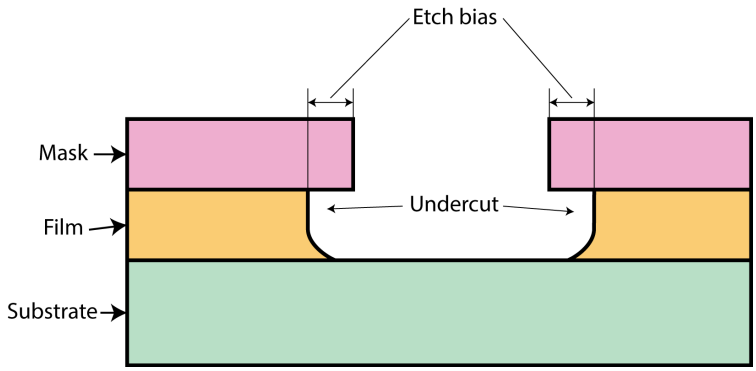

Figure 4.9 Undercut and etch bias that cause by anisotropic etching process

The fabrication process is shown in Figure 4.10. The details of the strain gauges patterning process are described as follows:

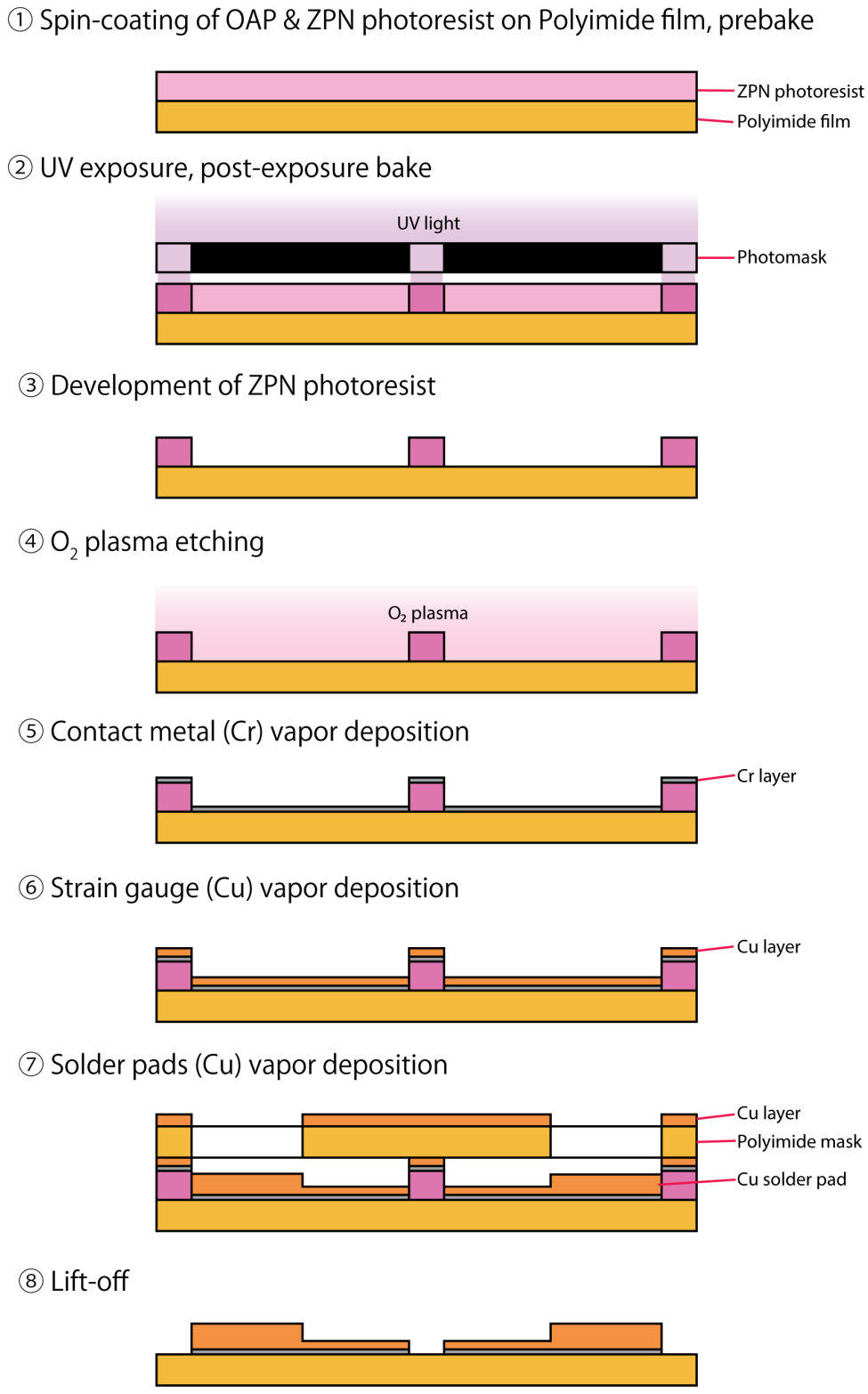

Figure 4.10 Fabrication process of strain gauges

1) Spin-coating of photoresist and prebake

Firstly, 50 μm-thick polyimide film (The Nilaco Corp.) was cut, cleaned and set on a glass substrate (Micro Slide Glass S9111, Matsunami Glass Ind., Ltd.) using Kapton tapes. A primer layer called hexamethyldisilazane (HMDS) (OAP, Tokyo Ohka Kogyo Co., Ltd) was spin-coated on the surface of the polyimide film to enhance the adhesion of the photoresist to the film using Mikasa Spincoater 1H-D7 (Mikasa Co., Ltd). Then, a negative type photoresist called ZPN1150-90 (ZEON Corp.) was spin-coated and the film was prebaked on a hotplate (EC Hotplate EC-1200N, AS ONE Corp.) to promote a strong adhesion of the photoresist to the polyimide film.

2) UV exposure and post-exposure bake (PEB)

After the film was cooled down to room temperature, a photomask (Tokyo Process Service Co., Ltd.) with the strain gauge pattern was placed on the film. The details of the design and dimensions of the photomask is described in the Appendix section of this dissertation. The film and photomask were then placed on a mask aligner (Union EMA-400, Union Optical Co., Ltd.) and exposed to UV light. Because negative type photoresist was used, the part that had been exposed to UV light would become insoluble to the developer liquids. After the exposure, the film was baked to enhance the crosslinking of the polymer structure of ZPN1150-90 photoresist.

3) Development of photoresist

NMD-3 2.38% developer (Tokyo Ohka Kogyo Co., Ltd) was used as the developer for the ZPN 1150-90 photoresist. The exposed film was immersed in the developer solution. In this step, the part that had not been exposed to UV light was removed. The film was then rinsed with pure water to remove the excess photoresist solution.

4) Oxygen (O_2) plasma etching

To enhance the adhesion between metal layer and polyimide film, the film was then etched with O_2 plasma. O_2 plasma etching is believed to increase the surface roughness of the polyimide film, thus increase the adhesion of metal to it [136]. After the development of photoresist, the film was dried in room temperature and etched in O_2 plasma chamber (Samco Plasma Etching System Model FA-1, Samco Inc.) for three minutes.

5) Chromium (Cr) vapor deposition

The film with patterned photoresist was set in the vacuum chamber for metal evaporation process. Cr grains (1 - 5 mm 99.9%, The Nilaco Corp.) were placed on the boat of the resistive thermal evaporation system (Sanyu Electron Co., Ltd.). The metal was then set to vapor-deposited to the film until the thickness became 35 nm. The Cr layer act as the contact layer between polyimide film and copper strain gauges [137].

6) Copper (Cu) strain gauge vapor deposition

Next, Cu wire (ϕ0.50 mm 99.9%, The Nilaco Corp) were cut to small pieces about 8 to 10 mm. The cut wires were then placed inside the evaporator boat and vapor-deposited to the film. The thickness was 110 nm.

7) Cu solder pad vapor deposition

The part of the strain gauge to be connected to the measurement system, or the solder pad, had to be thicker to make sure the wires would not be taken off from the strain gauge easily. So, more copper need to be vapor-deposited to the solder pad part. A polyimide mask was made by cutting a polyimide film to the shape of the solder pad, as shown in Figure 4.11, The mask was set on the strain gauge film, and then Cu was vapor-deposited to about 250 nm in thickness. It means that the total thickness for the solder pads was about 350 nm.

8) Lift-off process

The final process for the strain gauge making is the lift-off process. Acetone was used to wipe the photoresist off from the polyimide film. The fabricated strain gauge is shown in Figure 4.12.

The details for each process are summarized in the Appendix section of this dissertation.

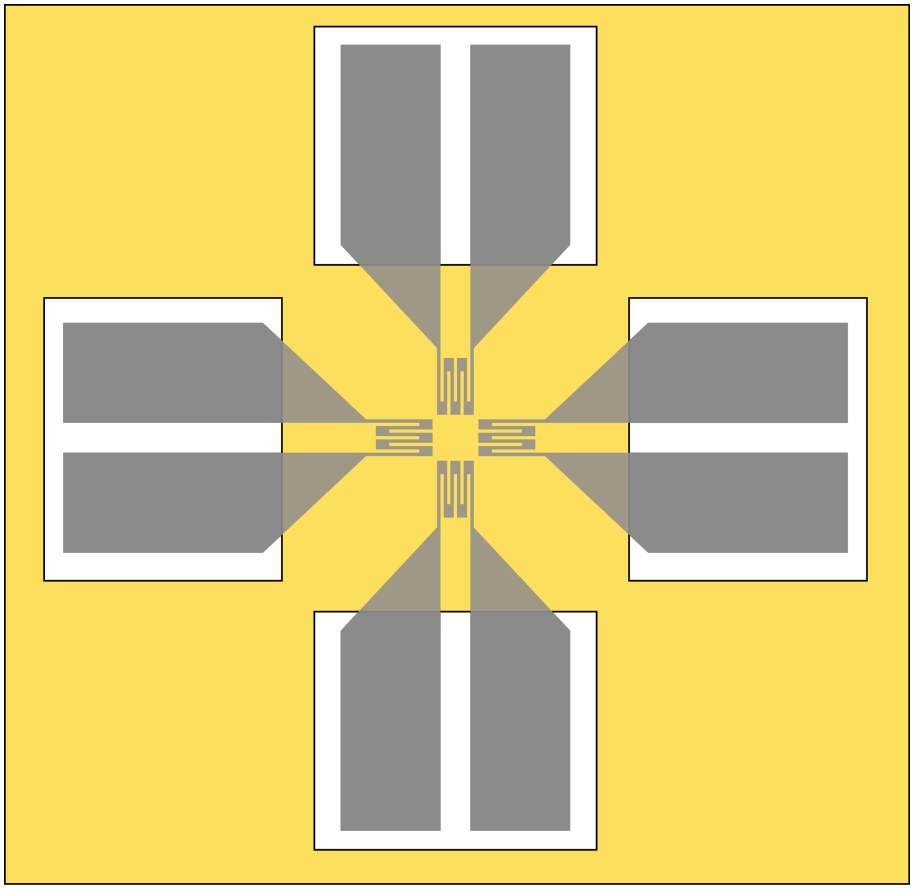

Figure 4.11 Polyimide mask for the solder pads of the strain gauges. The yellow area represents the polyimide mask, while the strain gauges are shown in grey. The polyimide mask exposed the solder pad parts of the strain gauge.

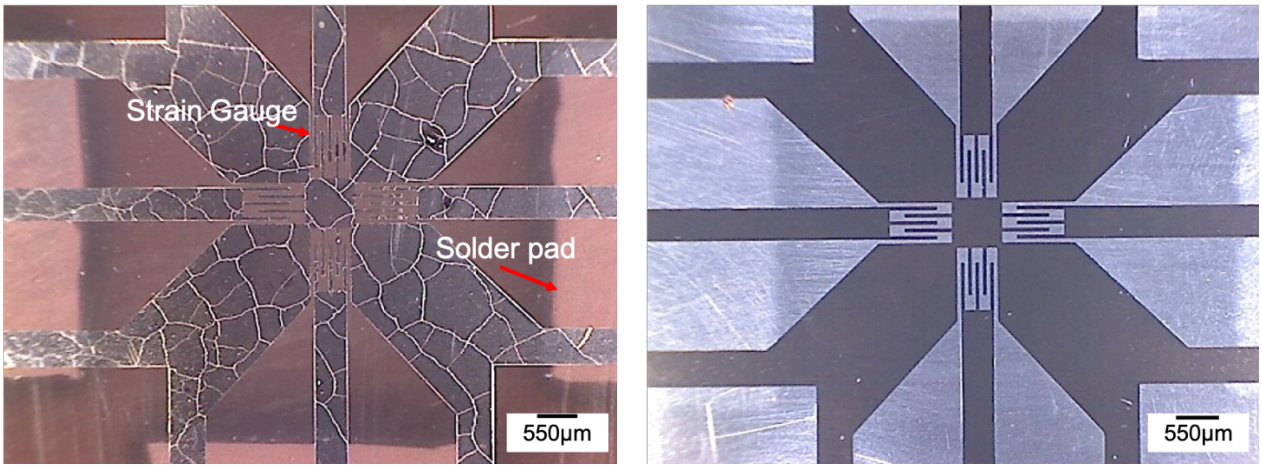

Figure 4.12 The fabricated strain gauges before lift-off process (left) and after lift-off process (right). The cracked area in the left figure is the area to be lifted off.

4.2 Assembly process

The base, pole, and strain gauges were then assembled to form the sensor device. The three steps of assembly process were illustrated in Figure 4.13.

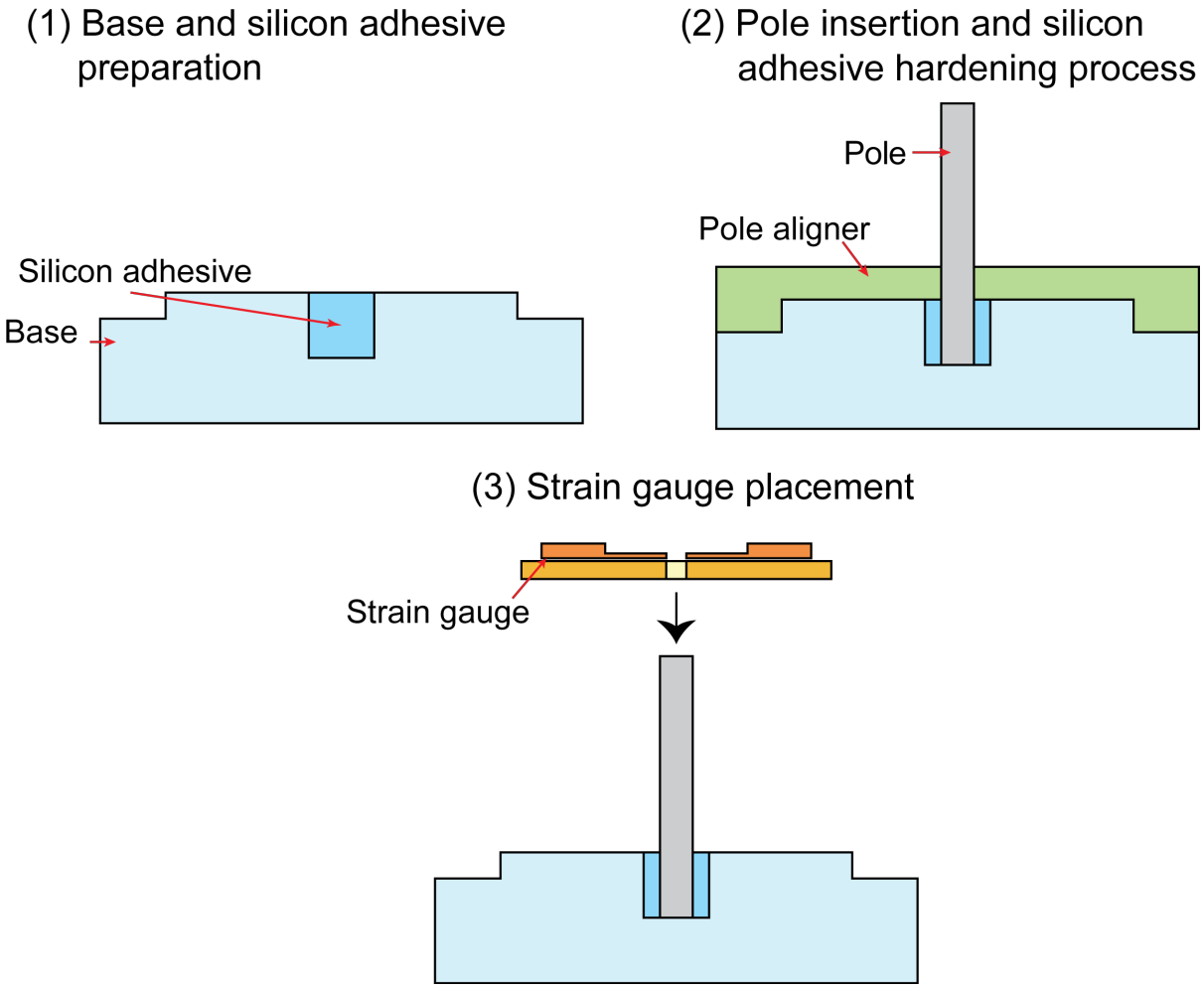

Figure 4.13 Assembly process of the sensor device's components

1) Silicon adhesive preparation

Silicon based adhesive paste（Dow Corning® 3145 RTV MIL-A-46146 adhesive/sealant, Dow Corning Corp.) were prepared by mixing the elastomer paste with thinner (RTV Thinner, Dow Corning Toray Co., Ltd) with the ratio of 2 mL of thinner for every 1 g of the paste. The mixture is then put in vacuum desiccator (VL-ALN, AS ONE Corp.) for about 30 minutes, or until all the air bubbles were dismissed. The silicon elastomer paste was then inserted in the hole of the device's base using tapered syringe, making sure no air bubbles trapped inside the hole.

2) Center pole setting

The stainless-steel center pole was inserted inside the hole. The silicon adhesive that flown out from the hole was wiped using cotton bud that was soaked with ethanol. An acrylic pole aligner, as shown in Figure 4.14, was inserted slowly through the tip of the pole to fit the base of the device. The pole aligner was made to make sure the pole stayed vertically in the center of the base, as shown in Figure 4.15. The device was then put inside a vacuum desiccator for 72 hours to cure the silicon adhesive.

3) Strain gauge placement

After the silicon adhesive was cured, the pole aligner was removed from the device. The top of the base where the polyimide-strain gauge film will be stuck to was marked with permanent marker pen. This was to make sure that the position of the strain gauge would be in the middle of the base. Double-sided tape was set on the base of the device to be the glue for the polyimide-strain gauge film. A ϕ2 mm hole was cut at the center of the double-sided tape, and the tape was insert through the hole of the pole of the device and stuck slowly on the base. The center of the polyimide film with strain gauges was cut in X shape, as shown in Figure 4.16, so that the strain gauges are separated from each other. The film was then fixed onto the acrylic base by piercing the pole through X hole of the polyimide-strain gauge film, from the bottom side of the film. The process was done carefully, making sure the pole was in the middle of the four strain gauges, and the strain gauges were leaned against the pole in upward manner.

The fabricated device is shown in Figure 4.17.

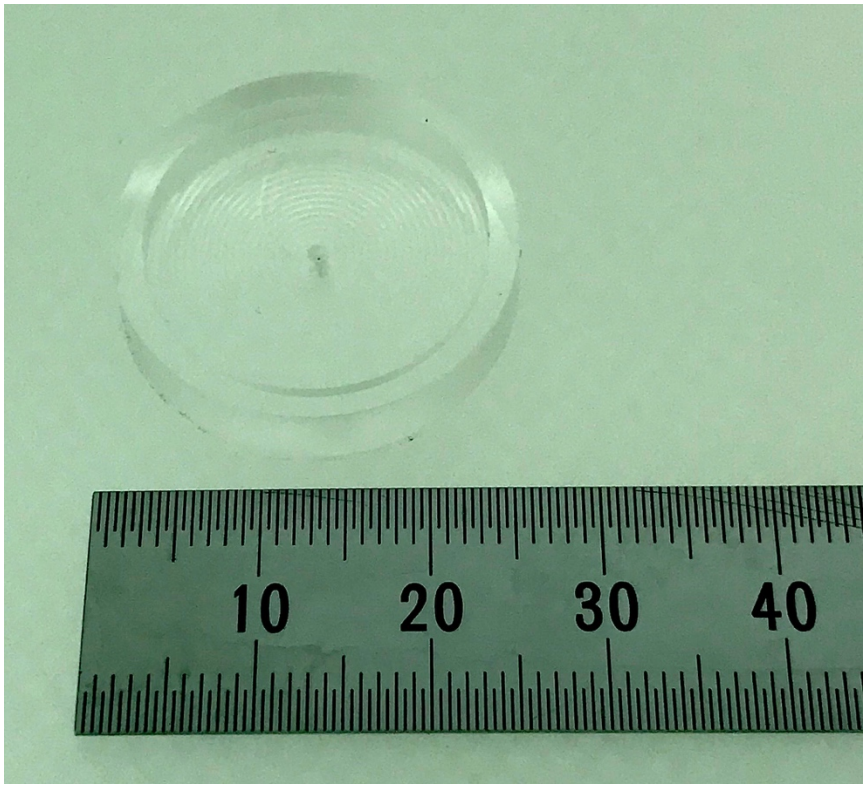

Figure 4.14 The acrylic pole aligner

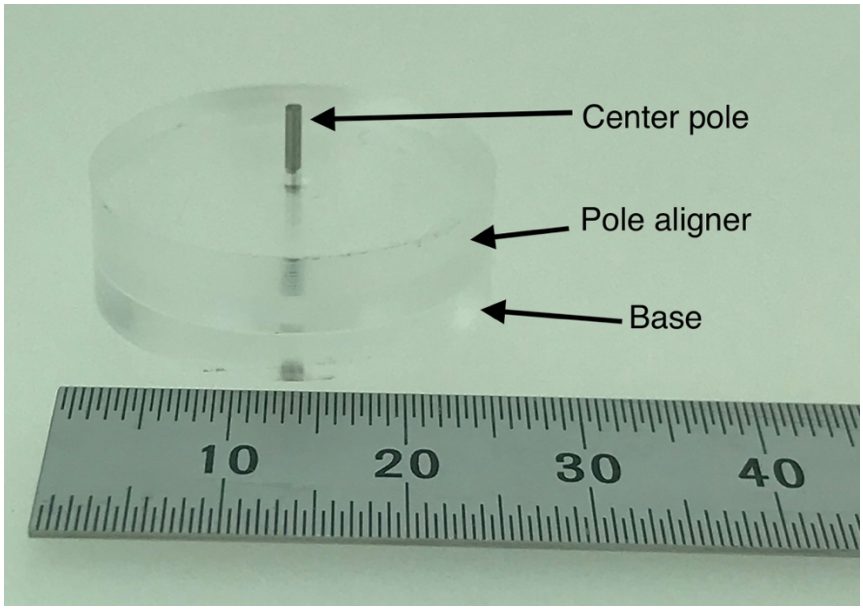

Figure 4.15 The setting of center pole to the base using pole aligner

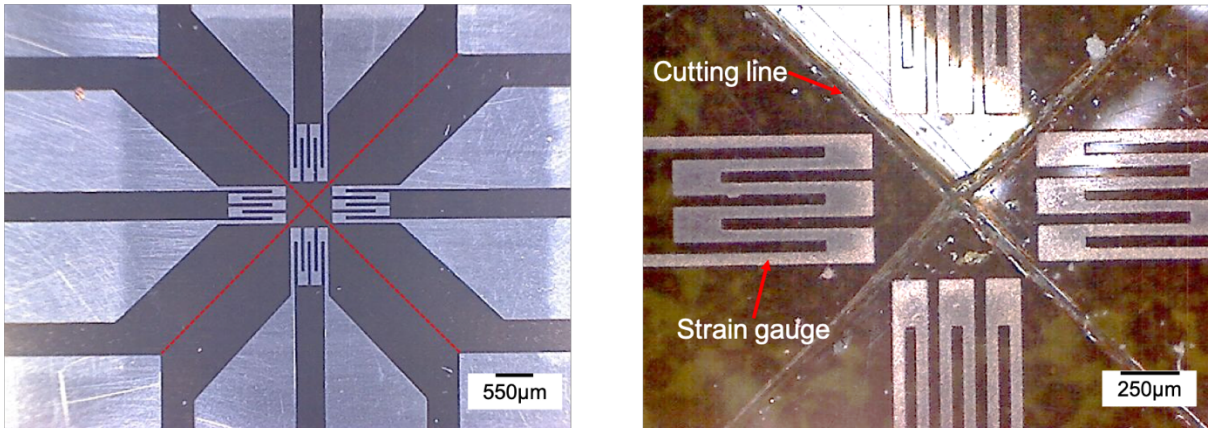

Figure 4.16 Strain gauges were separated by cutting the center in X shape. The red dotted line in the left figure shows the cutting line

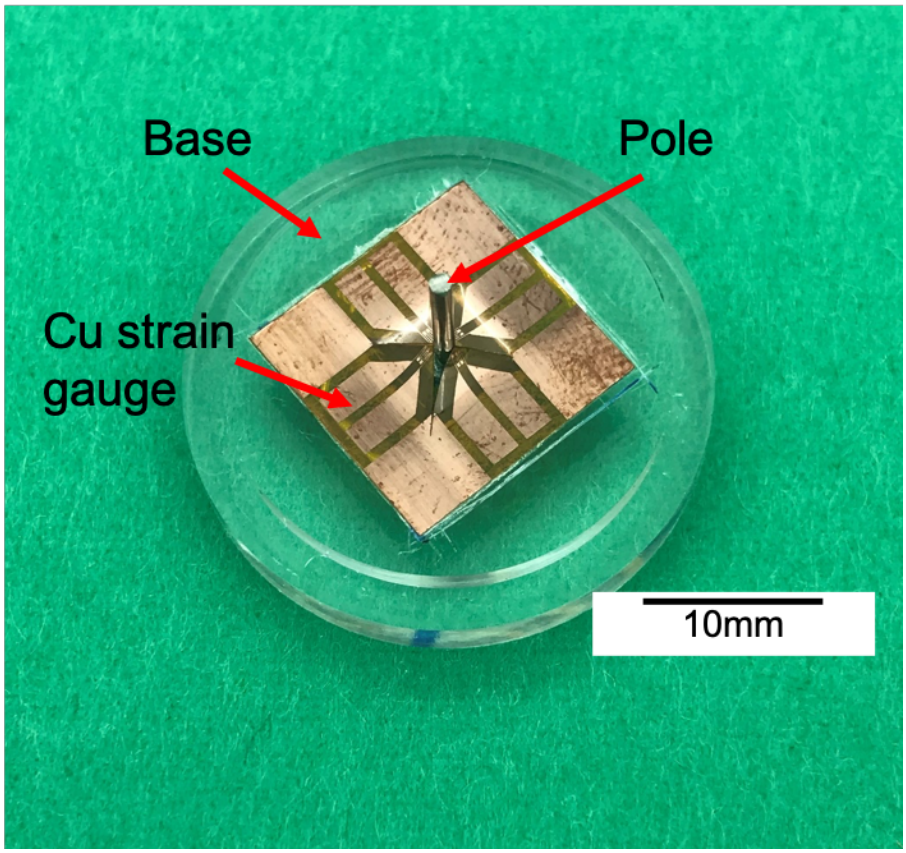

Figure 4.17 The fabricated device

5

EXPERIMENT RESULTS AND DISCUSSIONS

5.1 Result and discussion from the fabrication process

The resistance of the fabricated strain gauge can be calculated using equation 1.1. The resistivity of copper is 1.68×10^{-8} Ω · m [138]. From the calculation, the resistance of the fabricated strain gauge would be 11.7 Ω. On the other hand, the resistance of the fabricated strain gauge that was measured using a digital multimeter is 42.6 ± 12.9 Ω. There was quite a large difference in the theoretical and actual values of the resistance. The reason behind this phenomenon might be because of the inconsistency of the copper coverage on the polyimide film during vapor-deposition process.

The angle of the deflection of strain gauges after the fabrication process was measured from the surface of the base using a laser microscope (Keyence Corp.). The strain gauges were labelled as SG 1, SG 2, SG 3 and SG 4 each, arranged in a counter-clockwise manner. The deflection angles were summarized in Table 5.1.

Table 5.1 Deflection angle of each strain gauge in a sensor device

Strain Gauge	Deflection angle (°)
SG 1	41.4
SG 2	35.5
SG 3	34.2
SG 4	39.5

From the values of the deflection angles, it is spotted that the highest angle difference was between SG 1 and SG 3, which is 7.2°. Difference in the angle values for all four strain gauges occurred due to the misalignment during the fabrication process of the device. The initial angles were not so high, therefore there were a still a lot of space for the strain gauge to bend during pressure application.

5.2 Measurement Systems

Experiments were done to evaluate the device ability to detect pressure applied to the sides of the device. The test involved is the sensitivity test, the detection of direction of load, and the repeatability and frequency test. During these experiments, pressure would be applied to the side around the center pole, while the change of resistance of each strain gauge would be measured.

5.2.1 Pressure Application System

The fabricated sensor device was set on the middle of a rotary stage (High-Grade transmission type rotary stage ϕ 40, Chuo Precision Industrial Co., Ltd.) using double sided tape. The middle of SG 1 was set as 0°. Pressure was applied to the sides of the center pole using micro strength evaluation system (Shimadzu Micro Autograph MST-I, Shimadzu Corp.) while the system (Shimadzu TRAPEZIUM X materials testing software, Shimadzu Corp.) recorded the values of load and displacement of the jig throughout the experiment. The photograph of the system is shown in Figure 5.1.

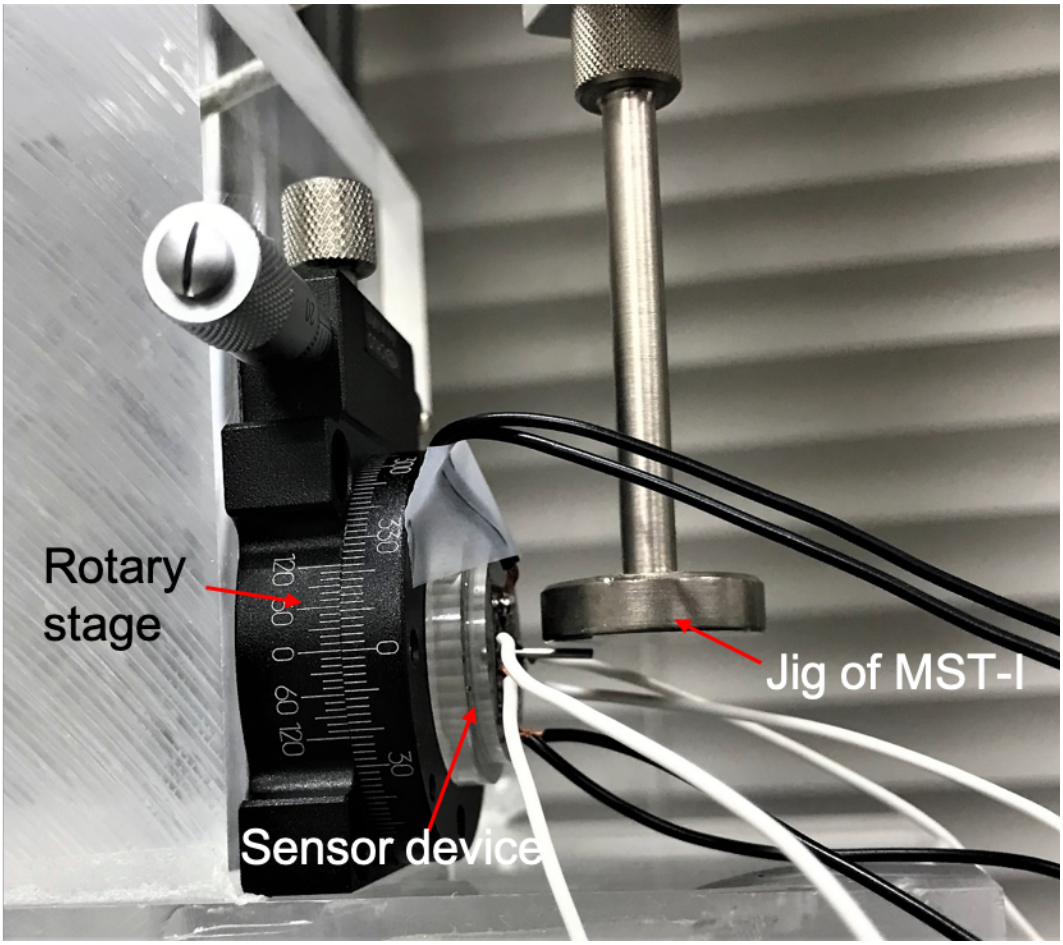

Figure 5.1 The experiment setup shows the sensor device fixed vertically on a rotary stage near the jig of micro strength evaluation system MST-I

5.2.2 Resistance Measurement Systems

The bending of the strain gauge during pressure application will cause resistance change. In this research, the resistances of the strain gauges were measured using four wire resistance measurement method. This method was chosen because the circuit is simple and easy to manage. Wires were soldered to the solder pads of the strain gauges, and the other ends were connected to a circuit as shown in Figure 5.2. The voltages at the strain gauges and the 100 Ω resistor were measured using data logger (Keyence NR 500 series, Keyence HA 08 High Speed Analog Measurement System, Keyence Corp.), and recorded using Keyence NR-H7W software (Keyence Corp.). The resistances of the strain gauges could be calculated from the measured values the equation as follows:

$$R_{SG} = \frac{V_{SG}}{V_{100}} R_{100} \qquad \text{Eq. 5.1}$$

In this equation, R_{SG} is the resistance of strain gauge, V_{SG} is voltage at the strain gauge, while R_{100} and V_{100} is the resistance and voltage across the 100 Ω resistor respectively.

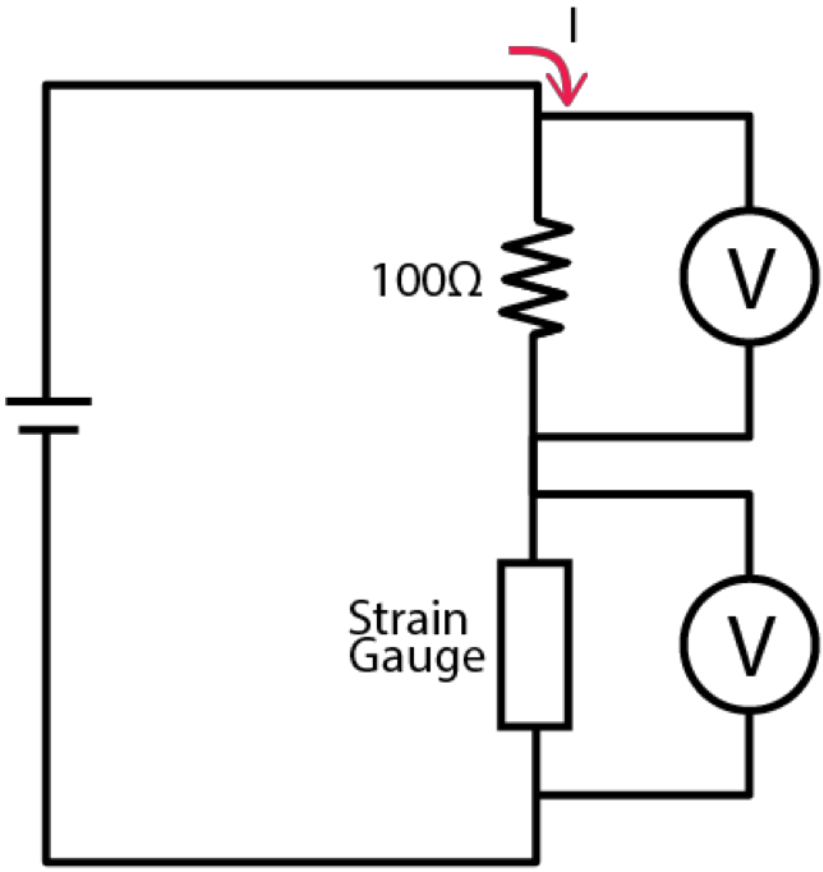

Figure 5.2 Four wire measurement circuit to measure the resistance of the strain gauges. The voltage of the100 Ω resistor and strain gauge were measured using data logger

5.3 Sensitivity Test

5.3.1 Experiment Method

Load was applied to the side of the center pole that has a strain gauge bent and leaned against it. The direction is illustrated in Figure 5.3. The jig of the micro strength evaluation system was placed at 4 mm from the tip of the pole. Loading and unloading speed was set to be 20 mm/min. The change of resistance of the strain gauge at the compressed side is measured and recorded during loading and unloading. The maximum displacement of the load was set to 1 mm, and the load was recorded throughout the experiment. The experiment was done four times.

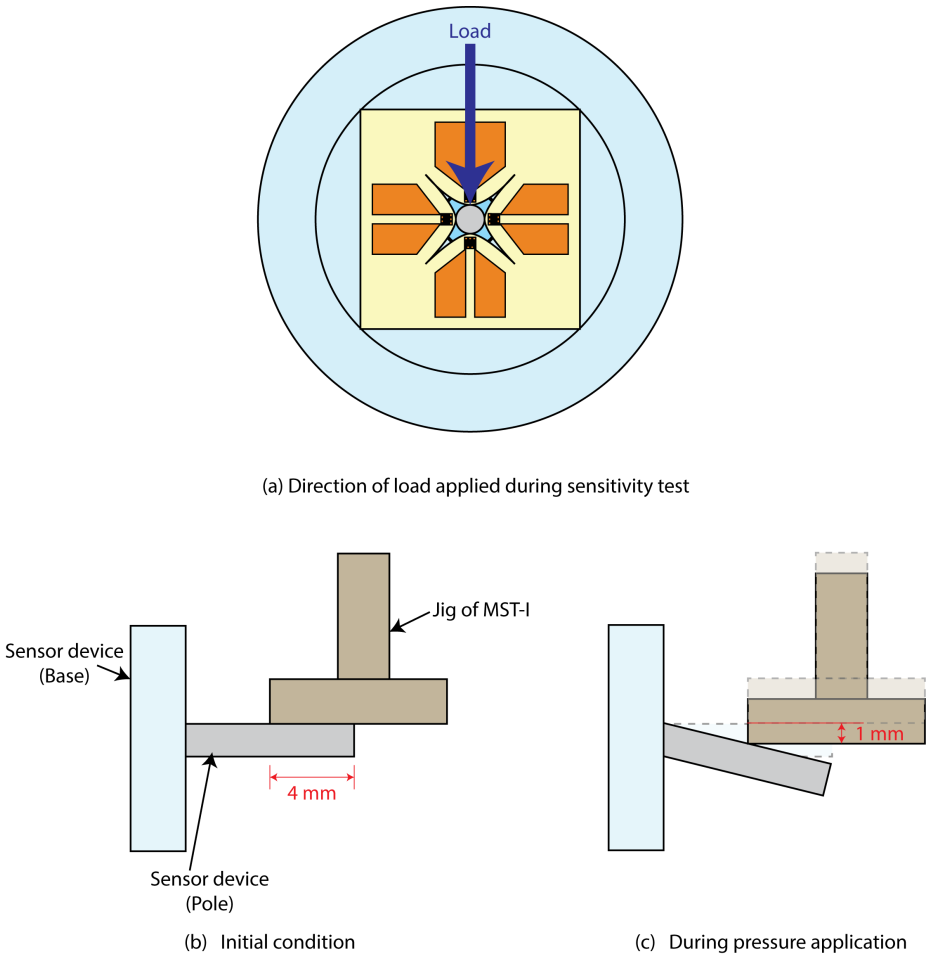

Figure 5.3 (a) Top view of the sensor device. Blue arrow shows the direction of load applied to the center pole. (b) The initial state of the experiment setup, and (c) movement of the center pole during load application with 1 mm jig displacement

5.3.2 Result and Discussions

The result of the sensitivity experiment is shown in Figure 5.4. It is observed that the change of resistance ratio of the strain gauge at the compression side of the device decreased with the increase of displacement and load applied to the center pole. The decreasing of the values of resistance is because the strain gauge at the compression side of the device became shorter that its initial length.

The sensitivity of this tactile pressure sensor device could be defined as the proportional coefficient between the resistance change ratio and the displacement of center pole, or the load applied to the center pole. From Figure 5.4 (a), it is observed that the sensitivity of the sensor device per unit 1 mm of displacement is -0.016 mm^{-1}. The sensitivity value per unit 1 N of load is appeared to be -0.313 N^{-1}, as read from the gradient of the graph in Figure 5.4 (b). The sensitivity values are comparable with tactile sensor devices that had been developed by other researchers [97], [139]–[141], and are good enough to detect small pressure and load while using resistance measurement systems that are available commercially.

Hysteresis were observed in both the graphs of the sensitivity tests. The one that appeared in the resistance change ratio vs load in Figure 5.4 (b) was larger than the one in Figure 5.4 (a). The hysteresis was believed to be caused by slip of the polyimide-copper strain gauge film from the pole. This is because the film was not glued to the pole, instead it leaned against the pole naturally by the fabrication process of the sensor device.

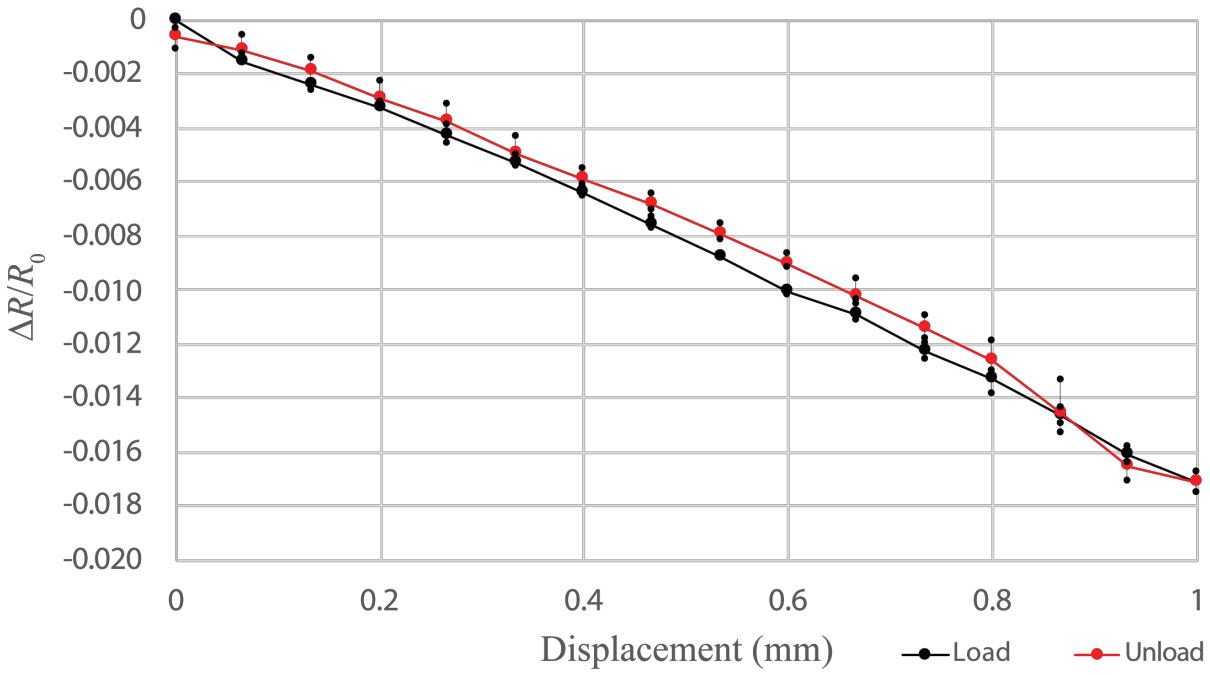

(a)

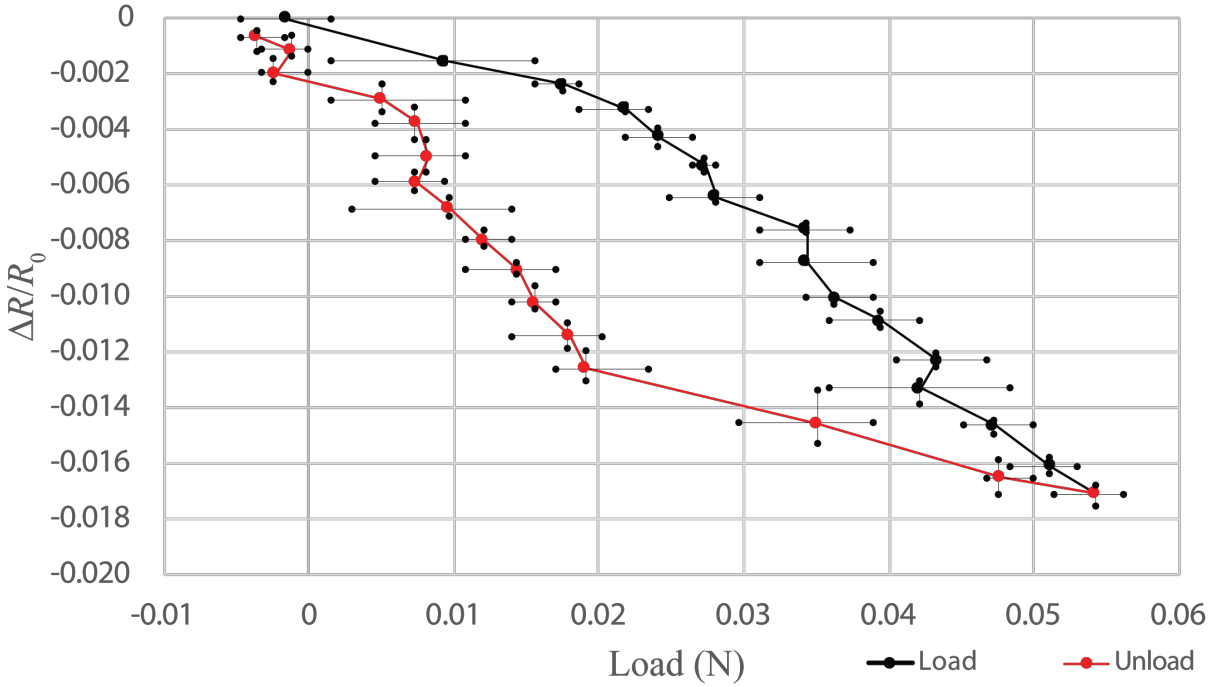

(b)

Figure 5.4 Results for the sensitivity of the sensor device, (a) resistance change ratio vs displacement of the center pole, and (b) resistance change ratio vs load applied to the side of center pole. The error bars represent the variance defined by maximum and minimum values from four tests.

5.4 Direction of Load

5.4.1 Experiment Method

Load was applied to the sides of the center pole, all 360° for every 15° intervals. The jig is placed at 4 mm from the tip of the center pole, as shown in Figure 5.3 (b). The displacement of the jig of the micro strength evaluation system MST-I was set to be 1 mm. The resistance of all of the strain gauges were recorded simultaneously when the displacement of the jig is 1 mm. 0° is defined as the middle of SG 1, as illustrated in Figure 5.5, and the rotary stage was rotated clockwise for the changing of the angles during the experiment.

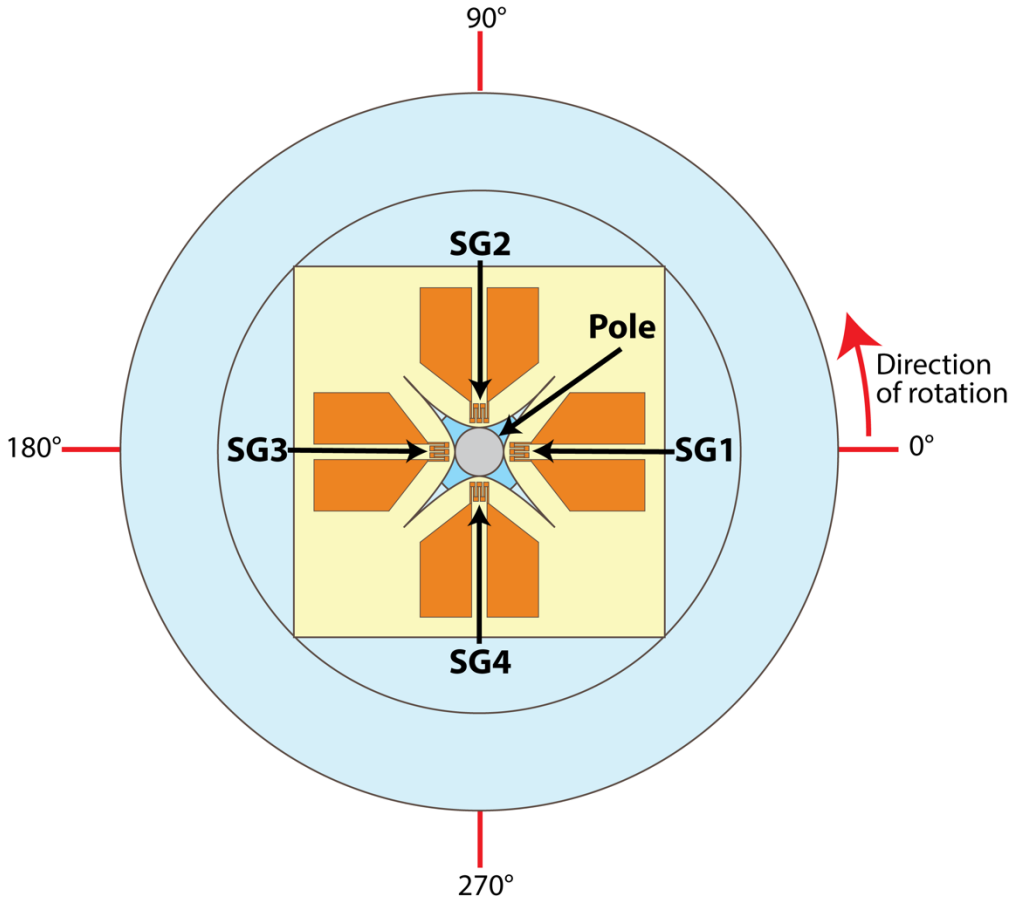

Figure 5.5 The direction of rotation from the top view of the sensor device for the test of direction of load

5.4.2 Result and Discussions

Figure 5.6 presents the result of the experiment of direction of load to the sensor device. The plotted graph shows the change of resistance ratios for each strain gauge were different according to the angle of load. The difference of resistance change ratio for each strain gauge in different angles proves that the device is capable to discriminate direction of load applied to it.

To see the trends of the resistance change ratios for each strain gauge, the results in Figure 5.6 was replotted and pictured in Figure 5.7 (b). For the replotting, 0° is defined as the opposite to the center of each strain gauge. It means that the angles depend on the position of the strain gauge, as illustrated in Figure 5.7 (a). The values of resistance change ratio express a sine-curve trend for each strain gauge, as can be seen in Figure 5.7 (b). The lowest values of resistance change ratio were at 180° and 195°, while the highest were coherent at 270° to 300°. The values of resistance change ratios were observed to be almost constant, but slightly decreasing starting from 315° to 330°, and ended at 75° to 105° from each strain gauge, before they decrease gradually with the increase of the angles.

The values of resistance change ratios were the lowest when load is applied from the opposite side of the middle of each strain gauge, i.e. 180° to 195° in Figure 5.7 (b) because the strain gauges were in the state of the highest bending moment during this time. This makes the length of the strain gauge to be the shortest compared to when load was applied to other directions. The constant values of resistance change ratios are believed as the expression of the limit of the elongation of the strain gauge during the releasing from its initial bending, that caused by the 1 mm displacement of the center pole. Meanwhile, the highest values at 270° to 300° may originate from the asymmetry wiring of the circuits. The consistent result validates a good elastic balancing of the center pole and the deflecting angle of the strain gauges against the pole.

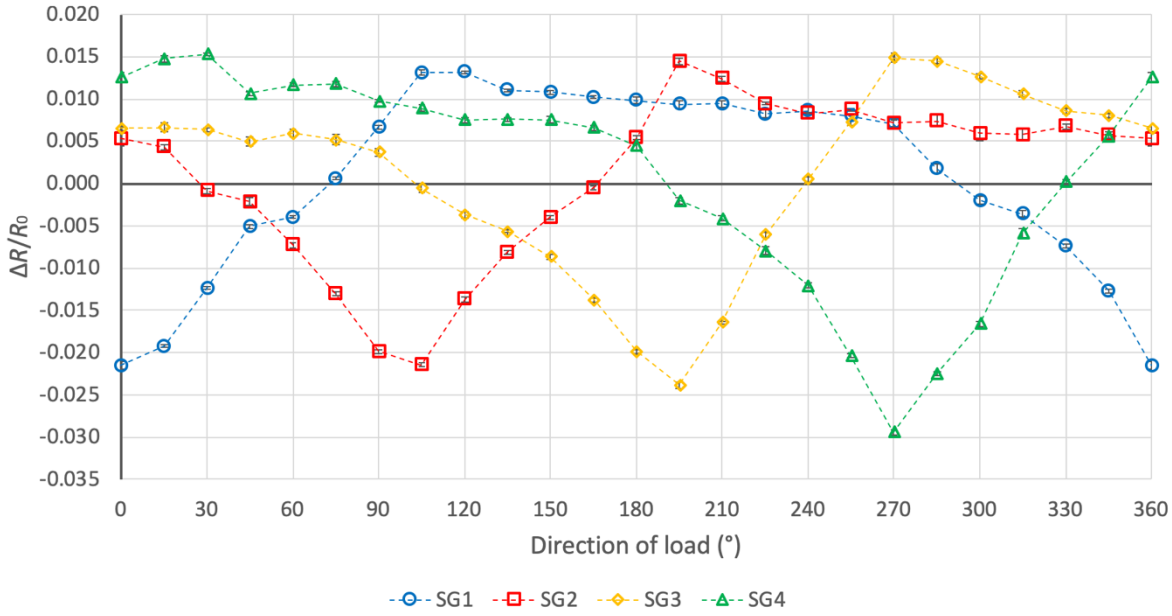

Figure 5.6 Result for the test for direction of load. 0° is defined as the middle of SG 1

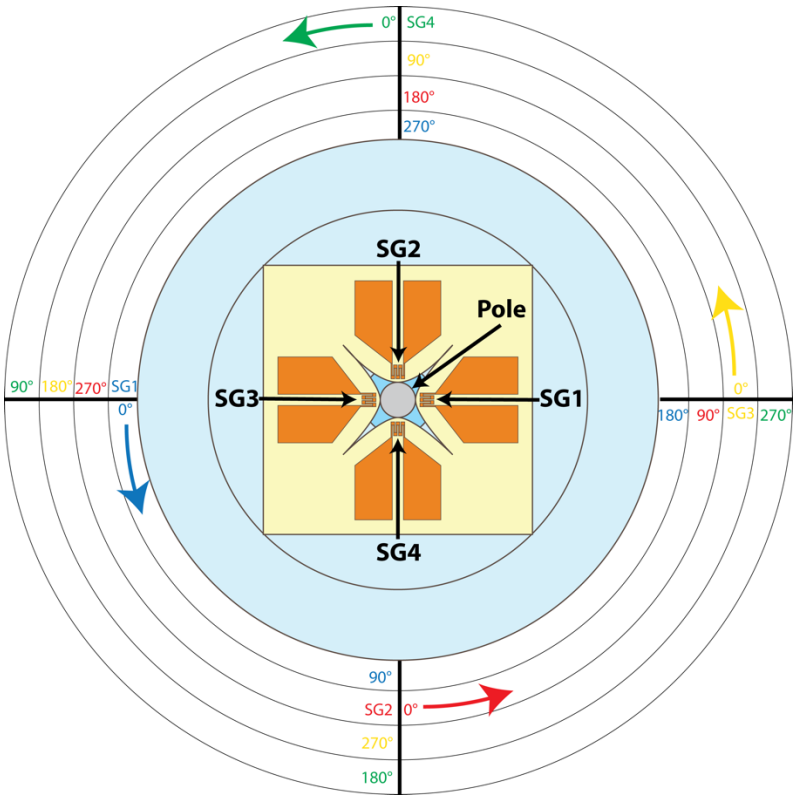

(a) Definition of angles for the replotted graph

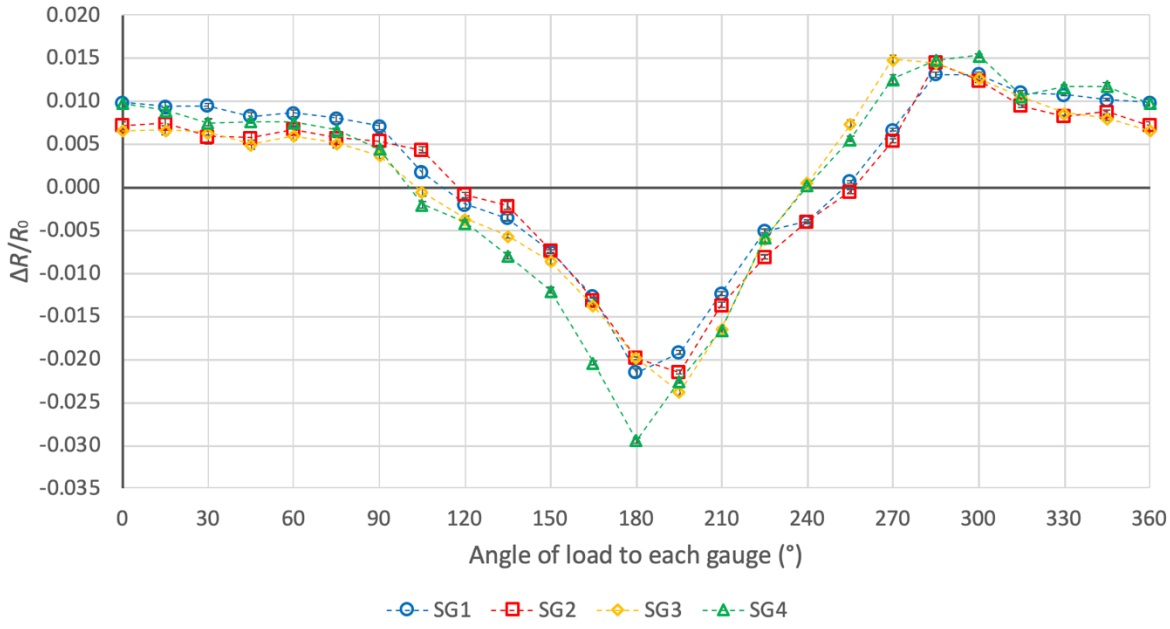

(b) Result for test of direction of load replotted with angles definition in (a)

Figure 5.7 The result of the test of direction of load replotted with 0° is defined as the opposite of each strain gauge

In applying this sensor device to the desired application, the sensor should interpret direction of force based on the obtained values of resistance change ratios. Thus, relations of the resistance change ratio of a strain gauge to its nearest strain gauge in a 90°counter-clockwise turn was calculated and summarized in Figure 5.8. The relative resistance change ratio of strain gauges ΔR_{SG} for each degree of force direction was calculated based on the equations below

$$\Delta R_{SG} = \frac{(\frac{\Delta R}{R_0})_{SG_{0°}}}{(\frac{\Delta R}{R_0})_{SG_{90°}}} \quad \text{Eq. 5.2}$$

Here, the numerator is the value of resistance change ratio of a strain gauge, and the value of resistance change ratio of the strain gauge 90° counter-clockwise from it would be the denominator.

In the x-axis of the graphs in Figure 5.8, 0° is the middle of SG 1 as illustrated in Figure 5.5. The values of relative resistance change ratios in each graph was simplified to maximum value of 5 and minimum value of -5 to illustrate a better view of the trend of the curves. Two sets of cubic curves were observed in each graph for all 360° of force direction, which means that using one relative resistance ratio could not give the exact value of force direction. It could be seen in the graphs that there were two infinity values for ΔR_{SG} for each relation. It is because the resistance change ratios of each strain gauge crosses 0 values at two angles, as seen in Figure 5.6. Therefore, by considering only when the denominator of equation 5.2 is in negative values ($\Delta R/R_0 \leq 0$), we can obtain the direction of force by only one cubic curve for each graph in Figure 5.8.

The algorithm of obtaining direction of force from the values of resistance change ratios of each strain gauge is shown in the flowchart in Figure 5.9. After the resistance change ratio of each strain gauge is obtained, the ones that have negative values would be the denominator of equation 5.2. Then, the resistance change ratio of the strain gauge that was positioned 90° counter-clockwise from it would be the numerator. The values would be whether from the relation of SG1/SG2, or SG2/SG3, or SG3/SG4, or SG4/SG1. After the ΔR_{SG} is obtained, the direction of load can be determined from the graphs in Figure 5.8.

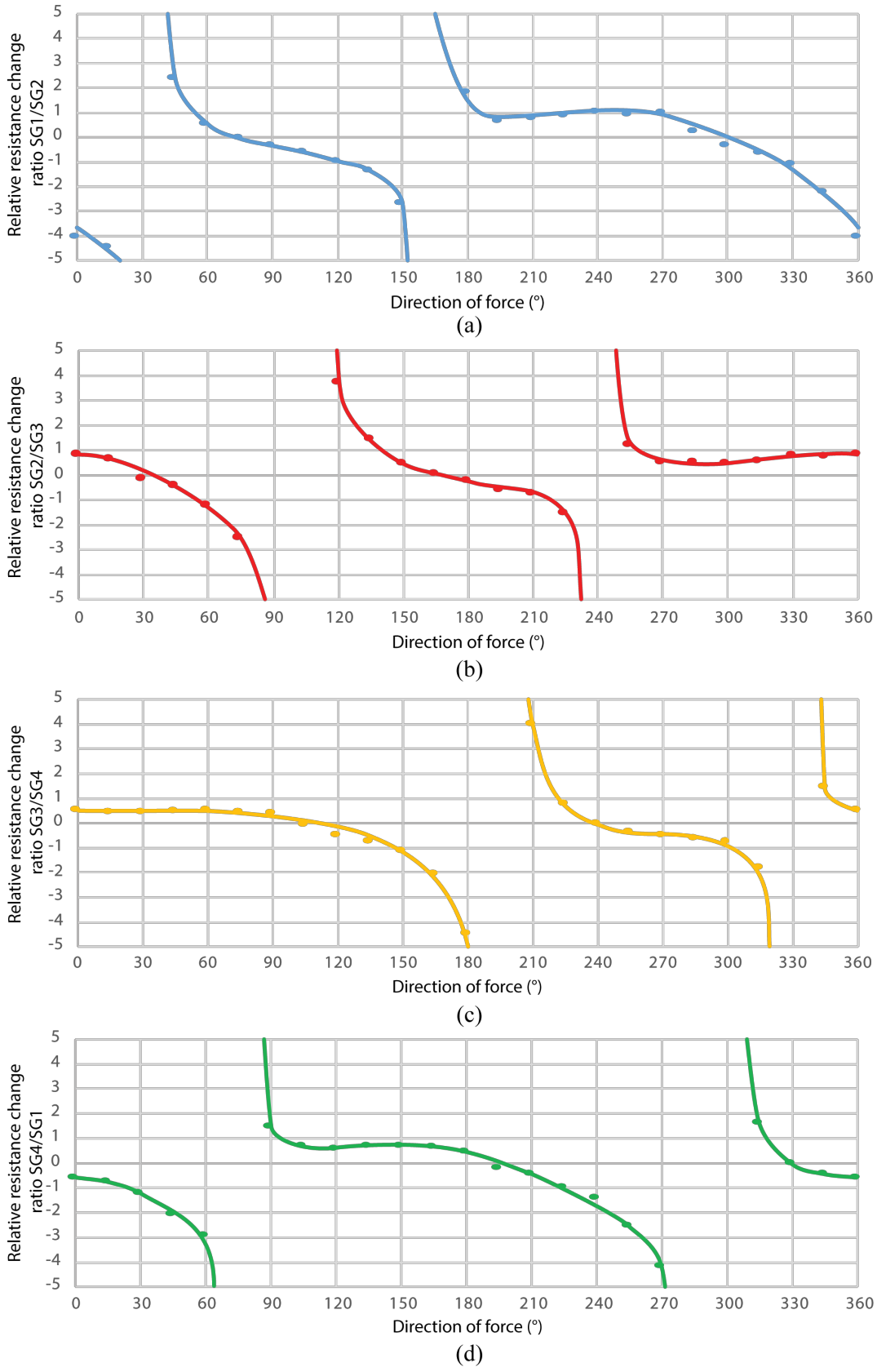

Figure 5.8 Relative resistance change ratio of (a) SG 1 to SG 2, (b) SG 2 to SG 3, (c) SG 3 to SG 4, and (d) SG 4 to SG 1

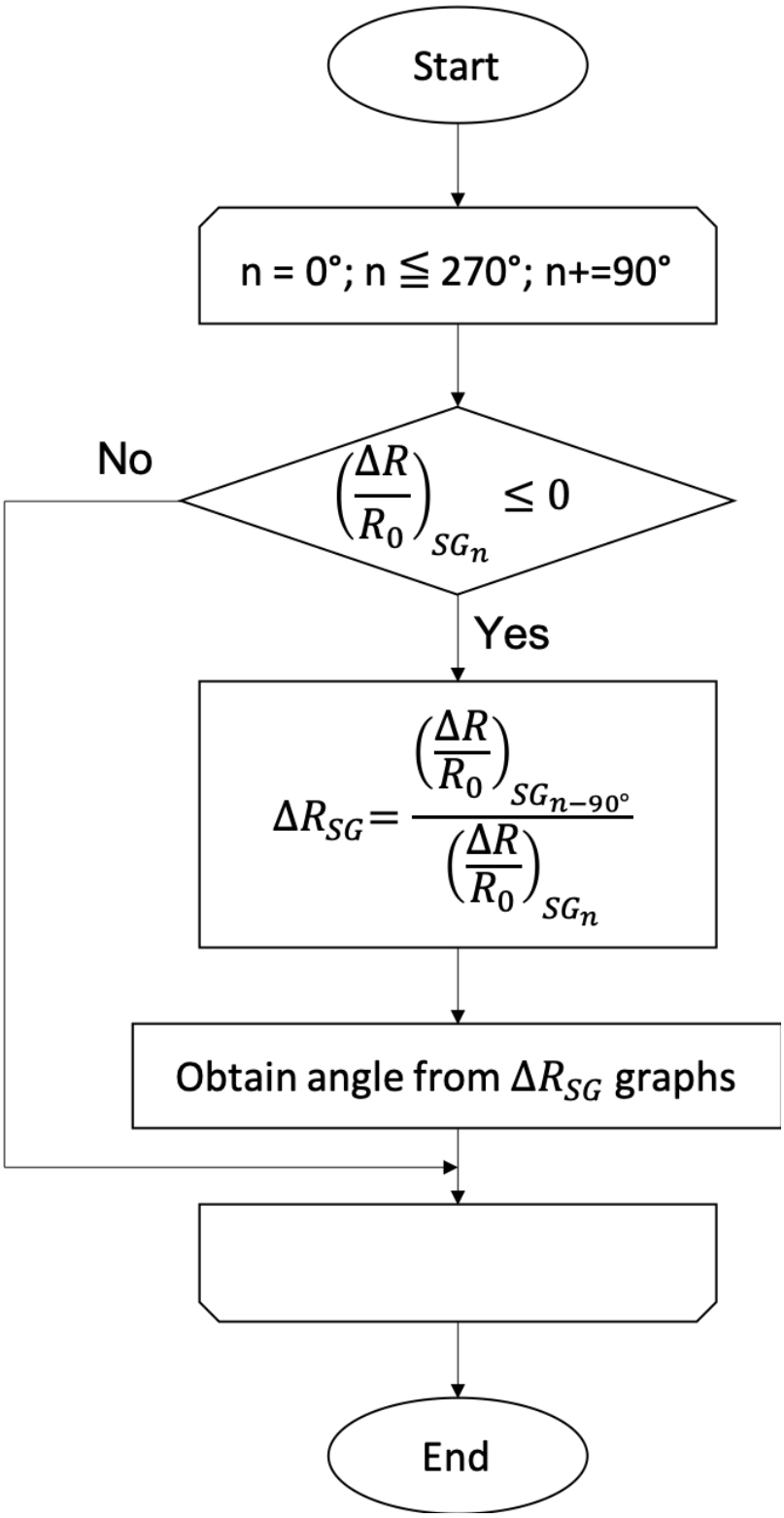

Figure 5.9 The algorithm of obtaining direction of force from the values of resistance change ratios of each strain gauge

5.5 Repeatability and Frequency Test

5.5.1 Experiment Method

Load was applied repetitively to the side of the center pole, directing to the middle of one strain gauge. The frequency of loading and unloading were set to be 0.05 Hz, 0.10 Hz, 0.15 Hz, 0.20 Hz, and 0.25 Hz, while the maximum displacement of the jig of the micro strength evaluation system MST-I was set to 1 mm. The jig is placed at 4 mm from the tip of the center pole, as shown in Figure 5.3 (b). The loading-unloading activity was repeated 10 times for each frequency. The highest resistance of the strain gauge was recorded for each cycle throughout the experiment.

5.5.2 Result and Discussions

The result for repeatability test is shown in Figure 5.10. From the graph, it is observed that the amplitudes of resistance change ratio were constant even the loading-unloading frequency were changed. Moreover, no significant delay was observed during the test, and no degradation of the sensor was seen after the test. This result approves loading repeatability of the sensor device in low frequency load application. The values of frequency tested was not high to suit the application of the sensor device, where movements in narrow channels are usually in low speed. The consistency of the amplitudes proves that the hysteresis observed in Figure 5.4 (b) did not give a significant effect on the performance of the sensor device.

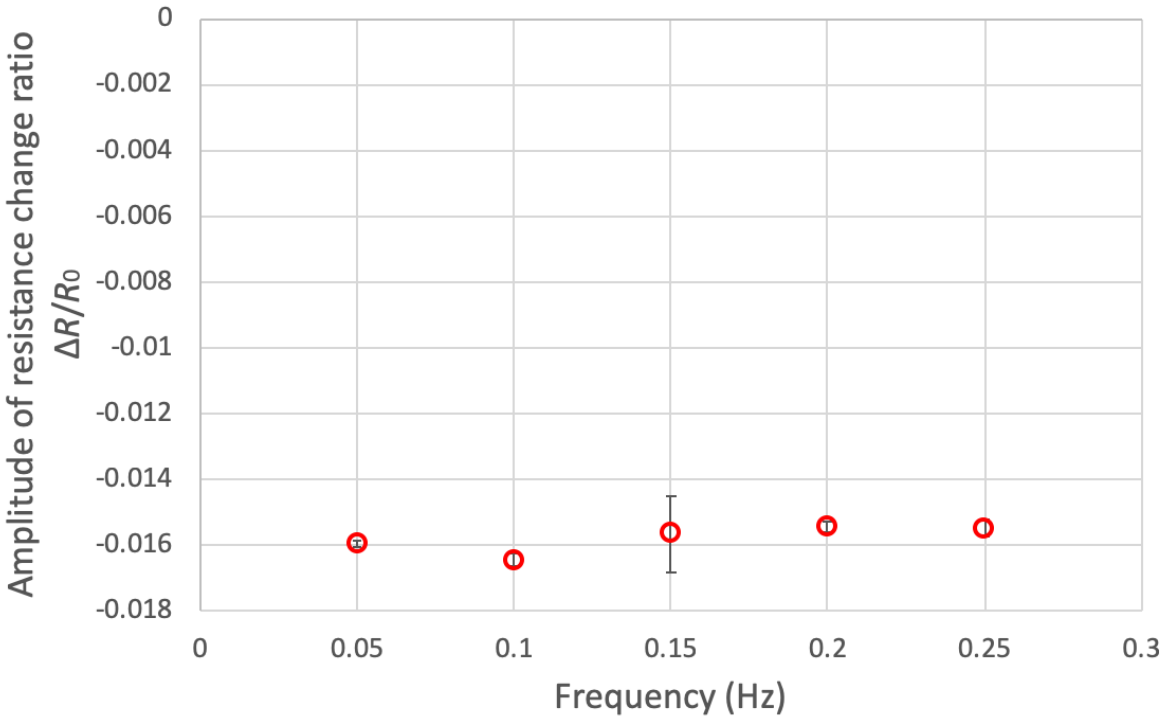

Figure 5.10 Result for repeatability test shows the constant amplitudes for different frequency of loading-unloading

6

CONCLUSION

6.1 Conclusion

This dissertation reports about design and fabrication process of a tooth-inspired tactile sensor for the detection of multidirectional force. There are various kinds of tactile sensors that had been developed by researchers around the world for various applications. Among the fields that demand the usage of tactile sensor is medical and surgery field because of the practical and advantageous application of minimally invasive surgery (MIS), and oil and gas field for pipeline inspection robots. Small yet sensitive tactile sensors are required as the operations should be done in narrow spaces. Besides, the sensor needed had to be able to detect force from different direction and distinguish the hardness and softness of surrounding objects. Various kinds of tactile sensors had been developed inspired by the skin, with flat and flexible features. These kinds of tactile sensor could not be applied in detecting forces in narrow channels, therefore, the objective of the research is to develop a non-flat tactile sensor with the function of detecting force applied to it from different directions.

Chapter 2 discuss about the design strategy of the tactile sensor. In this research, the sensor would be developed inspired by the anatomy of a tooth. A tooth can sense light touch and pressure that that is added to the enamel because of the movement of the tooth triggers the

tactile receptor that is located around its root. Parallel to that anatomy, the sensing element that surround the bottom of the center pole of this device acts as the 'tactile receptors' which sense the movement of the center pole. This design is very similar to the tooth that is fixed in its socket, with tactile receptor distributed in the periodontal ligaments around its root. The sensing mechanism of this sensor device is similar to the lever mechanism. The spring constant of the sensing element and the relative length of the sensing pole at the position of the sensing element and the position of force applied would determine the limit of pole displacement and magnitude of force applicable to the sensor device.

Chapter 3 discuss about the requirement and suitable mechanism and design of the sensor device. Capacitive tactile sensor with encapsulated liquid as dielectric was developed to enhance the sensitivity of the sensor device. The capacitive sensor could be a good candidate to be applied to the tooth-like sensor, but a few characteristics of capacitive sensor, like easily influenced with electrostatic charges from the environment, make it unsuitable to be applied to the tooth-like sensor. Moreover, the design needs to be revised because the sensing elements were not in three-dimensional state. Therefore, piezoresistive sensing element was chosen to be applied to the proposed tooth-inspired tactile sensor. Several attempts had been made in designing the piezoresistive tooth like tactile sensor. The first one was using nanocomposite piezoresistive principle. Experiment was done to choose the material, and the chosen conductive nanocomposite was injected in between two poles, making a tooth shape tactile sensor. The evaluation results of this sensor seem promising, but there are some disadvantages, such as it cannot detect low pressure. Plus, the measurement system was unstable and complicated. The second design was quite similar to the first one, except the sensing principle was changed to a strain gauge sensor. This sensor was not well fabricated as the location of the strain gauges in between two poles cannot be confirmed after assembly process. The evaluation result also showed that the sensor could not differentiate difference of pressure.

Thus, considering the pros and cons of these two mechanisms, the design of the sensor was improvised. The improvement made to the design is summarized in Table 6.1. A stainless-steel pole was glued using softer elastomer to an acrylic base. Four strain gauges were placed on the base, each slanted upwards against the pole. The length of the strain gauges would change according to the movement of the center pole, therefore the direction of the load applied to the center pole could be detected by measuring the resistance change of the strain gauges.

Table 6.1 Difference between previous devices and the latest one

Disadvantages of previous devices	Improvement made to the new device
High pressure sensing only due to the elastomer material that cannot be deformed by low pressure	Change of the material to the 'softer' one so that effects from low pressure could also be sensed and measured
Complicated data processing system: had to use switching system to measure resistance between six pairs of electrodes simultaneously	Using copper strain gauge with simpler measurement system
Sensor device could not detect different values of pressure, possibly because the space for the pole to move is too small to make a change in the resistance of the strain gauge	Put the strain gauge outside the device, instead of sandwiching it between two poles, to add the movable space for the strain gauge
Position of strain gauge might be shifted during the fabrication process	Put the strain gauge outside the device so that the position could be observed directly during fabrication process

Chapter 4 discuss the fabrication process of the newly proposed device. The components of the tactile sensor device were fabricated one by one, and then assembled step by step. The acrylic base and center pole were machined and cut to the desired shape first, and then assembled using silicon-based elastomer and a pole aligner to make sure the pole stayed perpendicularly in the middle of the base. The strain gauges were made using MEMS photolithography and lift-off process. The width of the strain gauges was 50 μm, which was too small to be fabricated by wet etching an 18 μm-thick copper film, like the ones that had been done to the previous two devices. The strain gauges were then cut and assembled to the device in a single-step procedure, with the strain gauges slanted upwards leaning against the center pole.

Chapter 5 is about the evaluation of the newly proposed tactile sensor device. The resistance of the fabricated strain gauges measured using a multimeter is $42.6 \pm 12.9\ \Omega$, which was about 3.6 times higher than the calculated resistance. There was a possibility of the inconsistency of copper coverage during vapor-deposition process, that made the resistance

values higher. Series of experiments were done to evaluate the fabricated device. First, the sensitivity of the device was checked by adding and removing load to and from the side of the center pole. The sensitivity of the fabricated device per unit 1 mm of displacement was -0.016 mm^{-1}, and the sensitivity per unit 1 N of load was -0.313 N^{-1}. The values of sensitivity are comparable to other tactile sensors that had been developed by other researchers. Next, load was applied to all 360° around the side of the center pole for every 15° to test the ability of the device to sense multidirectional load. The result shows a constant sine curve for each strain gauge, with the lowest point at 180° to 195°, and the highest at 270° to 300°, with the definition of 0° opposite to each strain gauge. The result proves that the direction of load applied to the tactile sensor can be deduced by the relative resistance change ratios of all four strain gauges. The last experiment is the repeatability test, where the center pole was charged with loading and unloading activity with five different frequencies, 10 times each. The amplitude of the resistance change ratio remained unchanged with the change of loading-unloading frequency. The result of this test confirmed that the sensor device can be used repetitively.

In conclusion, this research proposes a new design of tactile sensor that is inspired by the anatomy of a tooth, unlike the conventional ones that mimicked the skin. The skin is undoubtedly an organ that is sensitive to tactile stimulations, but it is not necessarily the only one that can serve the purpose. It is proved that the sensor can detect direction of load applied to the side of the center pole, because the resistance of the strain gauges at the bottom of the pole change according to the movement of the pole. A simple wiring system for resistance measurement, which uses the concept of four wire measurement, was built to prove the concept of the device by experiment. The reliability of the sensor to detect multidirectional load was proved successfully by experiment, where constant pattern of result was observed for all four strain gauges of the device. Also, the sensor device's sensitivity to detect low degree of force and the loading repeatability of the sensor device in low frequency were also tested and verified in this research.

6.2 Future Prospect

The fabricated device is believed to has a very good potential to be applied in MIS. The pole of the proposed sensor device is small enough to be applied to the tip of a catheter or an endoscope. The base and strain gauge can be further miniaturized for this purpose. By applying this device to endoscopes or catheters, one more 'sense' will be added during the procedure besides the existing cameras on the tip of the devices. Adding the sense of touch during MIS procedure will further upgrade the medical technology, where biopsies can be omitted in some procedures if the organ tissues can be touched in-vivo. To achieve this level of technology, this tactile sensor can be paired with a multi-dimension tactile display, that will interpret the data of the touched surface to a multi-dimension display. For example, if there was a strange lump seen in an organ inside the body during laparoscopy or endoscopy procedure, the lump would be touched by the tactile sensor, and the tactile stimulation received will be evaluated and interpreted in three-dimensional image by the tactile display that is paired to it outside the body. This technology will further simplify the medical procedure, thus improve the healing time and the quality of life of a patient.

Other than that, this sensor also could be applied to the pipeline inspection robot, especially the walking robot. In this moment, a lot of pipeline inspection robot are utilizing visual image as the feedback to operators. However, applying tactile sensor to the feet of walking robot could provide tactile feedback as well. Power consumption of this proposed sensor was very low, and the signal processing was uncomplicated. These features meet the demand of pipeline inspection robot, which had to be operated with limited power despite of its long operative hour.

REFERENCES

[1] A. Smith and F. Wempen, *CompTIA strata study guide*. John Wiley, 2012.

[2] Y. Wan, Y. Wang, and C. F. Guo, “Recent Progresses on Flexible Tactile Sensors,” *Mater. Today Phys.*, vol. 1, pp. 61–73, 2017.

[3] T. Yang, D. Xie, Z. Li, and H. Zhu, “Recent Advances in Wearable Tactile Sensors: Materials, Sensing Mechanisms, and Device Performance,” *Mater. Sci. Eng. R Reports*, vol. 115, pp. 1–37, 2017.

[4] D. Silvera-Tawil, D. Rye, and M. Velonaki, “Artificial Skin and Tactile Sensing for Socially Interactive Robots: A Review,” *Rob. Auton. Syst.*, vol. 63, no. P3, pp. 230–243, 2015.

[5] R. S. Dahiya, G. Metta, M. Valle, and G. Sandini, “Tactile Sensing—From Humans to Humanoids,” *IEEE Trans. Robot.*, vol. 26, no. 1, pp. 1–20, Feb. 2010.

[6] B. V. Jayawant, “Tactile Sensing in Robotics,” *J. Phys. E.*, vol. 22, no. 9, pp. 684–692, 1989.

[7] 下条誠, 前野隆司, 篠田裕之, and 佐野明人, 触覚認識メカニズムと応用技術 : 触覚センサ・触覚ディスプレイ. サイエンス&テクノロジー, 2010.

[8] Q. Hua, J. Sun, H. Liu, R. Bao, R. Yu, J. Zhai, C. Pan, and Z. L. Wang, “Skin-inspired Highly Stretchable and Conformable Matrix Networks for Multifunctional Sensing,” *Nat. Commun.*, vol. 9, no. 244, pp. 1–11, Dec. 2018.

[9] N. Thanh-Vinh, N. Binh-Khiem, H. Takahashi, K. Matsumoto, and I. Shimoyama, “High-sensitivity Triaxial Tactile Sensor with Elastic Microstructures Pressing on Piezoresistive Cantilevers,” *Sensors Actuators, A Phys.*, vol. 215, pp. 167–175, 2014.

[10] H. Takahashi, A. Nakai, N. Thanh-Vinh, K. Matsumoto, and I. Shimoyama, “A Triaxial Tactile Sensor without Crosstalk Using Pairs of Piezoresistive Beams with Sidewall Doping,” *Sensors Actuators, A Phys.*, vol. 199, pp. 43–48, 2013.

[11] G. Liang, Y. Wang, D. Mei, K. Xi, and Z. Chen, “Flexible Capacitive Tactile Sensor Array With Truncated Pyramids as Dielectric Layer for Three-Axis Force Measurement,” *J. Microelectromechanical Syst.*, vol. 24, no. 5, pp. 1510–1519, Oct. 2015.

[12] T. Nakadegawa, H. Ishizuka, and N. Miki, “Three-axis Scanning Force Sensor with

Liquid Metal Electrodes," *Sensors Actuators, A Phys.*, vol. 264, pp. 260–267, 2017.

[13] N. Morita, H. Nogami, E. Higurashi, and R. Sawada, "Grasping Force Control for a Robotic Hand by Slip Detection Using Developed Micro Laser Doppler Velocimeter," *Sensors (Switzerland)*, vol. 18, no. 2, pp. 1–17, 2018.

[14] R. Fernandez, I. Payo, A. S. Vazquez, and J. Becedas, "Slip Detection in Robotic Hands with Flexible Parts," Springer, Cham, 2014, pp. 153–167.

[15] Y. Murayama, M. Haruta, Y. Hatakeyama, T. Shiina, H. Sakuma, S. Takenoshita, S. Omata, and C. E. Constantinou, "Development of a New Instrument for Examination of Stiffness in the Breast Using Haptic Sensor Technology," *Sensors Actuators, A Phys.*, vol. 143, no. 2, pp. 430–438, 2008.

[16] M. Kalantari, M. Ramezanifard, R. Ahmadi, J. Dargahi, and J. Kovecses, "Design, Fabrication, and Testing of a Piezoresistive Hardness Sensor in Minimally Invasive Surgery," *2010 IEEE Haptics Symp. HAPTICS 2010*, pp. 431–437, 2010.

[17] R. Ahmadi, J. Dargahi, M. Packirisamy, and R. Cecere, "A New Hybrid Catheter-tip Tactile Sensor with Relative Hardness Measuring Capability for Use in Catheter-based Heart Surgery," *Proc. IEEE Sensors*, pp. 1592–1595, 2010.

[18] C. G. Li and J. J. Shen, "Design and Analysis of a Tactile Sensor Used in Minimally Invasive Surgery," in *2013 IEEE/ASME International Conference on Advanced Intelligent Mechatronics: Mechatronics for Human Wellbeing, AIM 2013*, 2013, pp. 1454–1457.

[19] M. Sohgawa, K. Watanabe, T. Kanashima, M. Okuyama, T. Abe, H. Noma, and T. Azuma, "Texture Measurement and Identification of Object Surface by MEMS Tactile Sensor," in *Proceedings of IEEE Sensors*, 2014, pp. 1706–1709.

[20] K. Takahashi, T. Abe, M. Sohgawa, M. Okuyama, and H. Noma, "Basic Study for Tactile and Visual Texture Measurement by Multimodal MEMS Sensor with Force and Light Sensitivity," in *2015 IEEE SENSORS*, 2015, pp. 1–4.

[21] R. Araki, T. Abe, H. Noma, and M. Sohgawa, "Miniaturization and High-Density Arrangement of Microcantilevers in Proximity and Tactile Sensor for Dexterous Gripping Control," *Micromachines*, vol. 9, no. 6, p. 301, 2018.

[22] F. Castelli, "An Integrated Tactile-thermal Robot Sensor with Capacitive Tactile Array," in *IAS '95. Conference Record of the 1995 IEEE Industry Applications Conference Thirtieth IAS Annual Meeting*, 1995, pp. 1970–1975.

[23] I. H. M. Hashim, S. Kumamoto, K. Takemura, T. Maeno, S. Okuda, and Y. Mori, "Tactile Evaluation Feedback System for Multi-layered Structure Inspired by Human Tactile Perception Mechanism," *Sensors (Switzerland)*, vol. 17, no. 11, 2017.

[24] P. Wang and Q. Liu, *Biomedical Sensors and Measurement*. Zhejiang University Press, 2011.

[25] A. H. Meitzler, "Effect of Strain Rate on the Behavior of Iso-elastic Wire Strain Gauges," *Rev. Sci. Instrum.*, vol. 27, no. 1, p. 56, 1956.

[26] H. S. Freynik, D. R. Roach, D. W. Deis, and D. G. Hirzel, "Evaluation of Metal-Foil Strain Gauges for Cryogenic Application in Magnetic Fields," in *Advances in Cryogenic Engineering*, Boston, MA: Springer US, 1978, pp. 473–479.

[27] J. Millett, N. Bourne, and Z. Rosenberg, "The Piezoresistance of Constantan Strain Gauges Under Shock Loading Conditions," *J. Phys. D. Appl. Phys.*, vol. 31, no. 9, pp. 1126–1130, May 1998.

[28] J.-F. Lei and H. A. Will, "Thin-film Thermocouples and Strain-gauge Technologies for Engine Applications," *Sensors Actuators A Phys.*, vol. 65, no. 2–3, pp. 187–193, Mar. 1998.

[29] C.-X. Liu, J.-W. Choi, C.-X. Liu, and J.-W. Choi, "Improved Dispersion of Carbon Nanotubes in Polymers at High Concentrations," *Nanomaterials*, vol. 2, no. 4, pp. 329–347, Oct. 2012.

[30] X. Z. Niu, S. L. Peng, L. Y. Liu, W. J. Wen, and P. Sheng, "Characterizing and Patterning of PDMS-Based Conducting Composites," *Adv. Mater.*, vol. 19, no. 18, pp. 2682–2686, Sep. 2007.

[31] H. Wang, D. Zhou, and J. Cao, "Development of a Skin-Like Tactile Sensor Array for Curved Surface," *IEEE Sens. J.*, vol. 14, no. 1, pp. 55–61, Jan. 2014.

[32] J.-J. Wang, C.-E. Lu, J.-L. Huang, R. Chen, and W. Fang, "Nanocomposite Rubber Elastomer with Piezoresistive Detection for Flexible Tactile Sense Application," in *2017 IEEE 30th International Conference on Micro Electro Mechanical Systems (MEMS)*, 2017, pp. 720–723.

[33] S.-H. Bae, Y. Lee, B. K. Sharma, H.-J. Lee, J.-H. Kim, and J.-H. Ahn, "Graphene-based Transparent Strain Sensor," *Carbon N. Y.*, vol. 51, pp. 236–242, Jan. 2013.

[34] N. A. A. Ridzuan and N. Miki, "A Bio-inspired Cylindrical Tactile Sensor for

Multidirectional Pressure Detection," in *2014 International Conference on Electronics Packaging (ICEP)*, 2014, pp. 394–399.

[35] N. T. Selvan, S. B. Eshwaran, A. Das, K. W. Stöckelhuber, S. Wießner, P. Pötschke, G. B. Nando, A. I. Chervanyov, and G. Heinrich, "Piezoresistive Natural Rubber-Multiwall Carbon Nanotube Nanocomposite for Sensor Applications," *Sensors Actuators A Phys.*, vol. 239, pp. 102–113, Mar. 2016.

[36] S. C. B. Mannsfeld, B. C.-K. Tee, R. M. Stoltenberg, C. V. H.-H. Chen, S. Barman, B. V. O. Muir, A. N. Sokolov, C. Reese, and Z. Bao, "Highly sensitive flexible pressure sensors with microstructured rubber dielectric layers," *Nat. Mater.*, vol. 9, no. 10, pp. 859–864, Oct. 2010.

[37] N. A. Ahmad Ridzuan, S. Masuda, and N. Miki, "Flexible Capacitive Sensor Encapsulating Liquids as Dielectric with a Largely Deformable Polymer Membrane," *Micro Nano Lett.*, vol. 7, no. 12, pp. 1193–1196, Dec. 2012.

[38] G. Schwartz, B. C.-K. Tee, J. Mei, A. L. Appleton, D. H. Kim, H. Wang, and Z. Bao, "Flexible polymer transistors with high pressure sensitivity for application in electronic skin and health monitoring," *Nat. Commun.*, vol. 4, no. 1, p. 1859, Dec. 2013.

[39] Y. Mi, Y. Chan, D. Trau, P. Huang, and E. Chen, "Micromolding of PDMS scaffolds and microwells for tissue culture and cell patterning: A new method of microfabrication by the self-assembled micropatterns of diblock copolymer micelles," *Polymer (Guildf).*, vol. 47, no. 14, pp. 5124–5130, Jun. 2006.

[40] N. Q. Balaban, U. S. Schwarz, D. Riveline, P. Goichberg, G. Tzur, I. Sabanay, D. Mahalu, S. Safran, A. Bershadsky, L. Addadi, and B. Geiger, "Force and Focal Adhesion Assembly: A Close Relationship Studied Using Elastic Micropatterned Substrates," *Nat. Cell Biol.*, vol. 3, no. 5, pp. 466–472, May 2001.

[41] Z. Ji, H. Zhu, H. Liu, N. Liu, T. Chen, Z. Yang, and L. Sun, "The Design and Characterization of a Flexible Tactile Sensing Array for Robot Skin," *Sensors (Switzerland)*, vol. 16, no. 12, 2016.

[42] L. Wang, H. Peng, X. Wang, X. Chen, C. Yang, B. Yang, and J. Liu, "PDMS/MWCNT-based Tactile Sensor Array with Coplanar Electrodes for Crosstalk Suppression," *Microsystems Nanoeng.*, vol. 2, no. 1, p. 16065, Dec. 2016.

[43] P. Peng and R. Rajamani, "Flexible Microtactile Sensor for Normal and Shear Elasticity Measurements," *IEEE Trans. Ind. Electron.*, vol. 59, no. 12, pp. 4907–4913, Dec. 2012.

[44] J. Kim, T. Nga Ng, and W. Soo Kim, “Highly Sensitive Tactile Sensors Integrated with Organic Transistors,” *Appl. Phys. Lett.*, vol. 101, no. 10, p. 103308, Sep. 2012.

[45] J. A. Dobrzynska and M. A. M. Gijs, “Polymer-based Flexible Capacitive Sensor for Three-axial Force Measurements,” *J. Micromechanics Microengineering*, vol. 23, no. 1, p. 015009, Jan. 2013.

[46] C. Ledermann, S. Wirges, D. Oertel, M. Mende, and H. Woern, “Tactile Sensor on a Magnetic Basis Using Novel 3D Hall Sensor - First Prototypes and Results,” in *2013 IEEE 17th International Conference on Intelligent Engineering Systems (INES)*, 2013, pp. 55–60.

[47] A. Alfadhel and J. Kosel, “Magnetic Nanocomposite Cilia Tactile Sensor,” *Adv. Mater.*, vol. 27, no. 47, pp. 7888–7892, 2015.

[48] A. Alfadhel, A. A. A. Carreno, I. G. Foulds, and J. Kosel, “Three-Axis Magnetic Field Induction Sensor Realized on Buckled Cantilever Plate,” *IEEE Trans. Magn.*, vol. 49, no. 7, pp. 4144–4147, Jul. 2013.

[49] S. Wattanasarn, K. Noda, K. Matsumoto, and I. Shimoyama, “3D Flexible Tactile Sensor Using Electromagnetic Induction Coils,” *Proc. IEEE Int. Conf. Micro Electro Mech. Syst.*, no. February, pp. 488–491, 2012.

[50] M.-S. Kim, H.-R. Ahn, S. Lee, C. Kim, and Y.-J. Kim, “A Dome-shaped Piezoelectric Tactile Sensor Arrays Fabricated by an Air Inflation Technique,” *Sensors Actuators A Phys.*, vol. 212, pp. 151–158, Jun. 2014.

[51] C.-H. H. Chuang, T.-H. H. Li, I.-C. C. Chou, and Y.-J. J. Teng, “Piezoelectric Tactile Sensor for Submucosal Tumor Detection in Endoscopy,” *Sensors Actuators, A Phys.*, vol. 244, pp. 299–309, Jun. 2016.

[52] A. Spanu, L. Pinna, F. Viola, L. Seminara, M. Valle, A. Bonfiglio, and P. Cosseddu, “A High-sensitivity Tactile Sensor Based on Piezoelectric Polymer PVDF Coupled to an Ultra-low Voltage Organic Transistor,” *Org. Electron.*, vol. 36, pp. 57–60, Sep. 2016.

[53] W. Liu, P. Yu, C. Gu, X. Cheng, and X. Fu, “Fingertip Piezoelectric Tactile Sensor Array for Roughness Encoding Under Varying Scanning Velocity,” *IEEE Sens. J.*, vol. 17, no. 21, pp. 6867–6879, Nov. 2017.

[54] H. Xie, A. Jiang, L. Seneviratne, and K. Althoefer, “Pixel-based Optical Fiber Tactile Force Sensor for Robot Manipulation,” in *2012 IEEE Sensors*, 2012, pp. 1–4.

[55] R. Ahmadi, M. Packirisamy, J. Dargahi, and R. Cecere, “Discretely Loaded Beam-Type Optical Fiber Tactile Sensor for Tissue Manipulation and Palpation in Minimally Invasive Robotic Surgery,” *IEEE Sens. J.*, vol. 12, no. 1, pp. 22–32, Jan. 2012.

[56] C. Ledermann, J. Hergenhan, O. Weede, and H. Woern, “Combining Shape Sensor and Haptic Sensors for Highly Flexible Single Port System Using Fiber Bragg Sensor Technology,” in *Proceedings of 2012 IEEE/ASME 8th IEEE/ASME International Conference on Mechatronic and Embedded Systems and Applications*, 2012, pp. 196–201.

[57] J. Song, Q. Jiang, Y. Huang, Y. Li, Y. Jia, X. Rong, R. Song, and H. Liu, “Research on Pressure Tactile Sensing Technology Based on Fiber Bragg Grating Array,” *Photonic Sensors*, vol. 5, no. 3, pp. 263–272, Sep. 2015.

[58] P. Saccomandi, C. M. Oddo, L. Zollo, D. Formica, R. A. Romeo, C. Massaroni, M. A. Caponero, N. Vitiello, E. Guglielmelli, S. Silvestri, and E. Schena, “Feedforward Neural Network for Force Coding of an MRI-Compatible Tactile Sensor Array Based on Fiber Bragg Grating,” *J. Sensors*, vol. 2015, pp. 1–9, Aug. 2015.

[59] C. Chi, X. Sun, N. Xue, T. Li, and C. Liu, “Recent Progress in Technologies for Tactile Sensors.,” *Sensors*, vol. 18, no. 948, Mar. 2018.

[60] L. Kruger, *Pain and Touch*. Academic Press, 1996.

[61] A. Montagu, *Touching : the Human Significance of the Skin*. Perennial Library, 1986.

[62] M. Trulsson and R. S. Johansson, “Orofacial Mechanoreceptors in Humans: Encoding Characteristics and Responses During Natural Orofacial Behaviors.,” *Behav. Brain Res.*, vol. 135, no. 1–2, pp. 27–33, Sep. 2002.

[63] R. Porter, “Lingual Mechanoreceptors Activated by Muscle Twitch.,” *J. Physiol.*, vol. 183, no. 1, pp. 101–11, Mar. 1966.

[64] B. M. Eley, M. Soory, J. D. Manson, and J. D. Manson, *Periodontia*, 6th ed. Elsevier Health Sciences, 2012.

[65] J. D. Manson, *Periodontics for the Dental Practitioner: A Manual of Practical Periodontics*, 2nd ed. London: Henry Kimpton, 1970.

[66] J. Bell, S. Bolanowski, and M. H. Holmes, “The Structure and Function of Pacinian Corpuscles: A Review,” *Prog. Neurobiol.*, vol. 42, no. 1, pp. 79–128, Jan. 1994.

[67] M. S. Fleming and W. Luo, “The Anatomy, Function, and development of mammalian

Aβ low-threshold mechanoreceptors.," *Front. Biol. (Beijing).*, vol. 8, no. 4, Aug. 2013.

[68] M. Hollins and S. R. Risner, "Evidence for the Duplex Theory of Tactile Texture Perception.," *Percept. Psychophys.*, vol. 62, no. 4, pp. 695–705, May 2000.

[69] M. Hollins, S. . Bensmaïa, and E. . Roy, "Vibrotaction and Texture Perception," *Behav. Brain Res.*, vol. 135, no. 1–2, pp. 51–56, Sep. 2002.

[70] S. J. Lederman, J. M. Loomis, and D. A. Williams, "The Role of Vibration in the Tactual Perception of Roughness," 1982.

[71] S. J. Lederman, "Tactual Roughness Perception: Spatial and Temporal Determinants.," *Can. J. Psychol. Can. Psychol.*, vol. 37, no. 4, pp. 498–511, 1983.

[72] H. Shirado and T. Maeno, "Modeling of Human Texture Perception for Tactile Displays and Sensors," in *First Joint Eurohaptics Conference and Symposium on Haptic Interfaces for Virtual Environment and Teleoperator Systems*, 2005, pp. 629–630.

[73] T. Maeno, K. Kobayashi, and N. Yamazaki, "Relationship between the Structure of Human Finger Tissue and the Location of Tactile Receptors.," *JSME Int. J. Ser. C*, vol. 41, no. 1, pp. 94–100, Mar. 1998.

[74] G. J. Gerling and G. W. Thomas, "Fingerprint Lines May Not Directly Affect SA-I Mechanoreceptor Response," *Somatosens. Mot. Res.*, vol. 25, no. 1, pp. 61–76, Jan. 2008.

[75] J. Z. Wu, K. Krajnak, D. E. Welcome, and R. G. Dong, "Three-Dimensional Finite Element Simulations of the Dynamic Response of a Fingertip to Vibration," *J. Biomech. Eng.*, vol. 130, no. 5, p. 054501, Jul. 2008.

[76] S. Shimawaki and N. Sakai, "Quasi-static Deformation Analysis of a Human Finger using a Three-dimensional Finite Element Model Constructed from CT Images," *J. Environ. Eng.*, vol. 2, no. 1, pp. 56–63, 2007.

[77] A. K. Afifi and R. A. Bergman, *Functional Neuroanatomy : Text and Atlas*. Lange Medical Books/McGraw-Hill, 2005.

[78] N. Cauna and L. L. Ross, "The Fine Structure of Meissner's Touch Corpuscles of Human Fingers.," *J. Biophys. Biochem. Cytol.*, vol. 8, pp. 467–82, Oct. 1960.

[79] J. N. Hoffmann, A. G. Montag, and N. J. Dominy, "Meissner Corpuscles and Somatosensory Acuity: The Prehensile Appendages of Primates and Elephants," *Anat. Rec.*, vol. 281A, no. 1, pp. 1138–1147, Nov. 2004.

[80] W.-Y. Tseng, J. S. Fisher, J. L. Prieto, K. Rinaldi, G. Alapati, and A. P. Lee, "A Slow-

adapting Microfluidic-based Tactile Sensor," *J. Micromechanics Microengineering*, vol. 19, no. 8, p. 085002, Aug. 2009.

[81] R. S. Johansson and Å. B. Vallbo, "Tactile Sensory Coding in the Glabrous Skin of the Human Hand," *Trends Neurosci.*, vol. 6, pp. 27–32, Jan. 1983.

[82] E. R. Kandel, J. Schwartz, and T. Jessell, *Principles of Neural Science*. McGraw-Hill Medical, 2000.

[83] W. R. Provancher, "On Tactile Sensing and Display," Stanford University, 2003.

[84] M. Seale, E. Mastropaolo, N. Nakayama, C. Cummins, and I. M. Viola, "Design Principles of Hair-like Structures as Biological Machines," *J. R. Soc. Interface*, vol. 15, no. 20180206, pp. 1–16, 2018.

[85] Y. Zhang and N. Miki, "An Optimal Design of Epidermal Ridges to the Tactile Sensor for Sensitivity Enhancement during Shear Force Detection," *IEEJ Trans. Sensors Micromachines*, vol. 131, no. 4, pp. 141–147, Apr. 2011.

[86] S. Salehi, J.-J. Cabibihan, and S. S. Ge, "Artificial Skin Ridges Enhance Local Tactile Shape Discrimination," *Sensors*, vol. 11, no. 9, pp. 8626–8642, Sep. 2011.

[87] S. Ding, Y. Pan, M. Tong, and X. Zhao, "Tactile Perception of Roughness and Hardness to Discriminate Materials by Friction-Induced Vibration," *Sensors*, vol. 17, no. 2748, pp. 1–14, 2017.

[88] J. Zhang, L. Hao, F. Yang, W. Jiao, W. Liu, Y. Li, R. Wang, and X. He, "Biomimic Hairy Skin Tactile Sensor Based on Ferromagnetic Microwires," *ACS Appl. Mater. Interfaces*, vol. 8, no. 49, pp. 33848–33855, Dec. 2016.

[89] K. Takei, Z. Yu, M. Zheng, H. Ota, T. Takahashi, and A. Javey, "Highly sensitive electronic whiskers based on patterned carbon nanotube and silver nanoparticle composite films.," *Proc. Natl. Acad. Sci. U. S. A.*, vol. 111, no. 5, pp. 1703–1707, Feb. 2014.

[90] S. Harada, W. Honda, T. Arie, S. Akita, and K. Takei, "Fully Printed, Highly Sensitive Multifunctional Artificial Electronic Whisker Arrays Integrated with Strain and Temperature Sensors," *ACS Nano*, vol. 8, no. 4, pp. 3921–3927, Apr. 2014.

[91] J. C. Sullivan, B. Mitchinson, M. J. Pearson, M. Evans, N. F. Lepora, C. W. Fox, C. Melhuish, and T. J. Prescott, "Tactile Discrimination Using Active Whisker Sensors," *IEEE Sens. J.*, vol. 12, pp. 350–362, 2012.

[92] F. Ju and S.-F. Ling, “Bioinspired Active Whisker Sensor for Robotic Vibrissal Tactile Sensing,” *Smart Mater. Struct.*, vol. 23, no. 12, p. 125003, Dec. 2014.

[93] C. Roke, C. Melhuish, T. Pipe, D. Drury, and C. Chorley, “Lump Localisation Through a Deformation-based Tactile Feedback System Using a Biologically Inspired Finger Sensor,” *Rob. Auton. Syst.*, vol. 60, no. 11, pp. 1442–1448, Nov. 2012.

[94] T. Assaf, C. Roke, J. Rossiter, T. Pipe, and C. Melhuish, “Seeing by Touch: Evaluation of a Soft Biologically-inspired Artificial Fingertip in Real-time Active Touch,” *Sensors*, vol. 14, no. 2, pp. 2561–2577, 2014.

[95] M. S. Suen, Y. C. Lin, and R. Chen, “A Flexible Multifunctional Tactile Sensor Using Interlocked Zinc Oxide Nanorod Arrays for Artificial Electronic Skin,” *Sensors Actuators, A Phys.*, vol. 269, pp. 574–584, 2018.

[96] T. Li, S. Zhang, G. W. Lu, and Y. Sunami, “Vibro-perception of Optical Bio-inspired Fiber-skin,” *Sensors*, vol. 18, no. 1531, pp. 1–15, 2018.

[97] Y. Jung, D. G. Lee, J. Park, H. Ko, and H. Lim, “Piezoresistive tactile sensor discriminating multidirectional forces,” *Sensors*, vol. 15, no. 10, pp. 25463–25473, 2015.

[98] Y. Hotta, Y. Zhang, and N. Miki, “A Flexible Capacitive Sensor with Encapsulated Liquids as Dielectrics,” *Micromachines*, vol. 3, no. 1, pp. 137–149, Mar. 2012.

[99] Y. Okayama, K. Nakahara, X. Arouette, T. Ninomiya, Y. Matsumoto, Y. Orimo, A. Hotta, M. Omiya, and N. Miki, “Characterization of a bonding-in-liquid technique for liquid encapsulation into MEMS devices,” *J. Micromechanics Microengineering*, vol. 20, no. 9, 2010.

[100] J. Fu and F. Li, “A Forefinger-like Tactile Sensor for Elasticity Sensing Based on Piezoelectric Cantilevers,” *Sensors Actuators, A Phys.*, vol. 234, pp. 351–358, 2015.

[101] Z. Yi, Y. Zhang, and J. Peters, “Bioinspired Tactile Sensor for Surface Roughness Discrimination,” *Sensors Actuators, A Phys.*, vol. 255, pp. 46–53, 2017.

[102] T. E. Alves De Oliveira, A. M. Cretu, and E. M. Petriu, “Multimodal Bio-Inspired Tactile Sensing Module,” *Sensors*, vol. 17, no. 1187, pp. 1–19, 2017.

[103] M. Tanaka, T. Iijima, Y. Tanahashi, and S. Chonan, “Development of a 3D tactile sensor,” *J. Mater. Process. Technol.*, vol. 181, pp. 286–290, 2007.

[104] X. Chen, J. Shao, H. Tian, X. Li, Y. Tian, and C. Wang, “Flexible Three-axial Tactile Sensors with Microstructure-Enhanced Piezoelectric Effect and Specially-Arranged

Piezoelectric Arrays," *Smart Mater. Struct.*, vol. 27, no. 2, 2018.

[105] S. McKinley, A. Garg, S. Sen, R. Kapadia, A. Murali, K. Nichols, S. Lim, S. Patil, P. Abbeel, A. M. Okamura, and K. Goldberg, "A Single-use Haptic Palpation Probe for Locating Subcutaneous Blood Vessels in Robot-assisted Minimally Invasive Surgery," in *IEEE International Conference on Automation Science and Engineering*, 2015, pp. 1151–1158.

[106] O. V. Baranova, G. L. Markina, Y. L. Kolesnikov, and I. V. Zakharov, "Robot Engineering Implementation for Monitoring Small-diameter Pipelines," *Indian J. Sci. Technol.*, vol. 9, no. 11, 2016.

[107] Y. X. Zhao, G. P. He, and D. W. Gao, "Micro In-pipe Robot Mechanical Structure Design of Shape Memory Alloy Driving," *2009 IEEE Int. Conf. Robot. Biomimetics, ROBIO 2009*, pp. 360–365, 2009.

[108] J. Okamoto, J. C. Adamowski, M. S. . Tsuzuki, F. Buiochi, and C. S. Camerini, "Autonomous System for Oil Pipelines Inspection," *Mechatronics*, vol. 9, no. 7, pp. 731–743, 1999.

[109] H. Ogai and B. Bhattacharya, "Pipe Inspection Robots for Gas and Oil Pipelines," in *Pipe Inspection Robots for Structural Health and Condition Monitoring*, vol. 89, India: Springer (India) Private Ltd, 2018, pp. 13–43.

[110] S. J. Nelson and M. M. Ash, *Wheeler's Dental Anatomy, Physiology, and Occlusion*. Saunders/Elsevier, 2010.

[111] S. Jónsdóttir, E. Giesen, and J. Maltha, "Biomechanical Behaviour of the Periodontal Ligament of The Beagle Dog During the First 5 Hours of Orthodontic Force Application," *Eur. J. Orthod.*, vol. 28, no. 6, pp. 547–552, Dec. 2006.

[112] T. S. Fill, J. P. Carey, R. W. Toogood, and P. W. Major, "Experimentally Determined Mechanical Properties of, and Models for, the Periodontal Ligament: Critical Review of Current Literature.," *J. Dent. Biomech.*, vol. 2011, p. 312980, 2011.

[113] J. Z. Gul, K. Y. Su, and K. H. Choi, "Fully 3D Printed Multi-Material Soft Bio-Inspired Whisker Sensor for Underwater-Induced Vortex Detection," *Soft Robot.*, vol. 00, no. 00, pp. 1–11, 2017.

[114] Y. Hu, R. B. Katragadda, H. Tu, Q. Zheng, Y. Li, and Y. Xu, "Bioinspired 3-D Tactile Sensor for Minimally Invasive Surgery," *J. Microelectromechanical Syst.*, vol. 19, no. 6, pp. 1400–1408, 2010.

[115] D. Benfield, E. Lou, and W. A. Moussa, “Parametric Evaluation of Shear Sensitivity in Piezoresistive Interfacial Force Sensors,” *J. Micromechanics Microengineering*, vol. 21, no. 045005, 2011.

[116] W. Wang, Y. Zhao, and Q. Lin, “An Integrated MEMS Tactile Tri-axial Micro-force Probe Sensor for Minimally Invasive Surgery,” in *2009 IEEE 3rd International Conference on Nano/Molecular Medicine and Engineering, NANOMED 2009*, 2009, pp. 71–76.

[117] A. L. Trejos, R. V. Patel, and M. D. Naish, “Force Sensing and Its Application in Minimally Invasive Surgery and Therapy: A Survey,” *Proc. Inst. Mech. Eng. Part C J. Mech. Eng. Sci.*, vol. 224, no. 7, pp. 1435–1454, 2010.

[118] J. D. Brown, J. Rosen, M. Moreyra, M. Sinanan, and B. Hannaford, “Computer-Controlled Motorized Endoscopic Grasper for In Vivo Measurement of Soft Tissue Biomechanical Characteristics,” in *Medicine Meets Virtual Reality*, Newport Beach, CA: IOS Press, 2002, pp. 71–73.

[119] A. L. Trejos, S. Jayaraman, R. V. Patel, M. D. Naish, and C. M. Schlachta, “Force Sensing in Natural Orifice Transluminal Endoscopic Surgery,” *Surg. Endosc.*, vol. 25, no. 1, pp. 186–192, 2011.

[120] B. B. V. L. Deepak, M. V. A. Raju Bahubalendruni, and B. B. Biswal, “Development of In-pipe Robots for Inspection and Cleaning Tasks: Survey, Classification and Comparison,” *Int. J. Intell. Unmanned Syst.*, vol. 4, no. 3, pp. 182–210, Jul. 2016.

[121] S. Schostek, C. N. Ho, D. Kalanovic, and M. O. Schurr, “Artificial Tactile Sensing in Minimally Invasive Surgery - A New Technical Approach,” *Minim. Invasive Ther. Allied Technol.*, vol. 15, no. 5, pp. 296–304, 2006.

[122] B. T. Bethea, A. M. Okamura, M. Kitagawa, T. P. Fitton, S. M. Cattaneo, V. L. Gott, W. A. Baumgartner, and D. D. Yuh, “Application of Haptic Feedback to Robotic Surgery,” *J. Laparoendosc. Adv. Surg. Tech. A*, vol. 14, no. 3, pp. 191–195, 2004.

[123] J. Jezný and M. Čurilla, “Position Measurement with Hall Effect Sensors,” *Am. J. Mech. Eng.*, vol. 1, no. 7, pp. 231–235, 2013.

[124] H. A. Sodano, D. J. Inman, and G. Park, “A Review of Power Harvesting from Vibration using Piezoelectric Materials,” *Shock Vib. Dig.*, vol. 36, no. 3, pp. 197–205, 2004.

[125] N. A. A. Ridzuan, “Development of a Cylindrical Tactile Sensor for Multidirectional Pressure Detection,” Keio University, 2014.

[126] N. A. Ahmad Ridzuan and N. Miki, “The Effects of Varying Fillers and Insulating Materials to Flexible Conductive Composites,” in *The Proceedings of the Symposium on Micro-Nano Science and Technology*, 2013, vol. 2013.5, no. 0, pp. 219–220.

[127] S. Y. Kwon, Y. K. Park, and M. S. Kim, “Piezoresistive Properties of Multi-walled Carbon Nanotubes–Poly(dimethylsiloxane) Composite for Low-pressure-sensing Applications,” *Nano*, vol. 07, no. 01, p. 1250005, Feb. 2012.

[128] N. Hu, Y. Karube, M. Arai, T. Watanabe, C. Yan, Y. Li, Y. Liu, and H. Fukunaga, “Investigation on Sensitivity of a Polymer/Carbon Nanotube Composite Strain Sensor,” *Carbon N. Y.*, vol. 48, no. 3, pp. 680–687, Mar. 2010.

[129] Q. Zhu, L. Ba, C. Zhou, E. Li, W. Dong, J. Wu, Y. Huang, and J. Mei, “Fabrication and Computer Simulation of Nanoparticle/Rubber Composite Elastomer with Precious Piezoresistance Response,” 2009, vol. 7493, p. 749304.

[130] M. Kalantari, J. Dargahi, J. Kövecses, M. G. Mardasi, and S. Nouri, “A New Approach for Modeling Piezoresistive Force Sensors Based on Semiconductive Polymer Composites,” *IEEE/ASME Trans. Mechatronics*, vol. 17, no. 3, pp. 572–581, Jun. 2012.

[131] K. Weiss and H. Worn, “The Working Principle of Resistive Tactile Sensor Cells,” in *IEEE International Conference Mechatronics and Automation, 2005*, pp. 471–476.

[132] R. Holm, *Electric Contacts*. Berlin, Heidelberg: Springer Berlin Heidelberg, 1967.

[133] Z. Wang, “Polydimethylsiloxane Mechanical Properties Measured by Macroscopic Compression and Nanoindentation Techniques,” University of South Florida, 2011.

[134] N. A. A. Ridzuan and N. Miki, “Development of a Cylindrical Tactile Sensor with a Tooth-Like Mechanism,” in *ICEP-IAAC 2015 - 2015 International Conference on Electronic Packaging and iMAPS All Asia Conference*, 2015, pp. 401–404.

[135] D. M. Mattox, *Handbook of Physical Vapor Deposition (PVD) Processing*. Elsevier Inc., 2010.

[136] Y. Nakamura, Y. Suzuki, and Y. Watanabe, “Effect of Oxygen Plasma Etching on Adhesion Between Polyimide Films and Metal,” *Thin Solid Films*, vol. 290–291, no. 1996, pp. 367–369, 1996.

[137] B. Noh, J. Yoon, J. Choi, and S. Jung, “Effect of Cr Thickness on Adhesion Strength of Cu/Cr/Polyimide Flexible Copper Clad Laminate Fabricated by Roll-to-Roll Process - 85.pdf,” *Mater. Trans.*, vol. 51, no. 1, pp. 85–89, 2010.

[138] R. A. Matula, “Electrical Resistivity of Copper, Gold, Palladium, and Silver,” *J. Phys. Chem. Ref. Data*, vol. 8, no. 4, pp. 1147–1298, Oct. 1979.

[139] L. Beccai, S. Roccella, A. Arena, F. Valvo, P. Valdastri, A. Menciassi, M. C. Carrozza, and P. Dario, “Design and Fabrication of a Hybrid Silicon Three-axial Force Sensor for Biomechanical Applications,” *Sensors Actuators A Phys.*, vol. 120, no. 2, pp. 370–382, May 2005.

[140] P. Valdastri, S. Roccella, L. Beccai, E. Cattin, A. Menciassi, M. C. Carrozza, and P. Dario, “Characterization of a Novel Hybrid Silicon Three-axial Force Sensor,” *Sensors Actuators A Phys.*, vol. 123–124, pp. 249–257, Sep. 2005.

[141] B. Han, Y. J. Yoon, M. Hamidullah, A. T. H. Lin, and W. T. Park, “Silicon Nanowire-based Ring-shaped Tri-axial Force Sensor for Smart Integration on Guidewire,” *J. Micromechanics Microengineering*, vol. 24, no. 6, 2014.

APPENDIX

A. Dimension of strain gauge

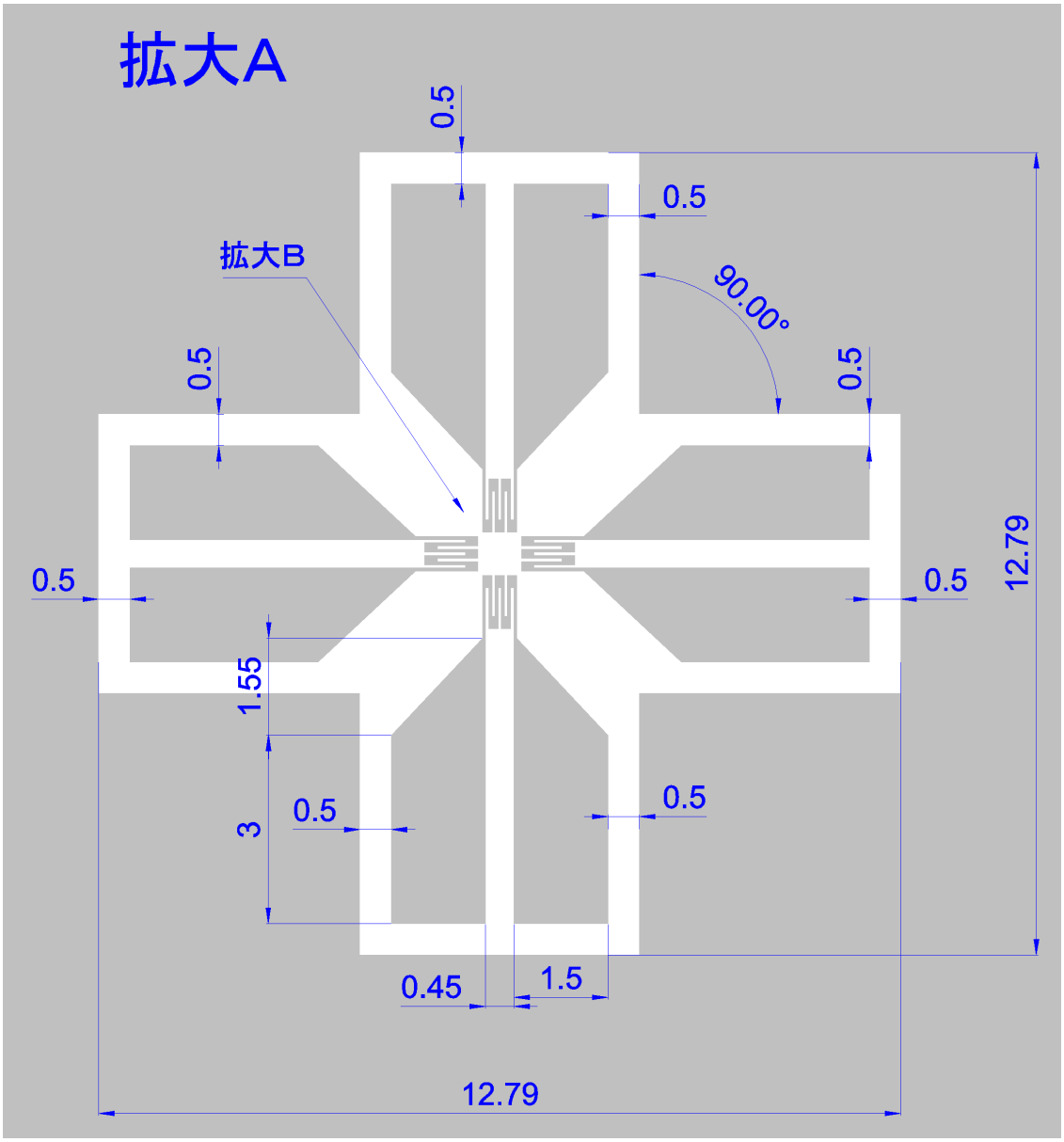

Figure A-1 Dimension of strain gauges (1) in mm (Tokyo Process Service Co., Ltd.)

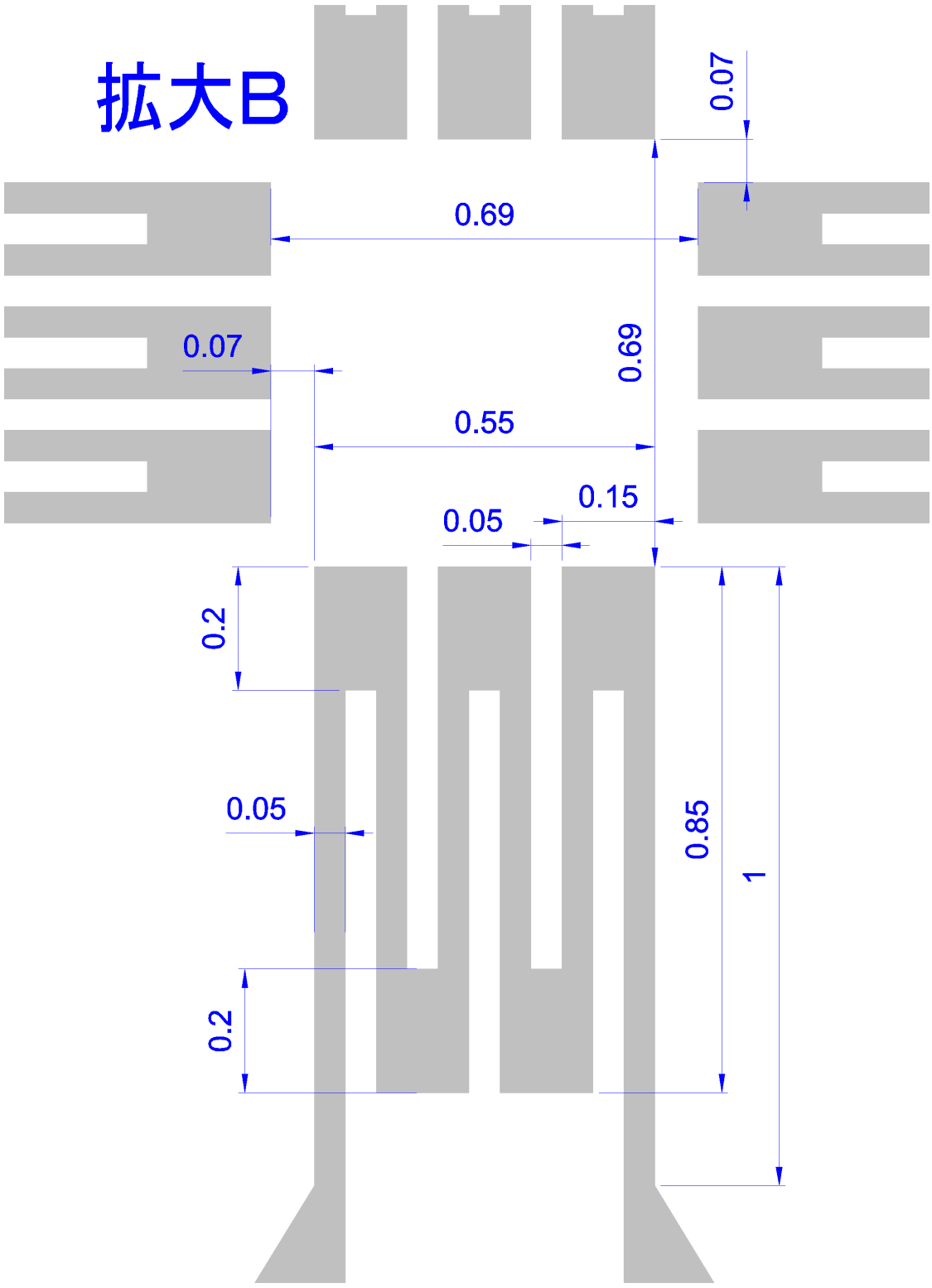

Figure A-2 Dimension of strain gauges (2) in mm (Tokyo Process Service Co., Ltd.)

B. Details of photomask

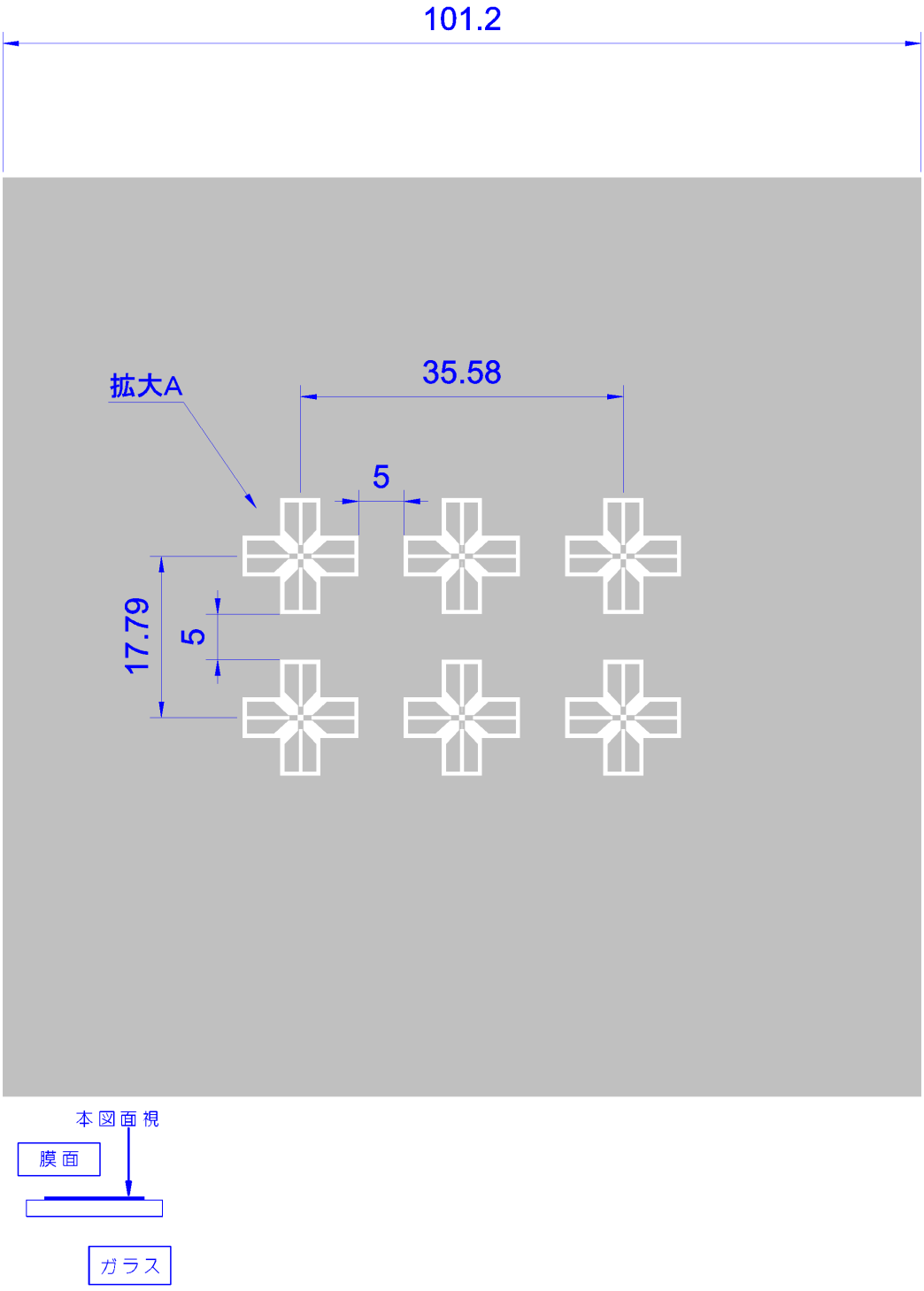

Figure B-1 Details and dimension of photomask for strain gauge patterning in mm (Tokyo Process Service Co., Ltd.)

C. Details of fabrication process of strain gauges

Table C-1 Details of fabrication process of strain gauges

Process	Machine/Materials	Details
Primer coating	Mikasa Spincoater 1H-D7 OAP	300 rpm, 8 s 2000 rpm, 12 s
Photoresist coating	Mikasa Spincoater 1H-D7 ZPN 1150-90	500 rpm, 8 s 3500 rpm, 20 s
Prebake	EC Hotplate EC-1200N	100°C, 90 s
UV exposure	Union EMA-400 Mask Aligner	16 mW/cm^2, 30 s
Post-exposure bake	EC Hotplate EC-1200N	100°C, 60 s
Photoresist development	NMD-3 2.38%	30 s
O_2 plasma etching	Samco Plasma Etching System Model FA-1	3 min
Contact metal vapor deposition	Sanyu Electron resistive thermal evaporation system Chromium grains	Thickness: 35 nm
Copper strain gauge vapor deposition	Sanyu Electron resistive thermal evaporation system Copper wires	Thickness: 110 nm
Copper solder pad vapor deposition	Sanyu Electron resistive thermal evaporation system Copper wires	Thickness: 250 nm
Lift-off process	Aceton	-

D. Dimension of pole aligner

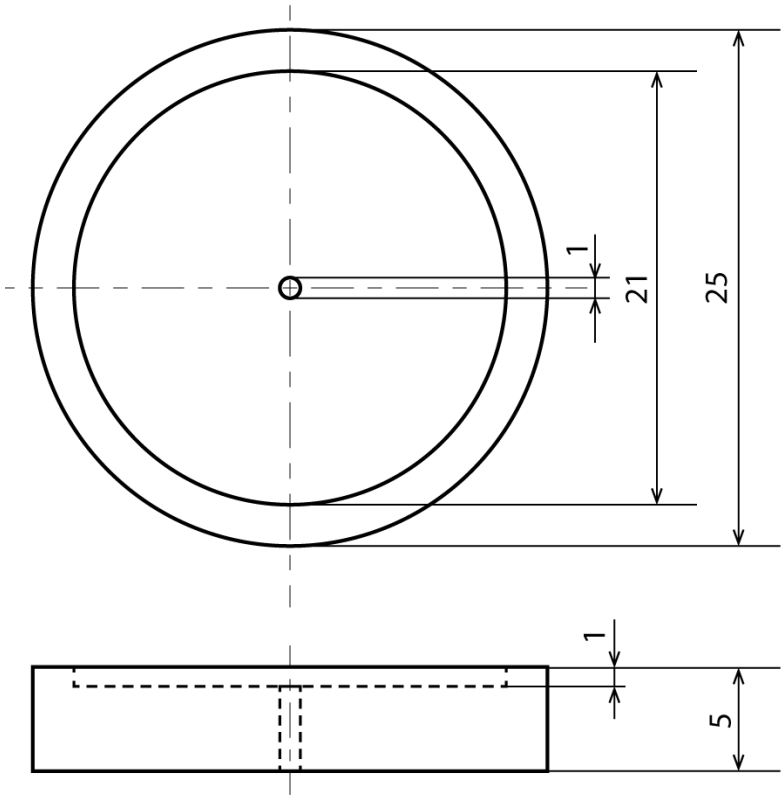

Figure D-1 Top view (top) and side view (bottom) of pole aligner with dimension in mm

PUBLICATIONS

1. Articles on periodicals (related to thesis)

N. A. Ahmad Ridzuan and N. Miki, "Tooth-Inspired Tactile Sensor for Detection of Multidirectional Force", Micromachines, 2019, Vol. 10, Iss. 18, pp. 1-10

N. A. Ahmad Ridzuan, S. Masuda, and N. Miki, "Flexible Capacitive Sensor Encapsulating Liquids as Dielectric with a Largely Deformable Polymer Membrane", Micro & Nano Letters, 2012, Vol. 7, Iss. 12, pp. 1193-1196

2. Articles on international conference proceedings (reviewed full-length articles)

N. A. Ahmad Ridzuan* and N. Miki, "Development of a Cylindrical Tactile Sensor with a Tooth-like Mechanism", 2015 International Conference on Electronic Packaging and iMAPS All Asia Conference (ICEP-IAAC 2015), Kyoto, Japan, 2015, pp. 401-404

N. A. Ahmad Ridzuan* and N. Miki, "A Bio-Inspired Cylindrical Tactile Sensor for Multidirectional Pressure Detection", 2014 International Conference on Electronics Packaging (ICEP 2014), Toyama, Japan, 2014, pp. 394-399

3. Presentations at international conferences

N. A. Ahmad Ridzuan*, Y Hotta, Y. Zhang and N. Miki, "Development of a Flexible Capacitive Sensor with Encapsulated Liquid as Dielectric", The Sixth Asia Pacific Conference on Transducers and Micro/Nano Technologies (IEEE APCOT 2012), Nanjing, China, July 2012

4. Presentations at domestic meetings

N. A. Ahmad Ridzuan* and N. Miki, "A Multidirectional Pressure Detectable Cylindrical Tactile Sensor", The 6th JSME Micro and Nano Symposium, Shimane, Japan, Oct 2014

N. A. Ahmad Ridzuan* and N. Miki, "The Effects of Varying Fillers and Insulating Materials to Flexible Conductive Composite", The 5th JSME Micro and Nano Symposium, Sendai, Japan, Nov 2013

N. A. Ahmad Ridzuan*, Y Hotta, Y. Zhang and N. Miki, “Flexibility and Sensitivity Enhancement of a Capacitive Sensor by Encapsulating Liquids as Dielectric”, JSME Robotics and Mechatronics Conference ROBOMEC 2012, Hamamatsu, Japan, 2012

5. Award

2014 IEEE CPMT Japan Chapter Young Award, ICEP-IAAC 2015, 15th April 2015